

DOTTORATO DI RICERCA IN BIOINGEGNERIA – XIX CICLO
Sede Amministrativa: Università degli Studi di Bologna

COMPUTATIONAL ANALYSIS
OF CARDIAC CELL EXCITABILITY

Tesi di Dottorato di:

ELEONORA GRANDI

Supervisor:

**Chiar.mo Prof. Ing. SILVIO CAVALCANTI
Chiar.mo Prof. Ing. GIANNI GNUDI**

Controrelatore:

Chiar.mo Prof. Ing. MAURO URSINO

ING-INF/06 BIOINGEGNERIA ELETTRONICA E INFORMATICA

Anno Accademico 2005-2006

**COMPUTATIONAL ANALYSIS OF EXCITABILITY
IN CARDIAC MYOCYTES**

by
Eleonora Grandi

A dissertation submitted to University of Bologna in conformity with the
requirements for the degree of Doctor of Philosophy

Bologna, 2007

Prof. Gianni Gnudi
Supervisor of Dissertation

Prof. Silvio Cavalcanti
Co-supervisor of Dissertation

Prof. Mauro Ursino
Reviewer of Dissertation

Keywords

Sodium Channelopathies – Action Potential Simulation
Cardiac Cell Models – Computational Biology
Inherited and Acquired Diseases

Acknowledgments

I would like to thank my primary advisor, Prof Silvio Cavalcanti, for sharing his vision and excitement for the field of computational biology. I am particularly grateful to Dr Stefano Severi and Dr Stefania Vecchietti for providing invaluable insight and support through all stages of my research.

The task of building computational models requires collaboration with experimentalists who provide not only data, but also expertise and insight. I have been fortunate to work with a number of experimental scientists at Fondazione Salvatore Maugeri (Pavia), Loyola University (Chicago) and Georg-August-University (Göttingen) who have contributed the essential data as well as valuable knowledge and discussions. I would like to thank Prof Silvia Priori, Dr Carlo Napolitano and Dr Ilaria Rivolta for the exciting work on Brugada and Long QT syndromes. I would like to thank Dr Donald Bers for the stimulating research period I spent in his lab, and all the professors, postdocs and students that made this period exciting and productive. In particular, I'm grateful to Dr Sanda Despa, Dr Ken Ginsburg, Dr Fei Wang and Dr Pepe Puglisi for providing support and helpful discussions. I would like to thank Dr Lars Maier and Dr Stefan Wagner for their support in the CaMKII study. I would like to thank Dr Emanuele Giordano for his helpfulness. For reading my dissertation and advising me during my PhD I would like to thank Prof Gianni Gnudi and Prof Mauro Ursino.

I would also like to thank everyone in the biomedical engineering community at DEIS in Bologna and Cesena for providing a productive and enjoyable environment in which to live and work.

I would like to thank my family and my friends, who have always happily provided full support and encouragement for my endeavors.

CONTENTS

Introduction.....	IV
1 Cardiac Action Potential and Na ⁺ channel	1
Functioning of the heart	1
Cardiac Na ⁺ channel	6
2 Mathematical modeling of the myocyte	11
Markov models of ion channel kinetics	21
The Luo-Rudy phase 2 model (guinea pig)	28
The Shannon <i>et al.</i> model (rabbit)	34
3 Arrhythmogenic Syndromes and Na ⁺ channelopathies	41
Long QT syndrome	42
Brugada syndrome	46
4 In silico assessment of Na ⁺ channelopathies	61
Materials and Methods	63
Results	67
Discussion	72
Conclusion	77
5 CaMKII effects on the Na ⁺ channel gating	78
Ca/Calmodulin-dependent protein kinase II	78
CaMKII regulates cardiac Na ⁺ channels	81
Discussion	89
6 Cardiac I _{Na} Markov Model Identification	92
Introduction	92

Methods	92
Results	97
Discussion	100
Conclusions	100
7 Effects of CaMKII over-expression on cardiac excitability	102
Na current	102
Methods	102
Results	100
Discussion	105
L-type Ca ²⁺ and K ⁺ transient outward current	107
Methods	100
Results	100
Concluding remarks	112
References.....	115

Introduction

The cardiac cell is a complex biological system where various processes interact to generate electrical excitation (the action potential, AP) and contraction. During AP generation, membrane ion channels interact nonlinearly varying transmembrane voltage that in turn depends on the ionic fluxes through the cell membrane, and are subject to regulatory processes. In recent years, a large body of knowledge has accumulated on the molecular structure of cardiac ion channels, their function, and dysfunction due to genetic mutations that are associated with cardiac arrhythmias and sudden death. However, ion channels are typically studied in isolation (in expression systems or isolated membrane patches), away from the physiological environment of the cell where they interact to generate the AP. A major challenge remains the integration of ion-channel properties into the functioning, complex and highly interactive cell system, with the objective to relate molecular-level processes and their modification by disease to whole-cell function and clinical phenotype. In the present thesis, it is shown how computational biology can be used to achieve such integration.

Abnormal repolarization of the cell membrane provides a substrate for life threatening cardiac arrhythmias. The dependence of repolarization on a delicate balance between various currents makes it vulnerable to perturbation by disease or drugs. Mutations in genes that encode cardiac ion channels can lead to abnormal channel function (“channelopathy”) which perturbs the AP to cause arrhythmias (Keating & Sanguinetti, 1996; Priori *et al.*, 1999a; Priori *et al.*, 1999b). Mutation-induced alterations in ion channel function are studied in expression systems (e.g. *Xenopus Oocyte*) in isolation from the physiological environment of the cardiac cell where the channels interact to generate the AP. Computational biology can be used to integrate this information into the functioning cardiac cell in order to relate these molecular-level findings to whole-cell function and to the clinical phenotype. In the present thesis examples are provided from the hereditary Long QT syndrome (LQT) that clinically appears as prolongation of the QT interval on the electrocardiogram and the occurrence of life-threatening arrhythmias and sudden death. Specifically, the LQT type 3 (LQT3) that is associated with mutations in *SCN5A* (the gene that encodes the cardiac sodium channel) was simulated. The

Brugada syndrome (Brugada *et al.*, 1998), that is characterized by ST segment elevation in the right precordial leads of the electrocardiogram and is also associated with severe arrhythmias and sudden death, was also simulated. Amino acid 1795 site in the C-terminus of *SCN5A* is intriguing because one human mutation (Y1795C) causes a gain of function and LQT3, while a different human mutation at this same site (Y1795H) causes loss of function and Brugada Syndrome. Intriguingly, a single human mutation at this site (1795InsD) in *SCN5A* is linked to simultaneous LQT3 and BrS features depending on the heart rate. Because mutations affect specific structural elements and kinetic states of the channel and their interdependencies, single-channel based Markov models are required to conduct these simulations.

The heritable channelopathies have yielded important insights into the pathophysiology of some far more common, acquired diseases. Heart failure (HF) is a case in point. This disease afflicts hundreds of millions of people worldwide. We now know that heart failure represents a common, acquired form of channelopathy, specifically of long-QT syndrome. Myocytes from failing hearts show prolongation of action potentials, and repolarization *in vivo* is abnormally labile. Several are the ion channels and signaling pathways involved in HF alteration of cardiac excitability.

Emerging evidences now also link Na⁺ channel gating alterations to acquired diseases, e.g. drug-induced LQTS, cardiac ischemia and HF. In HF an enhanced persistent Na⁺ current contribute to a propensity to arrhythmias. Altered Na⁺ channel regulation may also occur in HF, causing a widespread form of acquired Na⁺ channel dysfunction. For example, Ca-Calmodulin dependent protein kinase II (CaMKII) is upregulated in HF and is more active (Maier and Bers, 2006). Wagner *et al.* (2006a) showed that CaMKII regulates Na⁺ channel gating, and that upregulation of CaMKII in cardiac myocytes causes an extremely similar spectrum of gating changes to those seen for the combined LQT/Brugada phenotype seen with 1795InsD. However, increased levels of CaMKII in HF may target several proteins in the ventricle. CaMKII phosphorylates Ca transport proteins such as phospholamban, ryanodine receptors and L-type calcium channels. In addition novel data suggest that other ion channels, including sarcolemmal Na⁺ and K⁺ channels, may be regulated by this CaMKII.

To assess how CaMKII alters Na⁺ channel gating and how it may participate in arrhythmogenesis, we used a Markov model of the Na current to isolate the impact of altered Na channel gating on the action potential morphology and duration in HF. A more comprehensive in silico study, accounting for the effects of CaMKII on the other sarcolemmal channels was also carried out.

Given the complexity of cardiac arrhythmias, such in silico simulations will undoubtedly feature more prominently in future investigations.

1 Cardiac Action Potential and Na⁺ channel

Functioning of the heart

The heart is a complex electrical, chemical, and mechanical system which is designed to pump blood efficiently based on the metabolic needs of the body. Many of the properties of the whole heart arise from the properties of individual myocytes, each of which may be considered a miniature, but still rather complex, electrical, chemical, and mechanical system. Meticulously timed opening and closing of cardiac ion channels result in cardiac electrical excitation and relaxation that is coupled to rhythmic contraction of the heart. Cardiac excitation originates in the sinoatrial node and propagates through the atria into the atrial-ventricular node. The impulse then enters the Purkinje conduction system, which delivers the excitatory wave to the ventricles. Ventricular excitation spreads from the endocardium to the epicardium and is coupled to the contraction of the ventricles that generates systolic blood pressure. The wave of excitation that spreads over the heart reflects membrane depolarization of cardiac myocytes. The contraction of heart tissue is a direct consequence of a process known as excitation/contraction (EC) coupling. The electrical excitation of a single myocyte produces an action potential (Fig. 1.1), the characteristic depolarization of the cell membrane that occurs as a result of the passage of ionic currents across the cell membrane. In response to excitation, there is an increase in the intracellular Ca²⁺ concentration, which in turn leads to activation of the myofilaments, and ultimately results in cell shortening. The coordinated activation and shortening of myocytes throughout the heart produce contraction of the whole organ. Defects in EC coupling are thought to play an important role in reducing the ability of the heart to pump effectively in diseased states. Since whole heart function, both in physiological and diseased states, often reflects the processes that occur in individual myocytes, it is critical to understand the physiological properties of single cardiac myocytes.

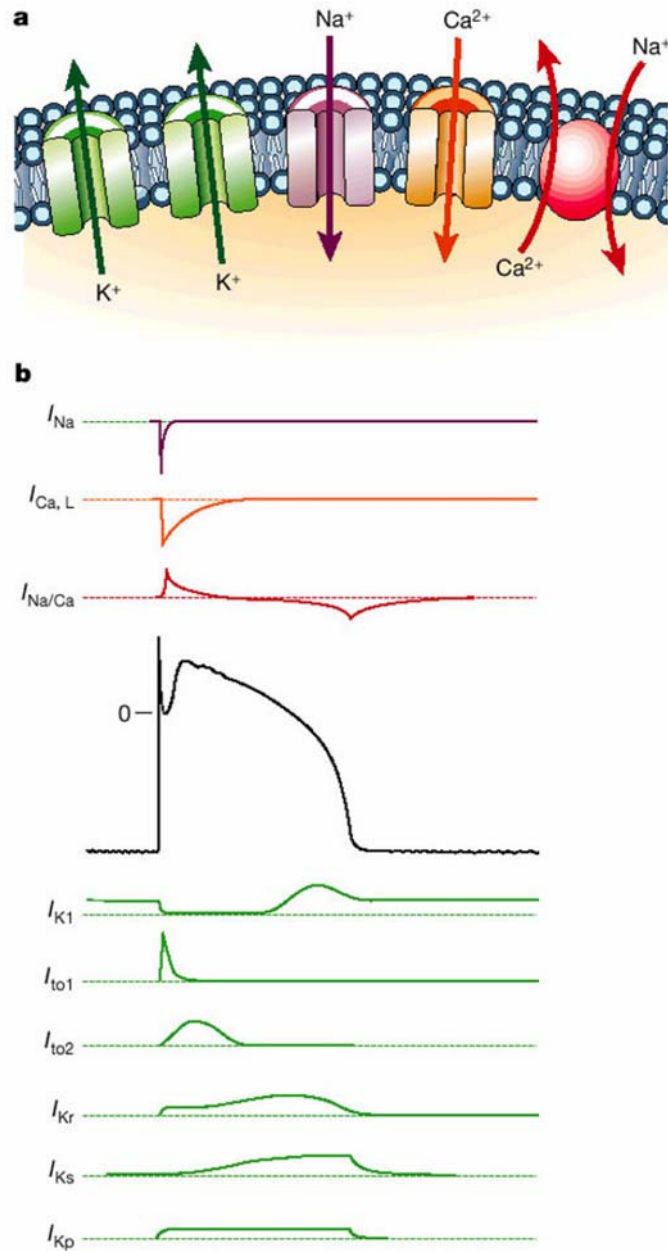


Figure 1.1

Figure 1.1: Panel A) Ion channels on the cell membrane. Panel B) Ion currents that underlie the cardiac action potential. Top, depolarizing currents as a function of time; Middle, a prototypical ventricular action potential; Bottom, repolarizing currents as a function of time. Figure from Marban, 2002.

A characteristic feature of the cardiac myocyte is its action potential (AP). The AP is a transient depolarization of the cell membrane which arises as a result of the dynamic behavior of a diverse population of membrane ion channels. A prototypical ventricular myocyte AP is shown in Fig. 1.1 (Marban, 2002). The AP exhibits a steep upstroke, followed by a sustained slowly decaying plateau phase, which eventually gives way to repolarization. Above the AP are shown the associated depolarizing currents, which are carried by inward Na⁺ and Ca²⁺ currents. Under physiological conditions, the Na⁺ current (I_{Na}) activates rapidly, producing the AP upstroke, and then inactivates completely (Marban *et al.*, 1998). L-type Ca²⁺ current (I_{CaL}) inactivates a bit more slowly, and incompletely, allowing for the inward Ca²⁺ current to maintain the plateau phase of the AP (Zeng and Rudy, 1995). The influx of Ca²⁺ via the L-type Ca²⁺ channels triggers the release of Ca²⁺ from the sarcoplasmic reticulum (SR), an internal Ca²⁺ storage compartment. This EC coupling event (Fig. 1.2) is known as Ca²⁺-induced Ca²⁺-release (CICR). The SR is a subcellular organelle that releases the majority of Ca²⁺ during each heartbeat (Bers, 2001). The rise in cytosolic Ca²⁺ ultimately leads to cell contraction. The SR also actively sequesters Ca²⁺, which is the primary mechanism by which Ca²⁺ is removed from the cytosol in order to allow relaxation in between heartbeats (Bassani *et al.*, 1994). The intracellular Ca²⁺ signal is not only triggered by membrane depolarization, but also feeds back on the L-type Ca²⁺ channel, mediating inactivation of the current, and therefore plays a role in influencing the AP shape. The lower part of Fig 1.1 shows the various types of K⁺ channels (and a Cl⁻ channel) that are involved in membrane repolarization. The inward rectifier current (I_{K1}) maintains and stabilizes the resting potential, the transient outward currents (I_{to1} and I_{to2}), carried by K⁺ and Cl⁻ respectively (Näbauer *et al.*, 1993; Collier *et al.*, 1996), contribute to the notch that follows the upstroke, and the components of the delayed rectifier K⁺ current (I_{Kr} and I_{Ks}) as well as the plateau K⁺ current (I_{Kp}) contribute to the repolarization of the AP (Yue and Marban, 1988). Each of these electrical processes can be detected on the body surface electrocardiogram (ECG) as a signal average of the temporal and spatial

gradients generated during each phase (Fig. 1.3). Electrical excitation in the atria (atrial depolarization) manifests on the ECG as P waves, while ventricular depolarization is seen as the QRS complex. Ventricular repolarization is reflected in the T wave.

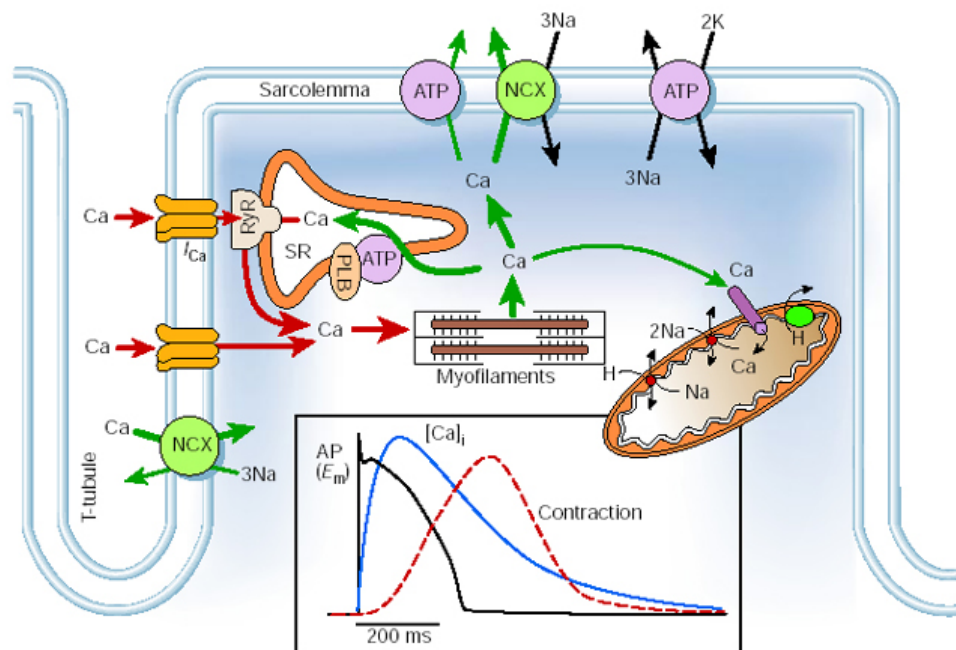


Figure 1.2: EC coupling.

ECG abnormalities are related to changes in cellular AP morphologies, which may be due to altered cell-to-cell coupling, heart disease, congenital ion channel abnormalities, drug intervention, or electrolyte imbalance. In general, membrane potential, extracellular and intracellular ion concentrations, as well as regulatory proteins that modulate the activity of ion channels influence ionic currents. The shape and duration of the AP is therefore an integrative cellular feature that is influenced by the interaction of many underlying cellular processes. For example, AP configurations display characteristic features in different regions of the mammalian heart as a result of the regional variation in underlying currents (reviewed in Katz, 1992).

Conduction abnormalities can be detected as changes in the QRS complex. Widening of the QRS reflects reduced conduction velocity, which typically stems from altered Na⁺ channel function (Tan *et al.* 2001). ST segment elevation reflects

transmural voltage differences during the AP plateau, a hallmark of congenital forms or drug-provoked Brugada syndrome (Yan and Antzelevitch 1999). Prolongation of the action potential duration (APD) (delayed repolarization) results in long QT intervals and may result in morphological changes in the T wave that can provide insight as to the underlying cellular mechanism of APD prolongation (Yan and Antzelevitch 1998).

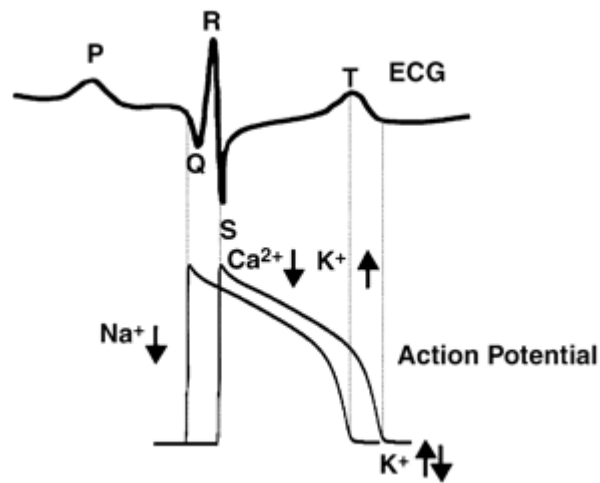


Figure 1.3: Electrical gradients in the myocardium can be detected on the body surface electrocardiogram (ECG) and reflect underlying cellular ionic current gradients. Up: illustration of a single cardiac cycle ECG detected as electrical gradients on the body surface. Down: schematic representation of the ventricular action potential gradients detected on the body surface ECG.

Cardiac Na⁺ channel

Voltage-gated sodium channels

Voltage-gated sodium channels (NaVChs) are important for the generation and propagation of signals in electrically excitable tissues like muscle, the heart, and nerve. Activation of NaVChs in these tissues causes the initial upstroke of the action potential, which in turn triggers other physiological events leading to muscular contraction and neuronal firing. NaVChs are also important targets for local anesthetics, anticonvulsants, and antiarrhythmic agents.

Structure

Sodium channels are heteromultimeric, integral membrane proteins belonging to a superfamily of ion channels that are gated (opened and closed) by changes in membrane potential. Sodium channel proteins from mammalian brain, muscle, and myocardium consist of a single large (approximately 260 kDa) pore-forming α subunit complexed with 1 or 2 smaller accessory β subunits (in Figure 1.4 the cardiac isoforms are shown). Nine genes (*SCN1A*, *SCN2A*, etc.) encoding distinct α subunit isoforms and 4 β subunit genes (*SCN1B*, *SCN2B*, etc.) have been identified in the human genome. Many isoforms are expressed in the central and peripheral nervous system, while skeletal muscle and cardiac muscle express more restricted NaVCh repertoires. The α subunits are constructed with a 4-fold symmetry consisting of structurally homologous domains (DI–DIV) each containing 6 membrane-spanning segments (S1–S6) and a region (S5–S6 pore loop) controlling ion selectivity and permeation (Figure 1.4). The S4 segment (green bars in Figure), which functions as a voltage sensor, is amphipathic with multiple basic amino acids (arginine or lysine) at every third position surrounded by hydrophobic residues.

Gating

NaVChs switch between 3 functional states depending on the membrane potential (Figure 1.5) (Hodgkin and Huxley, 1952). In excitable membranes, a sudden membrane

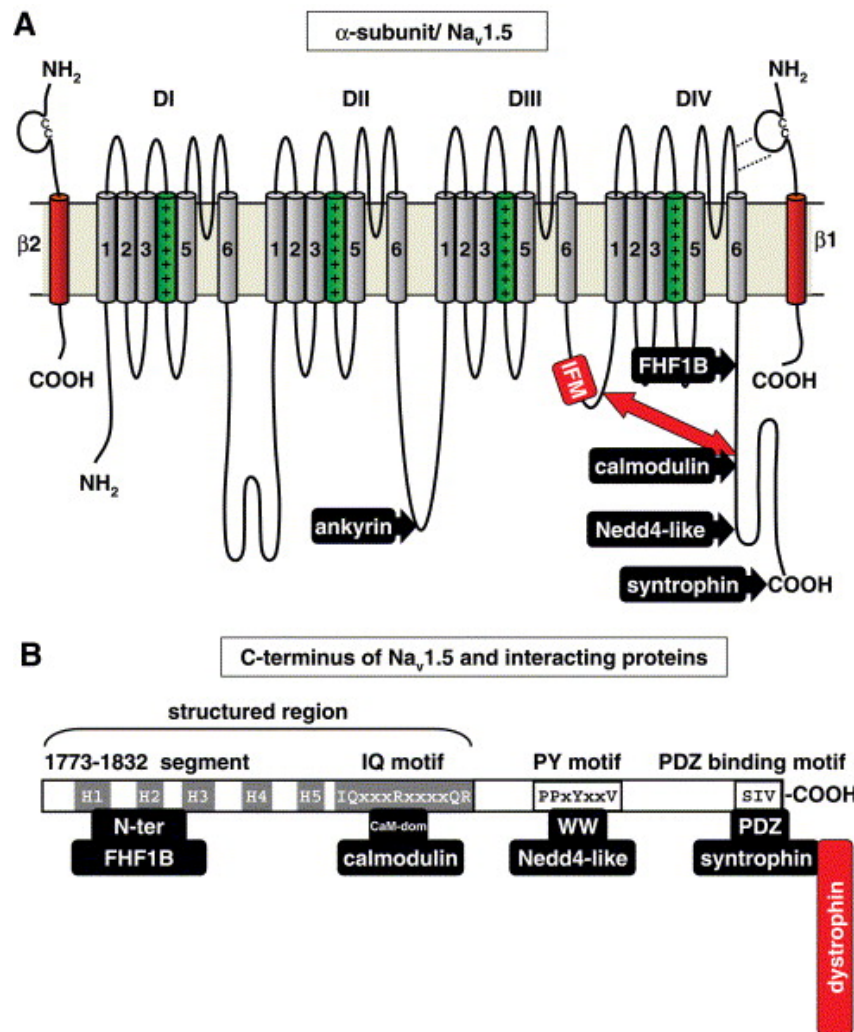


Figure 1.4: (A) Schematic representation of the α subunit of Nav1.5, the two associated β subunits, and interacting proteins. The predicted membrane topology of the α subunit of Nav1.5 is illustrated together with the $\beta 1$ and $\beta 2$ subunits (in red). DI–DIV indicate the four homologous domains of the α subunit; segments 5 and 6 are the pore-lining segments and the S4 helices (green) serve as voltage sensors. The isoleucine-phenylalanine-methionine (IFM) residues are key amino acids for fast inactivation gating. Five proteins that have been reported to interact with Nav1.5 are represented schematically with their approximate binding sites. The red arrow indicates the intramolecular interaction between the III–IV linker and the C terminus (C-T) domain (Motoike *et al.* 2004). (B) Scheme of the C-T of Nav1.5 and interacting proteins. The proximal part of the Nav1.5 C-T (structured region) has been proposed to be composed of six α helices (gray boxes H1–H5, plus the box comprising the IQ motif) (Cormier *et al.* 2002). The distal part seems to be unstructured. Four regions have been reported to be implicated in protein–protein interactions. The N terminus of FH1FB interacts with the proximal C-T domain. Figure from Abriel and Kass 2005.

depolarization causes a rapid rise in local Na⁺ permeability due to the opening (*activation*) of NaVChs from their resting closed state. For this to occur, voltage sensors (the 4 S4 segments) within the NaVCh protein must move in an outward direction, propelled by the change in membrane potential, and then translate this conformational energy to other structures (most likely S6 segments) that swing out of the way of incoming Na⁺ ions.

This increase in Na⁺ permeability causes the sudden membrane depolarization that characterizes the initial phase of an action potential. Normally, activation of NaVChs is transient owing to *inactivation*, another gating process mediated by structures located on the cytoplasmic face of the channel protein (mainly the DIII–DIV linker). NaVChs cannot reopen until the membrane is repolarized and they undergo *recovery from inactivation*. Membrane repolarization is achieved by fast inactivation of NaVChs and activation of voltage-gated potassium channels. During recovery from inactivation, NaVChs may undergo *deactivation*, the transition from the open to the closed state. Activation, inactivation, and recovery from inactivation occur within a few milliseconds. In addition to these rapid gating transitions, NaVChs are also susceptible to closing by slower inactivating processes (*slow inactivation*) if the membrane remains depolarized for a longer time. These slower events may contribute to determining the availability of active channels under various physiological conditions.

Cardiac isoform

The cardiac Na⁺ channel is a glycosylated membrane protein consisting of the main α subunit Na_v1.5—which consists of 2016 residues, with an apparent molecular mass of ~240 kDa—and auxiliary β subunits (~30–35 kDa, β 1– β 4 subunits). All four β subunits have been shown to be expressed in heart. However, the α subunit is the principal component of the cardiac Na⁺ channel forming the pore and all essential gating elements (Figure 1.4A), and is sufficient by itself for generating voltage-dependent Na⁺ currents (I_{Na}) in heterologous expression systems. As the other NaVChs, the Na_v1.5 protein has four homologous domains (DI–DIV, Figure 1.4A) each made up

of six transmembrane segments (S1–S6). The three interdomain regions (linker loops) and both N and C termini of the channel are cytoplasmic. The charged S4 transmembrane segments are involved in activation gating of the channel (Figure 1.4A, in *green*), and a cluster of three hydrophobic residues (isoleucine-phenylalanine-methionine [IFM]) in the III–IV linker facilitates intramolecular interactions that underlie fast inactivation gating (Figure 1.4A, in *red*). The C terminus (C-T) segment of Na_v1.5 has 243 residues, and has been only recently recognized as an important part of the channel (Cormier *et al.*, 2002, Mantegazza *et al.*, 2001). The C-T domain is involved in the inactivation gating, and contains sequences of amino acids forming consensus protein–protein interaction domains (Figure 1.4B). Furthermore, intramolecular interactions between the C-T domain and the cytoplasmic III–IV linker region have recently been demonstrated (Motoike *et al.* 2004). Based on modeling and experimental data, Cormier *et al.* (2002) proposed that the proximal 150 residues of the C-T form a well-structured region comprising six α helices (Figure 1.4B, *gray boxes*). The protein interaction sites are a calmodulin (CaM)-binding IQ motif found in I1908-R1918 (Tan *et al.*, 2002), a PY motif in P1974-Y1977 (Abriel *et al.*, 2000), and a postsynaptic density protein-95 large/zona occludens-1 (PDZ)-binding domain represented by the last three residues serine-isoleucine-valine (Ou *et al.*, 2003). A less well-characterized proximal segment interacts with the protein FHF1B (Liu *et al.* 2003). In addition, underlining the importance of this region, many mutations associated with LQTS, BrS, or conduction defects have been found in the Na_v1.5 C-T tail (Tan *et al.* 2003).

Na⁺ channelopathies

The essential nature of NaVChs is emphasized by the existence of inherited disorders (sodium “channelopathies”) caused by mutations in genes that encode these vital proteins. Nearly 20 disorders affecting skeletal muscle contraction, cardiac rhythm, or neuronal function and ranging in severity from mild or latent disease to life-threatening or incapacitating conditions have been linked to mutations in human

NaVCh genes. Most sodium channelopathies are dominantly inherited, but some are transmitted by recessive inheritance or appear sporadic. Additionally, certain pharmacogenetic syndromes have been traced to variants in NaVCh genes. The clinical manifestations of these disorders depend primarily on the expression pattern of the mutant gene at the tissue level and the biophysical character of NaVCh dysfunction at the molecular level.

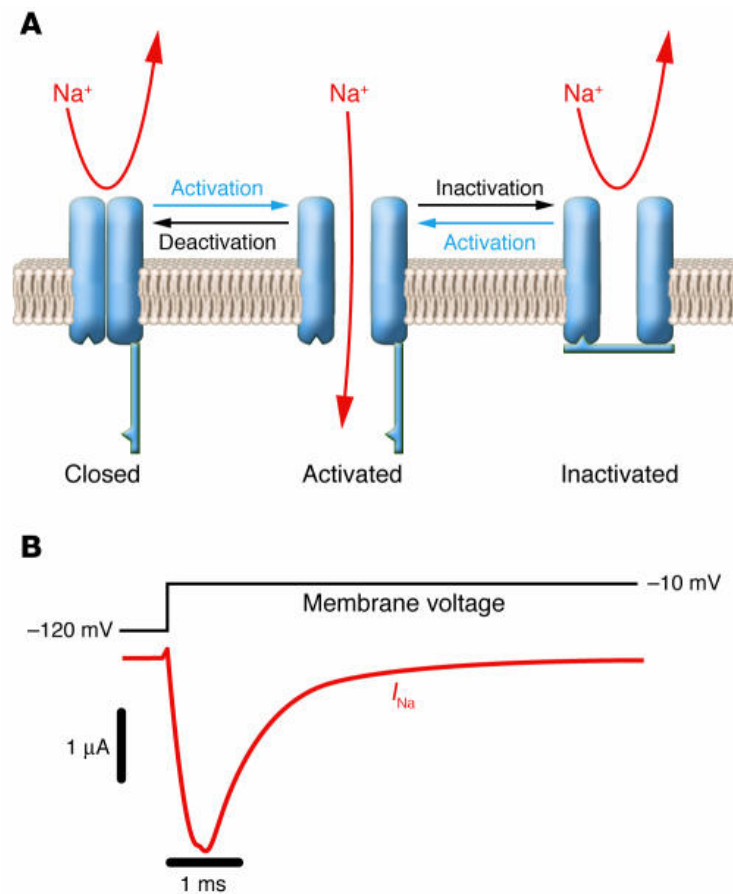


Figure 1.5: Functional properties of NaVChs. (A) Schematic representation of an NaVCh undergoing the major gating transitions. (B) Voltage-clamp recording of NaVCh activity in response to membrane depolarization. Downward deflection of the current trace (red) corresponds to inward movement of Na⁺. Figure from George 2005.

Mutations in *SCN5A*, the gene encoding the Nav1.5 protein, cause inherited susceptibility to ventricular arrhythmia and impaired cardiac conduction. In chapter 3, a review of the Na⁺ channelopathies in the heart is provided.

2 Mathematical modeling of the myocyte

Given the highly integrative nature of the dynamic processes which occur during excitation and contraction of a cardiac myocyte, the approach of integrative modeling is used in order to address fundamental questions about the function of the heart. This is accomplished by developing experimentally based, biophysically detailed, mathematical descriptions of individual cellular components, such as ion channels, pumps, exchangers, and subcellular compartments. Mathematical models of each cellular component are developed based on separate sets of experiments obtained under conditions designed to isolate and characterize a particular current or other subcellular component. Models of each individual system component are then incorporated into single integrative myocyte model in which these subcellular systems can interact. The power and utility of an integrative model stems from the fact that it is “transparent” under all conditions. Transparency refers to the fact that all variables of interest (e.g. membrane potential, ionic concentrations, ionic currents, channel open probability) can be monitored simultaneously at all times during any simulation, i.e. one can “see” into the cell and observe every aspect of the subcellular processes. This is obviously not possible in experimental approaches. Experimental techniques generally isolate and characterize the properties of a single subcellular component. The manipulations that are necessary to perform such experiments often require the presence of pharmacological agents, exogenous buffers, and/or non-physiological solutions. Integrative modeling can therefore be an important tool in interpreting experimental data by helping to elucidate mechanisms underlying phenomena which may otherwise be difficult to understand based on experiments alone. Moreover, models can be used as an exploratory tool to make quantitative predictions, and to guide the design of future experiments. While the transparency of integrative models is their key empowering feature, it is important to recognize that the predictive ability of any model

is limited by the fact that there are likely to be mechanisms and/or components that are missing or incompletely characterized. Taken together, the components of a fully comprehensive integrative model represent the collection of the actual body of knowledge obtained from experiments (and possibly previous models). The inability of a model to reproduce phenomena observed in experiments indicates that there are gaps in our knowledge of the system. However, the model may yield clues as to where these gaps are, and consequently would help guiding the necessary experiments designed to obtain new data and fill such gaps. The model can then be updated based on newly obtained data, and may then be used to make further predictions. This iterative interaction between experiment and simulation has been key to the broadening of our knowledge of the underlying mechanisms of the cardiac ventricular action potential (reviewed in Noble, 2001).

Much of the current knowledge regarding ion channel kinetics and functional current density in excitable tissues has been obtained using the voltage clamp technique. This approach was pioneered by Hodgkin, Huxley, and Katz (1949) now more than five decades ago, and continues to be the best biophysical technique for the study of ion channels (Hille, 1992). “Clamping” of the membrane potential to a constant value using a feedback amplifier with current passing electrodes allows for the quantitative characterization of voltage dependent ion channel gating kinetics. The development of this technique paved the way for the use of integrative modeling as an approach to understanding excitable cells.

In 1952, Hodgkin and Huxley published a series of papers (Hodgkin and Huxley, 1952d; Hodgkin and Huxley, 1952b; Hodgkin and Huxley, 1952a; Hodgkin and Huxley, 1952c) describing both voltage clamp measurements of membrane currents and an integrative model of the action potential for the squid giant axon (Fig. 2.1, left). The researchers successfully formulated simple quantitative descriptions of Na^+ and K^+ currents. Their modeling approach postulated that membrane permeability was regulated by gating mechanisms, whereby distinct entities (i.e., gates) controlled the

flux of both Na^+ and K^+ ions. The position of these gates defined three functional states of the channel: a closed resting state, an open state, and a closed refractory state. By combining their descriptions of the Na^+ and K^+ currents with a leak conductance into an integrative model, Hodgkin and Huxley were able to describe in detail how the interaction of these elements combine to generate an AP. The spectacular success of the Hodgkin-Huxley (HH) model is evident in the fact that, to this day, it serves as a paradigm for describing cell membrane excitability.

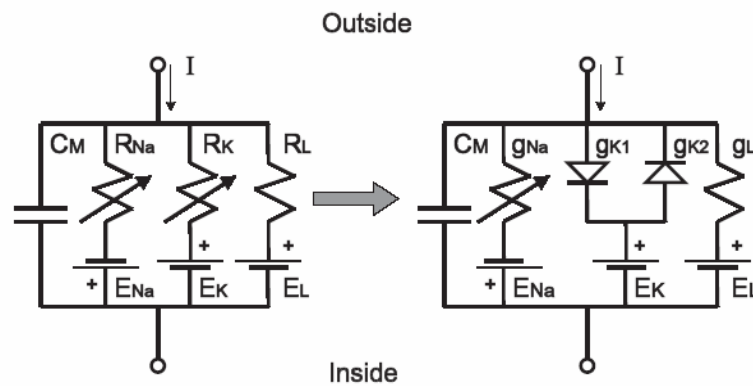


Figure 2.1: The basic Hodgkin and Huxley representation of the squid axon (left) was modified to represent the Purkinje cell (right). In the latter K^+ current is assumed to flow through two non-linear resistances. The conductance g_{K1} is assumed to be an instantaneous function of the membrane potential, while g_{K2} slowly rises when membrane is depolarized. Figure from Puglisi *et al.* 2004.

Soon after Hodgkin and Huxley laid the foundation for the use of integrative models in biology, the first cardiac cell models were developed using a similar approach. The models of Fitzhugh (1960) and Noble (1962) addressed the issue of whether Na^+ and K^+ current descriptions similar to those of Hodgkin and Huxley could be employed to account for the long plateau of the cardiac AP in Purkinje fibers (Figure 2.1, right, reviewed in Noble, 2001 and Puglisi *et al.*, 2004). Modifications to Na^+ and K^+ current kinetics were able to generate a plateau, which was supported by the inward Na^+ current. These early models could therefore reproduce APs, but not other relevant features of cardiac cells, in part, due to the fact that Ca^{2+} currents had not yet been discovered.

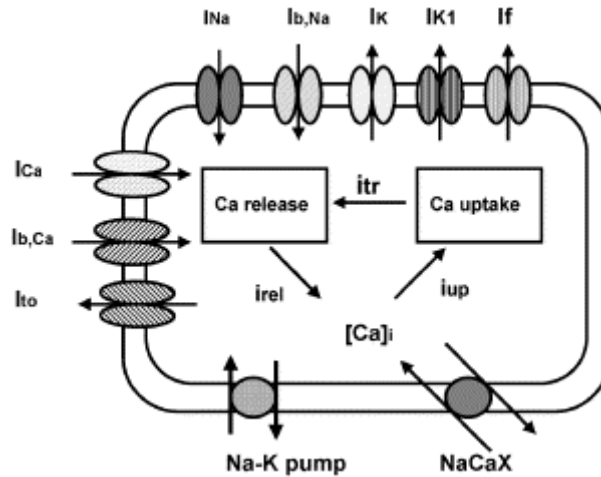


Figure 2.2: The Di Francesco & Noble Model. Besides the ionic currents it incorporated ionic pumps and exchanger mechanisms. It also included a description for Ca^{2+} movement inside of the cell (in the sarcoplasmic reticulum, SR). An energy-consuming pump was assumed to transport Ca^{2+} inside the SR uptake store which then reprimed a release store. Release was assumed to be activated by cytoplasmic Ca^{2+} . Figure from Puglisi *et al.* 2004.

The continued interactive iteration between experiments and simulations has led to improved mechanistic insights into cardiac myocyte electrophysiology. Aspects of intracellular Ca^{2+} handling were introduced in the DiFrancesco-Noble Purkinje cell (Fig. 2.2 DiFrancesco and Noble, 1985) and the Luo-Rudy ventricular cell (Fig. 2.3 Luo and Rudy, 1994) models. New features of these models were the inclusion of the intracellular SR compartment, time varying intracellular and extracellular ion concentrations, and ion pumps and exchangers. Whereas each of these models generate APs using detailed kinetic descriptions of membrane currents, the Ca^{2+} subsystem in each is represented by a phenomenological model that mimics the process of Ca^{2+} -induced Ca^{2+} release, but fails to capture the biophysical details involved. More recent models of the guinea pig (Jafri *et al.*, 1998) and dog (Winslow *et al.*, 1999) cardiac ventricular myocyte attempted to improve upon its predecessors by incorporating detailed descriptions of Ca^{2+} handling processes. Several computational models have been developed to investigate properties of local Ca^{2+} release at the level of the cardiac dyad (Rice *et al.*, 1999; Stern *et al.*, 1999; Langer and Peskoff, 1996; Cannell and Soeller, 1997; Soeller and Cannell, 1997). In 2002 Greenstein and Winslow developed

a comprehensive model of the ventricular myocyte based on the theory of local control of SR Ca^{2+} release.

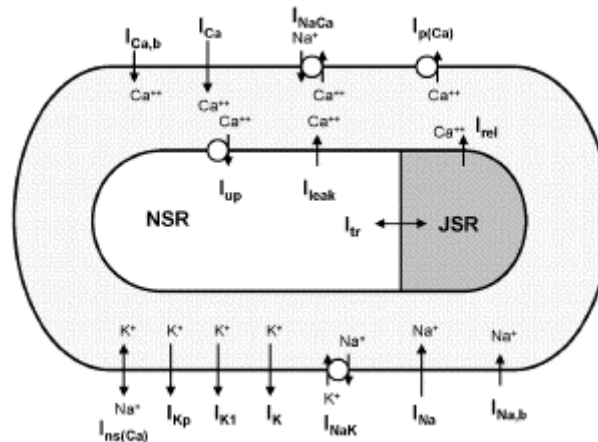


Figure 2.3: The Luo and Rudy Model. Schematic diagram showing the ionic currents, pumps and exchangers. The intracellular compartment is the SR, which is divided into two subcompartments the network SR (NSR) and the junctional SR (JSR). Dotted areas indicate the presence of Ca^{2+} buffers. (Figure from Puglisi *et al.* 2004)

Moving from a general to a species-dependent model

The availability of experimental data led also to the development of model of ventricular myocytes of different species. In fact, in the mid-1990s, the emphasis shifted from general models integrating voltage-clamp data from several species to more detailed models based on data obtained from isolated cells from one particular species. By 1995, electrophysiological studies had shown species differences in AP waveforms and ionic currents, e.g., mouse and rat APs have no phase 2 plateau, but exhibit rapid repolarization and very short AP duration if compared with the prominent plateau phase and long AP seen in humans, rabbit, guinea-pig and dog.

Mouse models are becoming increasingly important, too, as genetic manipulation in mice has proven to be a powerful tool to study the physiological effects of gene mutations, knockouts and transgenesis. Relevant computer models are important to understand the effects of these genetic manipulations, and to enable inferences to be made concerning the effects expected in other species. Rat models have been developed (Demir *et al.*, 1994; Pandit *et al.* 2001 and Pandit *et al.* 2003); the same group

further utilized the rat ventricular myocyte model to develop a model for the mouse left ventricular cells (Demir 2004). A computer model of action potential of mouse ventricular myocytes was proposed by Rasmusson's group (Bondarenko *et al.*, 2004).

Several models of rabbit sinoatrial (SA) node are available in the literature, e.g. Zang *et al.*, 2000, Oehmen *et al.*, 2002. A ventricular model was published by Puglisi and Bers in 2001 (LabHEART). A more recent model of the ventricular rabbit AP was published by Bers' group in 2004 (Shannon *et al.*, 2004).

Canine models have been published by several groups, including Winslow (ventricular cell, Winslow *et al.*, 1999; Greenstein *et al.*, 2000), Nattel (atrial model, Ramirez *et al.*, 2000; Kneller *et al.*, 2002), Cabo and Boyden (epicardial cell, Cabo and Boyden, 2003), Rudy (Hund and Rudy, 2004).

As the accuracy of models depends critically on the quality and extent of experimental data available for validation, during the 1990s development of a human myocyte model has proven elusive, due to the relative paucity of experimental data, specially from normal heart (Beuckelman *et al.*, 1992 and Beuckelman *et al.*, 1993; Li *et al.*, 1996; Piacentino *et al.*, 2003). Human models were published by Nygren *et al.* (1998, from Giles' group), Courtmanche *et al.* (1998, from Nattel's group) and Priebe and Beuckelmann (1998).

In recent years more and more data on human ionic currents have been gathered from human cardiomyocytes. In addition, a new technique has been developed, involving the cloning of human ion channels and heterologously expressing them in another cell type from which then voltage clamp measurements can be made. As a consequence, in recent years, several models for human ventricular cells have been formulated. The Priebe-Beuckelmann (1998) model and simplifications thereof (Bernus *et al.*, 2002) are the first human ventricular myocyte models developed. Their model was largely based on the Luo-Rudy phase 2 model for guinea pig ventricular cells (Luo and Rudy, 1994) in which formulations for the major ionic currents were adjusted to the scarce data available for human ventricular cells at that time. Early 2004, a new

model for human ventricular myocytes by Ten Tusscher *et al.* appeared (Ten Tusscher *et al.*, 2004). This model uses new formulations for all major ionic currents based on a now much wider set of experimental data, largely from human ventricular cell experiments but also from ion channel expression experiments.

Later on in 2004 another model for human ventricular myocytes by Iyer *et al.* (2004) was published. As compared to the Ten Tusscher model, the Iyer model is more strongly based on expression data on human cardiac ion channels than on data on human ventricular cells.

Recently, Ten Tusscher and Panfilov (2006) developed a new version of their human ventricular cell model, which is based on recent experimental measurements of human APD restitution and includes a more extensive description of intracellular calcium dynamics.

Single vs. multi-compartment models

An important issue in modeling the isolated cardiaomyocyte is intracellular calcium cycling. Calcium dynamics can be very important for arrhythmia initiation and its subsequent dynamics, given its involvement in early- and delayed- afterdepolarization (EAD and DAD) formation, alternans and wave instability.

The existence of microdomains of Ca^{2+} inside the cell was proposed and modeled by several authors (Leblanc and Hume, 1990; Bers and Peskoff, 1991; Stern and Lakatta, 1992). At this time, the requirement for modeling subcellular compartments to address essential features of the excitation–contraction coupling became evident. In 1993, Nordin published a guinea-pig model (Fig. 2.4) where the myoplasm was divided into three regions: superficial, medium and deep (Nordin, 1993). Ion flux between these compartments followed a simple gradient diffusion law and the volumes of each compartment were empirically adjusted. Although a heuristic idea this division matched experimental data related to rates of change in myoplasmic $[\text{Ca}^{2+}]$ (Nordin and Ming, 1995).

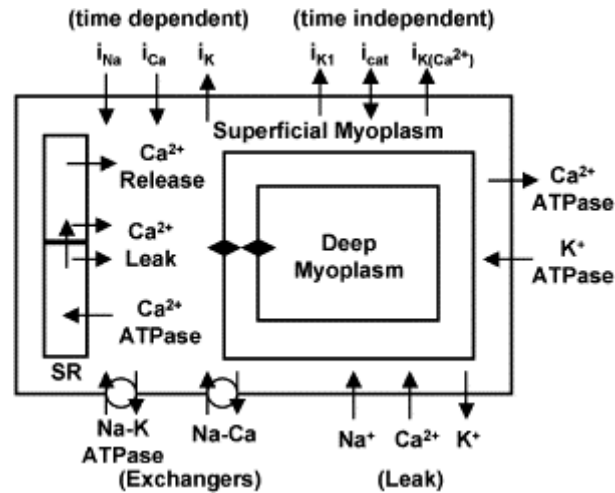


Figure 2.4: The Nordin Model. Myoplasm have been subdivided into superficial, middle, and deep compartments, separated by weak permeability barriers. The SR has been divided into two compartments. Ca^{2+} flux between superficial myoplasm and SR occurs through SR Ca^{2+} ATPase, Ca^{2+} -sensitive Ca^{2+} release channels and leakage fluxes from both SR compartments. Figure from Puglisi *et al.* 2004.

A similar approach was adopted by Nygren *et al.* (1998) in their model of human atrial cell. Based on the DiFrancesco and Noble formulation for ionic currents and SR uptake and release, a cleft and an intracellular space were used to represent ionic movement. Winslow's group worked with a more specific subspace: a restricted volume located between the junctional sarcoplasmic reticulum and the T-tubule. It possessed a buffer (calmodulin) and was the place where the L-type Ca^{2+} channel and the ryanodine receptors interacted (Jafri *et al.*, 1998). This representation allowed the study of phenomena such as adaptation of the ryanodine receptors (RyR).

An analogous scheme was adopted by Pandit *et al.* (2001 and 2003) for their model of rat ventricular myocyte. Shannon and Bers (2001) added a subsarcolemmal space (Fig. 2.5) based on experimental evidence that the Na^+/Ca^{2+} exchanger (NaCaX), I_{Na} , and Na/K-ATPase sense local ionic concentrations differing from both the bulk $[Ca^{2+}]_i$ and that in the junctional cleft. The design of these three compartments seems to be more suited to represent the essential steps in EC coupling; it possesses a dedicated volume for the L-type Ca^{2+} -channel and RyR interactions (the cleft), another volume

beneath the cell membrane for the interactions between transporters and their corresponding ions (the subsarcolemma space) and a cytosolic space where Ca^{2+} binds to myofilaments to generate force.

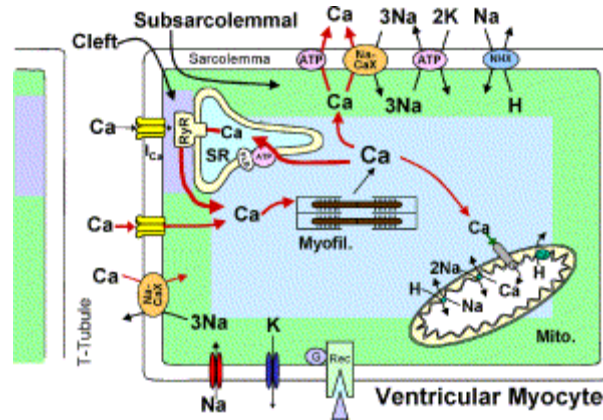


Figure 2.5: Shannon and Bers model. It included three compartments: (1) a junctional cleft where E–C coupling occurs, (2) a subsarcolemma space where I_{Na} , NaCaX and Na/K-ATPase sense ion concentrations and (3) a cytosolic volume where Ca^{2+} interacts with the myofilaments. Redrawn from Shannon and Bers, 2004.

In this regard, modeling the cleft space is crucial to represent accurately basic aspects of the EC coupling. The critical Ca^{2+} -induced Ca^{2+} -release takes place in this minute volume ($\sim 0.06\%$ of the total cell volume, Shannon *et al.*, 2001) and modelers have been challenged to find an adequate representation for a system with high gain, graded response and under a tight control of the I_{CaL} . Mechanistic models describing the interaction between RyR and the L-type Ca^{2+} channel (e.g. Soeller and Cannel, 1997) have proven extremely useful to provide us with insights that are far from intuitive.

Even if in recent years models of intracellular calcium handling have become increasingly complex, modeling individual L-type calcium channels, ryanodine channels, calcium release subunits, and their local, stochastic interactions (Rice *et al.*, 1999 and Greenstein and Winslow, 2002), their computational complexity caused modelers to use incorporate simplified models of intracellular calcium dynamics, by formulating an empirical description of Ca^{2+} release as a function of SR load and Ca^{2+}

influx (e.g. Luo and Rudy, 1994, used a fixed release time that starts 2 ms after the onset of I_{CaL}). In addition, despite ongoing experimental and modeling research important knowledge on the exact mechanisms as for example calcium release termination and recovery is still lacking. To model the role of calcium dynamics in arrhythmia initiation and progression, a model of calcium dynamics that is able to accurately describe both normal stable and abnormal alternating or spontaneously active behavior is needed.

Markov models of ion channel kinetics

Hodgkin and Huxley provided important insights into the mechanisms of cell excitability with the understanding that membrane permeability changes with the membrane potential, and they formulate a mathematical model to demonstrate that voltage dependent changes in the membrane permeability could justify the generation of an action potential. Further studies led to the following interpretation of their model based on voltage dependent ion conductances and open channel probabilities.

In the original Hodgkin and Huxley model of the action potential, each current is calculated using Ohm's law. For example, the equation for I_{Na} is

$$I_{Na} = g_{Na} \cdot (V - E_{Na})$$

where I_{Na} is the transmembrane Na^+ current density ($\mu A/cm^2$), g_{Na} is the Na^+ conductance (mS/cm^2), V is the membrane potential and E_{Na} is the reversal potential (computed using the Nernst equation). Thus $(V-E_{Na})$ is the driving force.

The conductance for each current can be considered as a function of the open probability of a series of hypothetical gates and the maximum conductance of the membrane for each ion species. The gates provide the voltage and time dependence of the conductance, and the maximum conductance is simply the conductance when all gates are open. Each gate can go through a first-order voltage-dependent transition from a closed to an open position or from an open to a closed position at a rate that is independent of the positions of all other gates. An ion can pass through the gate only in its open position. Na^+ current activation (increasing conductance) is accurately modeled by three identical activation gates that move from closed to open positions at depolarized V . The open probability of the activation gate is typically assigned the variable m that ranges from 0 (all gates closed) to 1 (all gates open), and the time-dependent change in m is described by the following first-order differential equation:

$$\frac{dm}{dt} = \alpha \cdot (1 - m) - \beta \cdot m$$

where m and $(1-m)$ are the gate open and closed probabilities, t is time (ms), and α and β are V -dependent opening and closing transition rates (ms^{-1}).

Since the transitions are assumed to be independent, the probability that all three gates are open is m^3 . At positive V all three gates transition rapidly (within milliseconds even at 6–7 °C, Fig. 2.6) to the open state, providing the depolarizing current necessary for the AP upstroke.

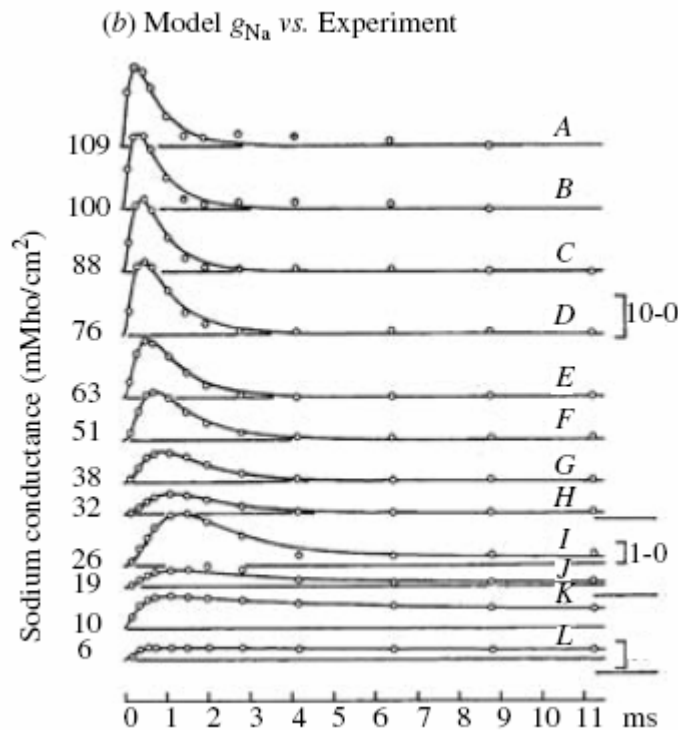


Figure 2.6: Hodgkin–Huxley model-simulated sodium conductance, g_{Na} , (solid line) is superimposed on experimental data (open circles). V values (mV) are indicated by numbers on each trace; conductance scales (mMho/cm^2) are provided on the right.

The voltage-clamp recordings (Fig. 2.6) also show a decrease in current shortly after activation. This process was termed inactivation, and was modeled by using a single first-order inactivation gate with open probability h . At hyperpolarized potentials, h is fully open. When the membrane is depolarized, the inactivation gate closes to cause the

monoexponential decrease observed in I_{Na} . Since h operates independently of m , the open probability for the Na^+ gates is m^3h , and the conductance is

$$g_{Na} = g_{Na,max} \cdot m^3 \cdot h$$

where $g_{Na,max}$ is the maximum experimental conductance (mS/ μ F).

As more information about ion-channel gating has been obtained, it has become clear that models with explicit representation of single ion-channel states are required. In the Hodgkin–Huxley formulation, the gating parameters (e.g. m , h) do not represent specific kinetic states of ion channels. It has also become apparent that the Hodgkin–Huxley formulation is not sufficient to describe various aspects of channel behavior. One such aspect is the inactivation of the Na^+ channel, which has a greater probability of occurring when the channel is open (Armstrong & Bezanilla, 1977; Bezanilla & Armstrong, 1977). If this is the case, then inactivation depends on activation and the assumption of independent gating that allows us to multiply m^3 and h to compute conductance no longer holds. What we require is a class of models that can accurately represent the dependence of a given transition on the occupancy of different states of the channel. For sodium channel inactivation, the model must account for the dependence of the inactivation transition on the probability that the channel occupies the open state. Markov-type models fit this profile, and are based on the assumption that transitions between channel states depend on the present conformation of the channel, but not on previous behavior. Because the molecular interactions of channels are often state dependent, Markov model transitions typically represent specific channel movements that have been characterized experimentally. This section describes the application of Markov-type models to simulate such interactions (from Rudy and Silva, 2006).

We begin by describing a simple hypothetical channel with a single open (O) and a single closed (C) state (Fig. 2.7a). The following first-order equations describe the rate of change of occupancy in the closed and open states :

$$\frac{dC}{dt} = -\alpha \cdot C + \beta \cdot O$$

$$\frac{dO}{dt} = \alpha \cdot C - \beta \cdot O$$

where O and C are the probabilities that the channel resides in the open or closed state; α and β are voltage dependent transition rates (ms^{-1}) between these states.

In addition to activation, many channels undergo inactivation. A hypothetical four-state model (closed, open, and two inactivated states) with two sets of forward and reverse transition rates is shown in Fig. 2.7b. One set of rates, α and β , describes movement between states where the channel is open (O) or closed (C) (states that are not inactivated), and between the two inactivated states I_O and I_C . In the Markov scheme of Fig. 2.7b, these are horizontal transitions. The second set, γ and δ , describes vertical transitions to and from the inactivated states. Channels are only open when the channel is both activated and not inactivated, in state O. If differential equations are used to compute the occupancy of each state they take the following form:

$$\frac{dC}{dt} = \beta \cdot O + \delta \cdot I_C - (\alpha + \gamma) \cdot C$$

$$\frac{dO}{dt} = \alpha \cdot C + \delta \cdot I_O - (\beta + \gamma) \cdot O$$

$$\frac{dI_C}{dt} = \beta \cdot I_O + \gamma \cdot C - (\alpha + \delta) \cdot I_C$$

$$\frac{dI_O}{dt} = \alpha \cdot I_C + \gamma \cdot O - (\beta + \delta) \cdot I_O$$

where α , β , γ and δ are transition rates, as shown in Figure 2.7b.

Because each state represents a channel conformation, calculating the occupancies of these states can provide mechanistic insight into how transitions within the channel itself govern its behavior and participation in the AP. For example, channels that move during depolarization from C to I_C to I_O are not available to conduct current and do not participate in the AP. In contrast, channels that arrive at I_O through O are available to

conduct current while occupying the open state and have an effect on the AP. Thus, the Markov formulation can be used to relate AP morphology and properties to specific kinetic states of ion channels and the transitions between them during the different AP phases.

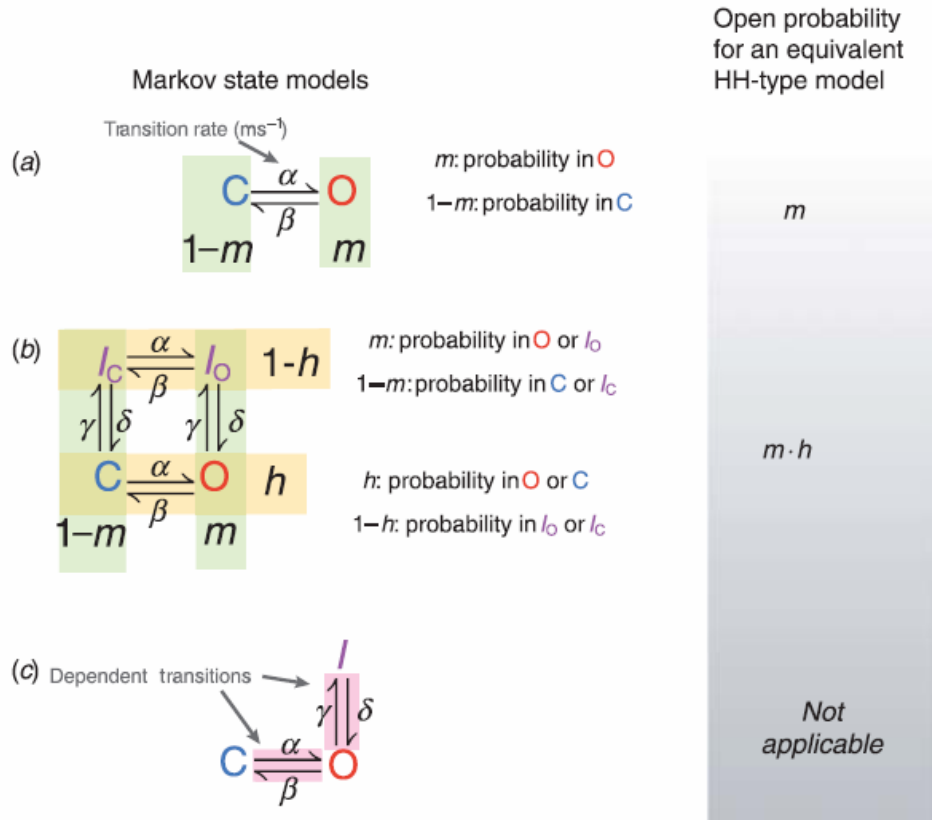


Figure 2.7: Examples of Markov and equivalent Hodgkin–Huxley (HH) models of ionic currents. (a) A two state closed (C) – open (O) model with α and β as forward and reverse transition rates. In the equivalent HH-type formulation, current activation is described by a single gating variable, such as m . (b) A four-state model with two independent transitions. C, Closed; O, open; I_C , closed-inactivated; I_O , open-inactivated. The transition rates α , β between I_C and I_O and between C and O are identical, as are transition rates γ , δ between C and I_C and between O and I_O . Thus activation and inactivation transitions are independent in this model. Independent transitions are readily modeled using the HH formulation. The probability for current activation is m and the probability that it is not inactivated is h ; the open probability is $m \cdot h$. (c) A three-state model with dependent transitions from C to O and O to I. There is no HH equivalent because of the dependent transitions.

When using Hodgkin–Huxley type formulations, the occupancy for each state is not explicitly calculated. Instead, these models assume independent gating, an assumption that improves computational efficiency, which was certainly necessary in 1952 when the Hodgkin–Huxley model was published. In the Markov model of Fig. 2.7b the vertical transitions (C to I_C and O to I_O) have identical transition rates (α and β). This implies that channel inactivation can be represented by a single gate. Similarly, the horizontal transition rates between I_C and I_O are identical to the transition rates between C and O, and can be represented by a single gate. Horizontal movement from [C, I_C] to [O, I_O] represents channel activation; we can assign an activation gate m to describe these transitions. Similarly, we assign a second gate, h , to the inactivation process. Because the rates of inactivation transitions from C or O are identical, inactivation does not depend on the position of the activation gate (i.e. whether it is in the C or O position). The probability that the channel is in C or in O is h , and the probability that the channel is in O or in I_O is m . Because the gates are independent, the open probability (O) is calculated as their product ($m h$). This expression is the same as would have been derived for the Hodgkin–Huxley formulation. Thus, under the assumption of independent gating the Markov formalism and the Hodgkin–Huxley formalism are interchangeable.

However, experiments have shown that typically channel activation and inactivation processes are not independent, but coupled. A simple version of activation and inactivation coupling, in a hypothetical channel, is shown in Fig. 2.7c. In this scheme, channel inactivation can only occur from the open state, and channel activation and inactivation do not involve independent transitions (such as the independent movement of several voltage sensors). Therefore, the state-to-state transitions are dependent, the assumption of independent gating is no longer valid, and the Hodgkin–Huxley formalism in terms of gating variables can not be applied ; each state must be described individually by a differential equation:

$$\frac{dC}{dt} = \alpha \cdot C - \beta \cdot O$$

$$\frac{dO}{dt} = \alpha \cdot C + \delta \cdot I - (\beta + \gamma) \cdot O$$

$$\frac{dI}{dt} = \gamma \cdot O - \delta \cdot I$$

where α , β , γ and δ and d are transition rates, as shown in Fig. 2.7c.

The Markov models compute occupancy of the channel in its various kinetic states as a function of voltage and time (and possibly other factors such as ligand binding). The channel conducts ions when it occupies its open state (or, in some cases, multiple open states). Therefore, the macroscopic current density through an ensemble of such channels is described by the following equation:

$$I_X = g_{sc,x} \cdot n \cdot O \cdot (V - E_X)$$

where for an arbitrary channel X, $g_{sc,x}$ is the single channel conductance, n is the number of channels per unit membrane area, O is the probability that a channel occupies the open state, and $(V - E_X)$ is the driving force.

This equation specifically accounts for the fact that current is generated by a population of ion channels that reside in the open state with a probability that depends on time and voltage. This single-channel based formulation of the current density can be incorporated into a model of the AP. Because in this scheme discrete channel states (i.e. open, closed, inactivated) are represented explicitly, the model can be used to describe not only the macroscopic current during the AP, but also the occupancies and transitions of channel states. This approach provides a mechanistic link between the whole-cell AP and the structure/function of ion channels.

The Luo-Rudy phase 2 model (guinea pig)

The dynamic Luo and Rudy model (LRd) was developed on the basis of the first formulation model of the guinea pig ventricular action potential by Luo and Rudy (LR91, Luo and Rudy 1991), inspired by Beeler & Reuter (1977). Figure 2.8 shows the flowchart of the model development.

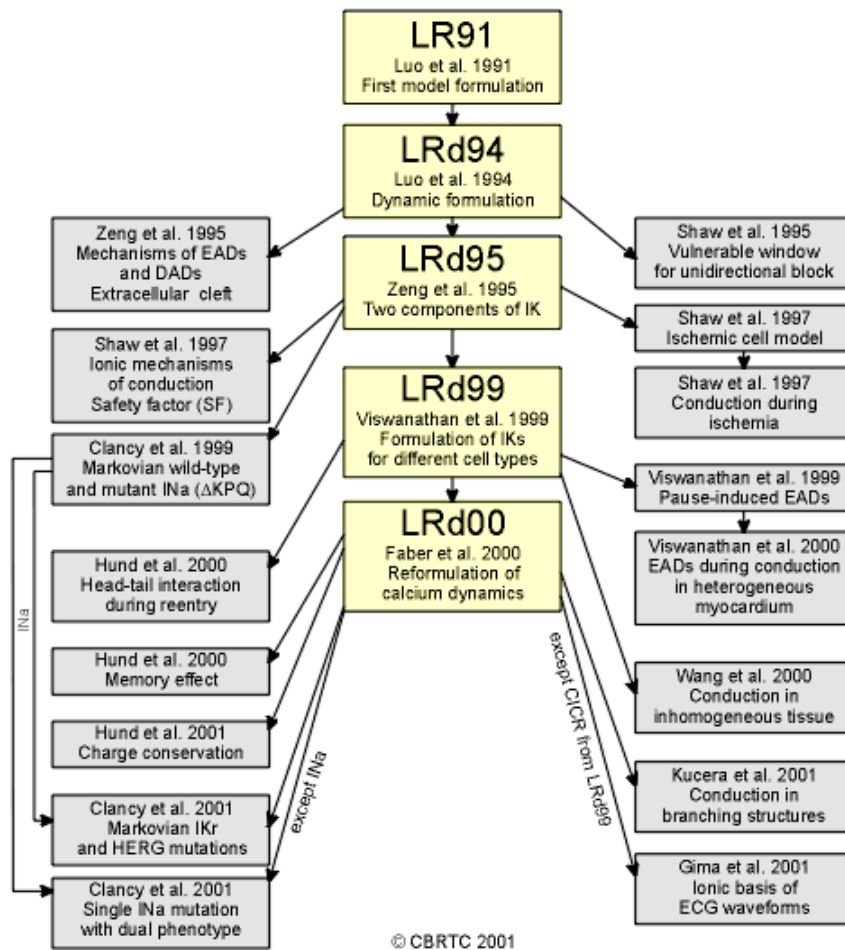


Figure 2.8: Development flowchart of the LRd model. [Figure from <http://rudylab.wustl.edu/research/cell/LRD.htm>]

The LR91 model, shaping the ventricular myocyte as a cylinder of 100 μm in length and 11 μm in radius, implements six transmembrane currents and, like the Beeler-Reuter model, takes into account concentration changes of intracellular Ca^{2+} only. The subsequent LR94 (Luo and Rudy 1994) includes formulation for most of the sarcolemmal currents, pumps and exchangers. It implements cell compartmentalization (myoplasm and sarcoplasmic reticulum). The sarcoplasmic reticulum is functionally and structurally divided into two compartments the junctional sarcoplasmic reticulum (JSR) and the network sarcoplasmic reticulum (NSR). The volume of the SR is 6% of the cell volume, the NSR is the 92% of the SR while the JSR is the 8% of the SR. The mitochondria volume is the 26%, while the myoplasm is the 68% of the cell volume. Ca^{2+} buffers in the myoplasm (troponin, calmodulin) and in the junctional sarcoplasmic reticulum (calsequestrin), and Ca^{2+} -induced release (CICR) are described. Ca^{2+} ions enter the NSR from the myoplasm through the uptake process, they translocate from the NSR to the JSR where they are released into the myoplasm by means of the CICR process. The LR94 model takes into account myoplasmic concentration changes of Na^+ and K^+ as well as Ca^{2+} concentration changes in all three compartments. LR95 (Zeng et al 1995) incorporates two components (rapid and slow) of the delayed rectifier K^+ current (I_{Kr} and I_{Ks}). In the LR99 model (Viswanathan *et al.* 1999), the formulation of the Ca^{2+} release process and I_{Ks} are modified, and the heterogeneity of the ventricular wall is included, by differentiating three different cell types: epi-, mid- and endocardial. Finally, in LR00 (Faber and Rudy 2000, schematic representation in Fig. 2.9) CICR and I_{NaCa} are re-formulated, and the Na^+ -activated K^+ current is added.

The ionic currents are described by Hodgkin and Huxley formalism (i.e. gating model), therefore they change the membrane voltage which subsequently affects ionic gates and currents (Tab. 2.1).

The action potential is calculated by numerically solving the differential equation describing the rate of change of the membrane potential (V), that is

$$C \frac{dV}{dt} = -(I_{CaL} + I_{Na} + I_{NaCa} + I_{Kr} + I_{Ks} + I_{K1} + I_{NaK} + I_{CaT} + I_{To} + I_{Kp} + I_{K(Na)} + I_{p(Ca)} + I_{Nab} + I_{Cab} + I_{st})$$

where I_{st} is the stimuli applied to the cell and C the cell membrane capacity (1 μ F).

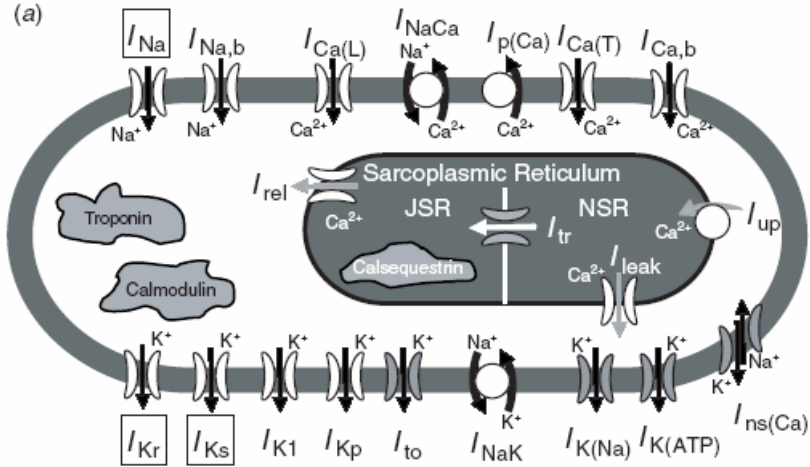


Figure 2.9: Schematic diagram of ventricular cell of Luo-Rudy model. I_{Na} - fast sodium current $I_{Na,b}$ - background sodium current $I_{Ca(L)}$ - L-type calcium current I_{NaCa} - sodium-calcium exchange current $I_{p(Ca)}$ - calcium pump current $I_{Ca(T)}$ - T-type calcium current $I_{Ca,b}$ - background calcium current I_{Kr} - rapid delayed rectifier potassium current I_{Ks} - slow delayed rectifier potassium current I_{K1} - time-independent potassium current I_{Kp} - plateau potassium current (ultra-rapid, I_{Kur}) I_{to} - transient outward current I_{NaK} - sodium-potassium pump current $I_{K(Na)}$ - sodium activated potassium current $I_{K(ATP)}$ - ATP activated potassium current $I_{ns(Ca)}$ - non-specific calcium activated current NSR - network sarcoplasmic reticulum JSR - junctional sarcoplasmic reticulum I_{up} - calcium uptake from myoplasm to NSR I_{tr} - calcium transfer from NSR to JSR I_{leak} - calcium leak from NSR to myoplasm I_{rel} - calcium release from JSR to myoplasm Troponin, Calmodulin, Calsequestrin - calcium buffers

Figure 2.10 shows the main ionic currents that are involved in the AP development. The Na^+ current (I_{Na} , shown on an expanded time scale in the inset) activates rapidly, producing the AP upstroke (phase 0), and rapidly inactivates. The transient outward potassium current (I_{to}) contributes to the notch that follows the upstroke (not shown); the L-type Ca^{2+} current (I_{CaL}) inactivates more slowly than I_{Na} , and incompletely, allowing for the inward Ca^{2+} current to maintain the plateau phase of the AP (Zeng and Rudy, 1995). The I_{NaK} current increases during depolarization and pumps Na^+ ions out of the cell and K^+ ion into the cell. The slow and rapid components of the delayed

Table 2.1 Dependence of current conductance of membrane currents on intra- and extracellular ion concentrations, voltage and time(Luo and Rudy, 1994a; Luo and Rudy, 1994b; Zeng *et al.*, 1995; Viswanathan *et al.*, 1999; Dumaine *et al.*, 1999).

Current	Time independent		Time dependent	
	Voltage	Concentration	Voltage	Concentration
I_{Na}			Activation (m) Inactivation (j,h)	
I_{CaL}	GHK model	$[Ca^{2+}]_i$ $[Ca^{2+}]_o$	Activation (d) Inactivation (f)	Inactivation ($f_{ca}([Ca^{2+}]_i)$)
$I_{Ca(T)}$			Activation (b) Inactivation (g)	
I_{To}			Activation (z) Inactivation (y)	
I_{Kr}	Inactivation (R)	$[K^+]_o$	Activation (X_r)	
I_{Ks}		$[Ca^{2+}]_i$	Activation (X_{s1}, X_{s2})	
I_{Kp}	Activation (K_p)			
I_{NaCa}	GHK model	$[Ca^{2+}]_i$ $[Ca^{2+}]_o$ $[Na^+]_i$ $[Na^+]_o$		
I_{NaK}	Activation (f_{NaK})	$[K^+]_o$ $[Na^+]_i$		
$I_{K(Na)}$	Inactivation (P_{ov})	$[Na^+]_i$		
I_{K1}	Inactivation (K_{1z})	$[K^+]_o$		
$I_{ns(Ca)}$	GHK model	$[Ca^{2+}]_i$ $[Ca^{2+}]_o$		
$I_{p(Ca)}$		$[Ca^{2+}]_i$		
I_{Cab}				
I_{Nab}				

GHK=Goldman-Hodgkin-Katz

rectifier current (I_{Ks} and I_{Kr}) as well as the plateau K^+ current (I_{Kp}) display voltage- and time-dependent properties that contribute to the repolarization of the AP (Yue and Marban, 1988). The I_{NaCa} extrudes Ca^{2+} ions out of the cell and intrude Na^+ ions into the cell mainly in late repolarization phase and diastole, constitutes an additional

inward current. The inward rectifier current (I_{K1}) maintains and stabilizes the resting potential.

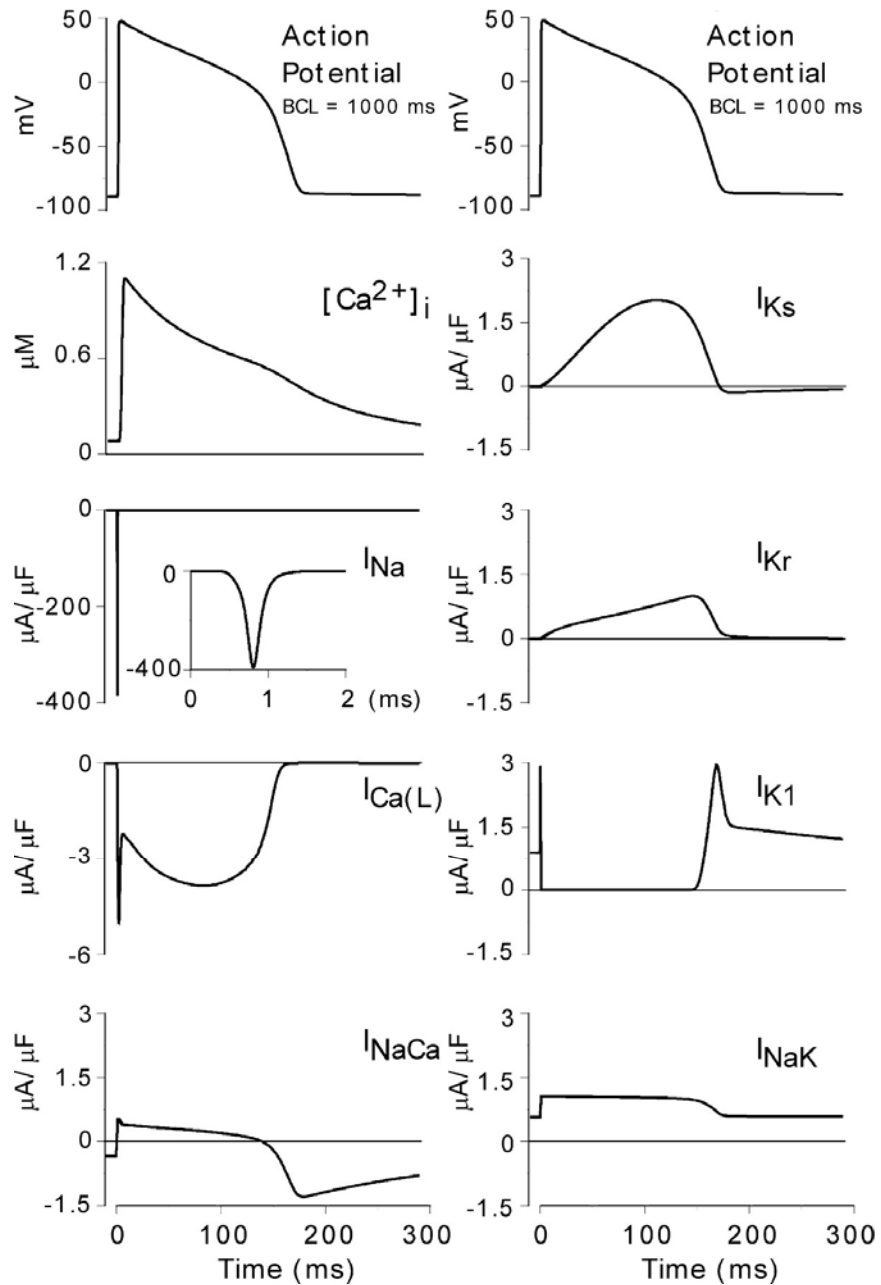


Figure 2.10: Tracing of the major ionic currents that determine the shape of AP.

Upon depolarization, Ca^{2+} entering the cell through the L-type current (I_{CaL}) triggers the release of Ca^{2+} from the JSR (I_{rel}), thus leading to the increase of the cytosolic

calcium concentration (Fig. 2.8, $[Ca^{2+}]_i$). Then, Ca^{2+} ions are removed from the cytosol to the NSR by means of the uptake process (I_{up}) and to the extracellular compartment through the Na^+/Ca^{2+} exchanger. The translocation process of Ca^{2+} from NSR to JSR is mediated by I_{tr} . There is also a small flux (I_{leak}) due to Ca^{2+} ions that move from NSR to myoplasm. The intracellular Ca^{2+} signal also feeds back on the L-type Ca^{2+} channel, mediating inactivation of the current, and therefore plays a role in influencing AP shape.

The complete list of equations for all ionic currents and other processes described in the dynamic Luo and Rudy model of the guinea pig ventricular action potential (Luo and Rudy 1994) and its subsequent releases (Faber and Rudy 2000; Viswanatan *et al.* 1999; Zeng *et al.* 1995) is available on <http://rudylab.wustl.edu/research/cell/LRD.htm>.

The Shannon *et al.* model (rabbit)

In 2004 Bers' group published a new model of rabbit cardiac myocyte Ca^{2+} and Na^+ homeostasis. Their goals were: [i] to track ion influx and efflux such that the model comes to steady-state with a realistic balance of Ca^{2+} fluxes, [ii] to incorporate a form of Ca^{2+} -induced Ca^{2+} release (CICR), [iii] to use parameters which are consistent with laboratory observations, [iv] to be able to simulate basic physiological phenomena when all of the components are combined and [v] to incorporate reasonable compromises to allow the model to be solved numerically on a desktop computer. The model includes the following novel features: [i] the addition of a subsarcolemmal compartment along with the junctional and bulk cytosolic compartments (Fig. 2.11) to allow proteins in the membrane to sense ion concentrations which differ from bulk, [ii] the use of realistic cytosolic Ca^{2+} buffering parameters, [iii] a reversible SR Ca^{2+} pump as suggested by the results of Shannon *et al.* (2000a), [iv] a $[\text{Na}^+]_i$ -dependent Na^+ - Ca^{2+} exchanger which is physiologically regulated by Ca^{2+} as proposed by Hilgemann *et al.* (1992, see also Weber *et al.* 2001) and [v] a model of SR Ca^{2+} release (Fabiato, 1985) including both inactivation/adaptation (Cheng *et al.*, 1995; Stern *et al.*, 1999) and SR Ca^{2+} load dependence (Shannon *et al.*, 2000b). The model data describes Ca^{2+} handling characteristics of the cardiac myocyte and the SR Ca^{2+} load dependence of these processes is accounted for. The model includes a realistic balance of cellular Ca^{2+} removal mechanisms (Bassani *et al.*, 1994; Puglisi *et al.*, 1999), and the phenomena of rest decay and frequency-dependent inotropy. A particular emphasis is placed upon reproducing the non-linear dependence of gain and fractional SR Ca^{2+} release upon SR Ca^{2+} load (Shannon *et al.*, 2000a).

The model is composed of a series of differential equations describing changes in $[\text{Ca}^{2+}]$, $[\text{Na}^+]$, and membrane voltage over time. The AP (Fig. 2.10) is generally reconstructed from individual equations representing sarcolemmal (SL) membrane

channels (Figures 2.11 and 2.12) as in Luo and Rudy (1994a,b) with variations in and additions to individual equations and parameters (see also Puglisi and Bers, 2001).

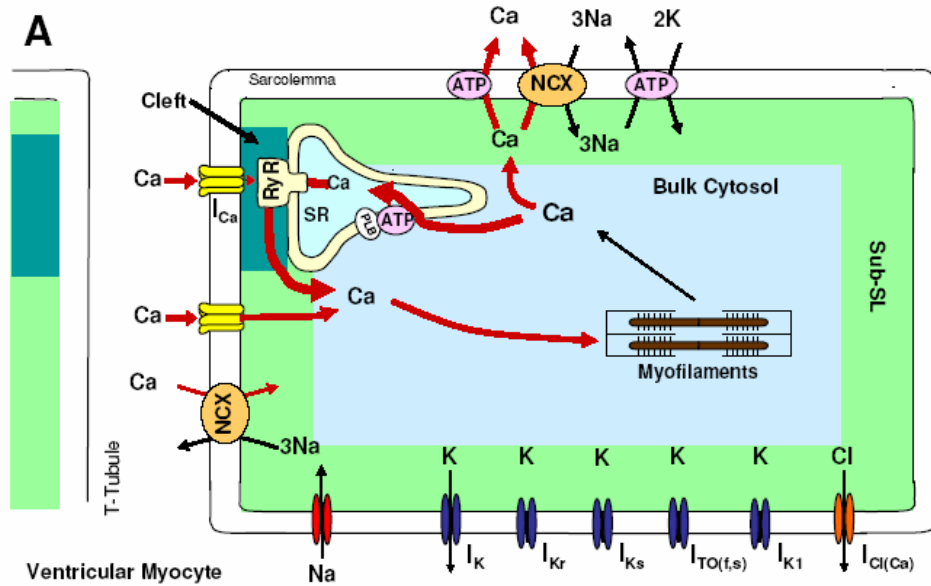


Figure 2.11: A: Diagram of the cell with Ca^{2+} - and Na^+ -dependent components of the model.

Combined, the currents produce a relatively normal AP waveform with duration of 235 ms at 1 Hz (Figure 2.10 and 2.11).

Cellular Structure

The cell (volume 33 pL) is separated into four lumped compartments (Figure 2.11): [i] the SR (Page *et al.*, 1971, 3.5% of the cell volume), [ii] the junctional cleft (Page and Surdyk-Droske, 1979; Soeller and Cannell, 1997, 0.077% assuming 11% of the cell membrane is junctional and that the cleft is 15 nm deep), [iii] the subsarcolemmal space (2% assuming 89% of the membrane is nonjunctional SL and by making the space 45 nm deep), and [iv] the bulk cytosolic space (Page *et al.*, 1971, 65% with the remainder of the volume accounted for by mitochondria). The accessible cleft volume is reduced by an additional third to 0.051% due to the occupation of this space by protein (Soeller and Cannell, 1997).

Na^+ buffers are located only in the junction and SL compartment and are modeled as rapidly binding molecules with the standard Hill equation. Parameters are taken from Bers *et al.* (1986).

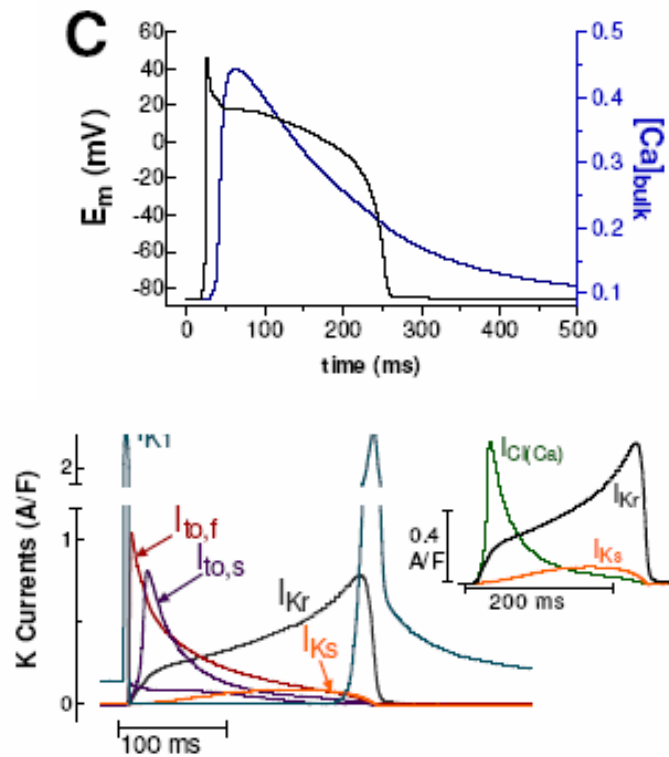


Figure 2.12: (upper panel) An action potential and the accompanying bulk cytosolic Ca^{2+} transient. (lower panel) Relevant K^+ and Cl^- currents.

Ca^{2+} buffers are distributed in each compartment as appropriate (Fig. 2.14). SR Ca^{2+} buffers (primarily calsequestrin) are modeled as rapidly binding molecules. Parameters are from Shannon *et al.* (1997, 2000). Cytosolic Ca^{2+} binding molecules are modeled in a time-dependent manner.

Ca^{2+} Currents

Ca current (Fig. 2.13) is formulated as previously described (Luo and Rudy, 1994a; Luo and Rudy, 1994b; Puglisi and Bers, 2001) with modifications. The formulations are based upon the Goldman-Hodgkin-Katz equation. Ca^{2+} -dependent inactivation was

modified to be calmodulin-dependent (Peterson *et al.*, 1999; Qin *et al.*, 1999). Ninety percent of the channels are located in the junctional cleft membrane (Scriven *et al.*, 2000), as shown in Figure 2.13A.

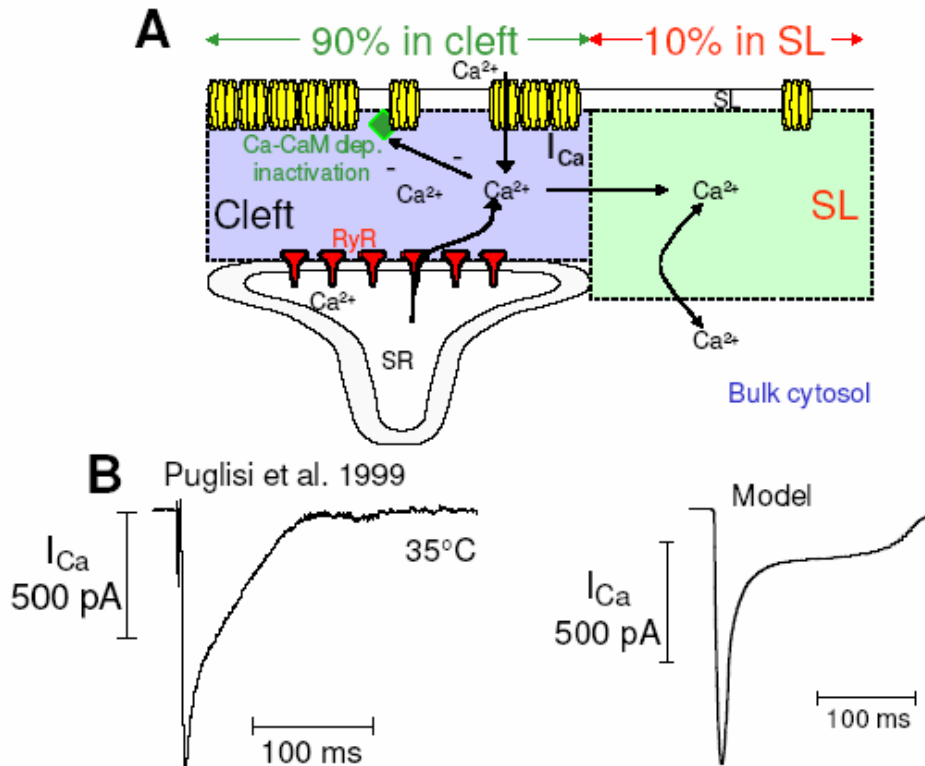


Figure 2.13: A. Diagram of the way in which the L-type Ca²⁺ channel operates. The model includes Ca-dependent inactivation which is Ca-calmodulin (CaM)-dependent. Most of the channels (90%) are in the cleft space (Scriven *et al.*, 2002). B. L-type Ca²⁺ current generated during the AP (right). The currents of Puglisi *et al.* (1999) are shown for comparison (left).

The SL Ca²⁺ leak flux is adjusted to match that calculated from Negretti *et al.* (1993).

The SL Ca²⁺ pump is formulated using the standard Hill equation and approximates cellular estimates of Bassani *et al.* (1994).

The $\text{Na}^+\text{-Ca}^{2+}$ exchanger is formulated essentially as described in Weber *et al.* (2001). The scheme is a general improvement over other models in that it is $[\text{Na}^+]_i$ -dependent and allosterically regulated by Ca^{2+} .

Sarcoplasmic Reticulum Ca^{2+} Transport

The SR Ca pump is a reversible enzyme formulated as in Shannon *et al.* (2000a).

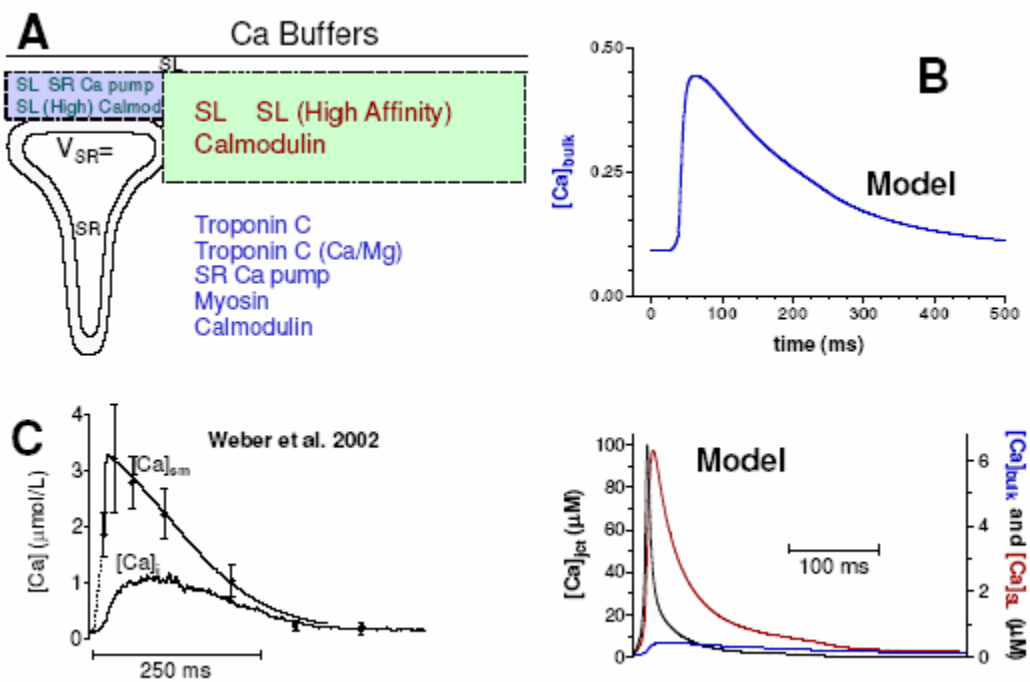


Figure 2.14: A. Ca^{2+} buffers in each compartment. B. Bulk cytosolic Ca^{2+} transient. C. Ca^{2+} transients in each of the three non-SR compartments. Data is compared to that of Weber *et al.* (2002).

The cytosolic Ca^{2+} dependence of the SR Ca^{2+} release channel (RyR) was modeled in a steady-state manner as in Stern *et al.* (1999, see Figure 2.15, based upon Fabiato, 1985 and Cheng *et al.*, 1995) with the addition of a dependence of RyR gating upon $[\text{Ca}^{2+}]_{\text{SR}}$. The model has four states: resting or closed (R), open (O), inactivated (I) and resting inactivated. All of the SR Ca^{2+} release takes place in the junctional

compartment. A passive leak from the SR into the junctional compartment was also added to give a total diastolic leak (passive and diastolic RyR leak) of $\sim 4 \mu\text{M/s}$ (Shannon *et al.*, 2001).

Other Currents

The equations used for the Na^+ and K^+ currents are based upon those of Luo and Rudy (1994a, b) with some modifications (Jafri *et al.*, 1998; Puglisi and Bers, 2001;

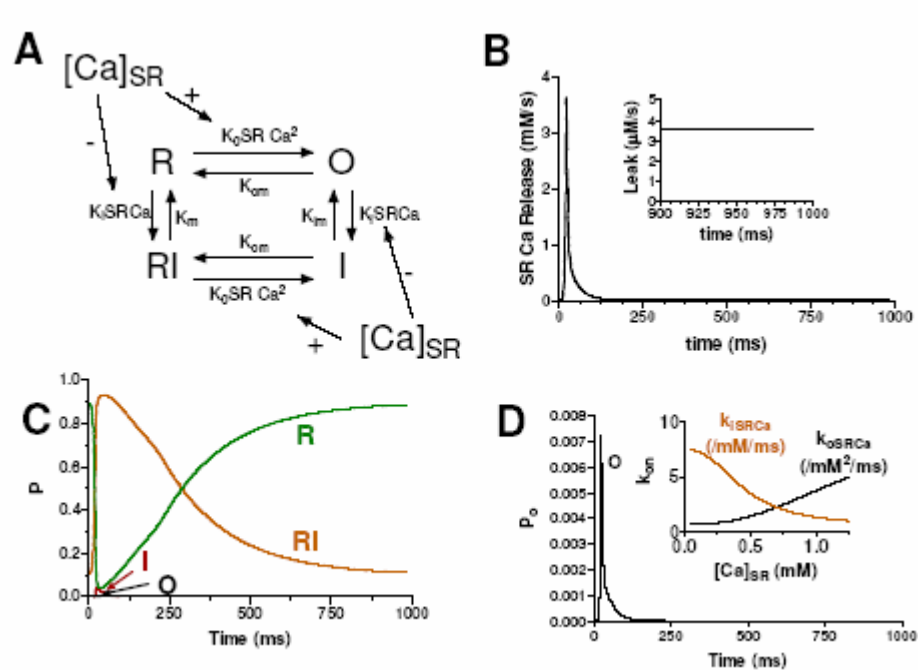


Figure 2.15: A. Markovian state model of the ryanodine receptor. The model was developed from that of Stern *et al.* (1999) with the addition of SR Ca^{2+} load dependence to the binding of Ca^{2+} to the activation and inactivation cytosolic sites. B. SR Ca^{2+} release flux with RyR-dependent SR Ca^{2+} leak (inset). Total leak is equal to this diastolic release plus the passive leak flux (4 $\mu\text{M/s}$). B. Profile of the four channel states over the course of an AP. C. Time-dependent profile of the channel open state with changes in the k_{on} for Ca^{2+} binding with $[\text{Ca}^{2+}]_{\text{SR}}$ (inset).

Bassani *et al.*, 2004). Two notable exceptions are in the I_{Ks} current and the Ca-dependent Cl current (I_{Cl}). I_{Ks} was modeled to resemble the data of Tohse (1990). Cl

currents were added to the model and scaled to approximate those of Zygmunt and Gibbons (1991) and Puglisi *et al.* (1996).

All of the channels and transporters (with the exception of the L-type Ca^{2+} channel) are evenly distributed through out the cell membrane, 89% in the SL compartment and 11% in the junctional membrane.

3 Arrhythmogenic Syndromes and Na⁺ channelopathies

Cardiac arrhythmias are a leading cause of morbidity and mortality. More than 300,000 individuals in the United States die suddenly every year, and in most cases it is assumed that the underlying cause of sudden death is ventricular tachyarrhythmia (Kannel *et al.*, 1987; Willich *et al.*, 1987). Despite their importance, until recently the understanding of the molecular mechanisms underlying life-threatening ventricular tachyarrhythmias was poor. The ability to predict, prevent, and treat these disorders remains a major scientific and medical challenge.

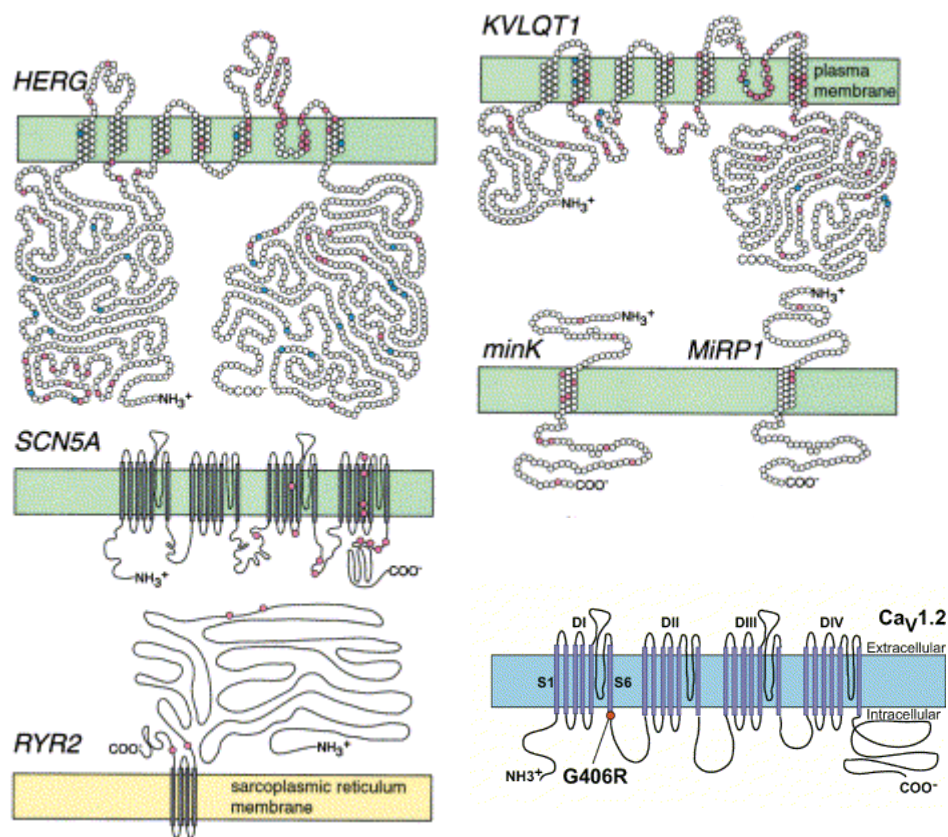


Figure 3.1: Cardiac ion channels and genes associated to arrhythmia susceptibility.

Mutations in cardiac ion channel genes have been shown to contribute to arrhythmia susceptibility. Over the last six years 14 genes related to cardiac arrhythmias were discovered (Fig.3.1). Mutations in *KCNQ1*, *KCNH2*, *SCN5A*, *ANK2*, *KCNE1*, *KCNE2*, *KCNJ2*, *CACNA1*, *CAV3*, *SCN4B* (see Table 3.1) cause Long QT syndrome (LQTS), a cardiac disease characterized by prolongation of the QT interval on the ECG. *SCN5A*, mutations can cause both LQTS and Brugada syndrome (Brugada *et al.*, 1997), that has a distinct electrocardiographic feature of elevation of the ST segment (recently, mutations in *GPDI-L*, *CACNA1* and *CACNA2* gene have been discovered in BrS families). A third familial cardiac arrhythmia, catecholaminergic ventricular tachycardia, is caused by mutations in *RYR2* - the ryanodine receptor gene (Priori *et al.*, 2000), and in *CASQ2* - the gene encoding the Ca²⁺ buffering protein in the lumen of SR. Mutations in *KCNQ1*, *KCNH2* and *KCNJ2* have been associated to Short QT syndrome (SQTS).

In general, arrhythmia susceptibility is more severe in homozygotes than in heterozygotes. Although some familial forms of arrhythmia susceptibility are associated with additional obvious phenotypic abnormalities (e.g., congenital neural deafness in Jervell and Lange-Nielsen syndrome, see Table 3.1), most of these individuals appear grossly normal and go undetected until their first arrhythmia strikes.

Long QT syndrome (reviewed in Ching *et al.* 2006)

Inherited LQTS is an uncommon cardiac disorder that affects 1 to 5,000-10,000 people (Ching *et al.*, 2006). LQTS causes 3,000-4,000 death/year in children and young adults in USA (Wehrens *et al.* 2002).

Long QT syndrome is a genetically heterogeneous disorder caused by various defects in ion channels (see Table 3.1), which result in prolongation of ventricular repolarization (QTc>440-460 ms). LQTS is usually inherited with only approximately 10% of cases being sporadic. Besides the congenital form, acquired LQTS can be caused by exposure to drugs, electrolyte abnormalities and cardiomyopathies. The

inherited LQTS, which was firstly associated to genetic defect in 1991 (Keating *et al.*, 1991), is present in two forms: i) the Romano-Ward syndrome is the most common and is transmitted as an autosomal dominant trait, i.e. the mutant gene is transmitted to 50% of the offspring of an affected individual. Mutations associated to Romano-Ward syndrome has been identified in 10 chromosomes: LQT1 to LQT10; ii) the Jerwell and Lange-Nielsen syndrome is relatively uncommon and is transmitted as an autosomal recessive trait (LQT1 and LQT5). It is associated to deafness (Wehrens *et al.* 2002).

Genetic Bases

The 10 forms of Long QT syndrome (Tab. 3.1) are related to specific ionic channel functional alterations. The pathogenic mutations lead to either a loss of function in potassium channels or a gain of function in sodium and calcium channel. The most common form of LQTS is LQT1 (~50%), followed by LQT2 (45%) and LQT3 (~10%) (Ching *et al.* 2006).

Table 3.1 - Summary of gene information for the various types of LQTS

Type	Locus	Channel	Gene	Transmission	Frequency among genotypes
LQT1	11p15	I _{Ks}	KCNQ1	AD	42–50%
LQT2	7q35	I _{Kr}	KCHN2	AD	45%
LQT3	3p21–24	I _{Na}	SCN5A	AD or M	7–8%
LQT4	4q25–27	Na/Ca	ANK2	AD	Rare
LQT5	21q22	I _{Ks}	KCNE1	AD	3%
LQT6	21q22	I _{Kr}	KCNE2	AD	2%
LQT7	17q23	I _{K1}	KCNJ2	AD	Rare
(Andersen's syndrome)					
LQT8 (Timothy syndrome)	12q13.3	I _{CaL}	CACNA1C	AD or M	Rare
LQT9	3p25.3	I _{Na}	CAV3	AD	Rare
LQT10	11q23.3	I _{Na}	SCN4B	AD	Rare
JLN Type I	11p15	I _{Ks}	KCNQ1	AR	Rare
JLN Type II	21q22	I _{Ks}	KCNE1	AR	Rare

AD: Autosomal dominant; AR: Autosomal recessive; JLN: Jervell–Lange-Nielsen; LQT: Long QT; M: Mosaicism documented.

Phenotype and Symptoms

The congenital form of LQTS is characterized by prolonged QT interval in the surface ECG (Fig. 3.2), increased risk of a typical polymorphic ventricular tachycardia, termed Torsade de Pointes (Fig. 3.2), and high risk of sudden cardiac death (SCD).

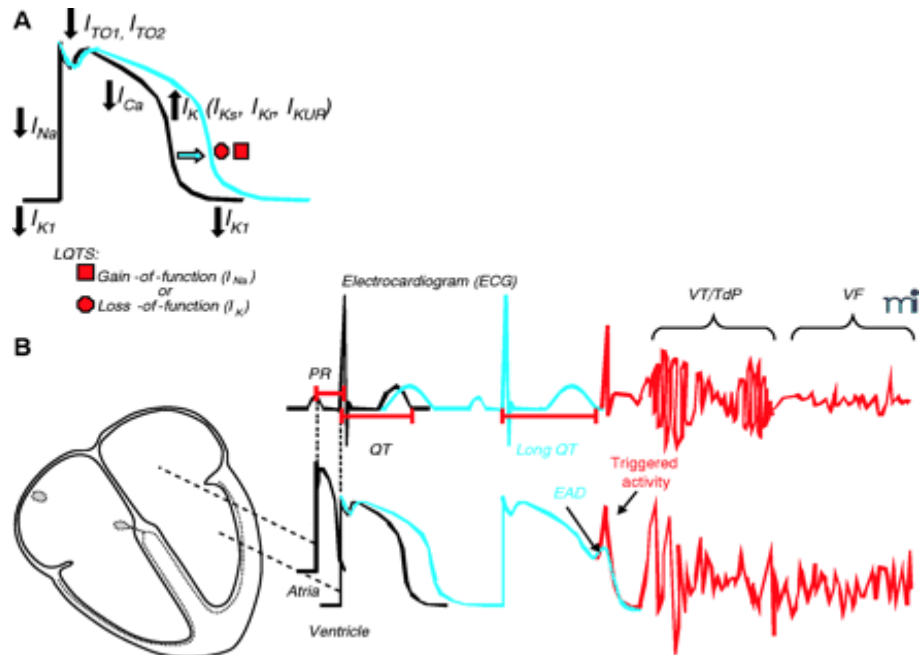


Figure 3.2: Panel A) LQTS is characterized by an action potential prolongation and is associated to mutations that lead to a loss of function in potassium channels or gain of function in sodium and calcium channel. Panel B) Time correspondence between representative ECG and atrial and ventricular action potentials. Prolongation of the ventricular action potential is reflected in the lengthening of the QT interval (blue line). The presence of early afterdepolarizations (EADs) leads to the development of Torsades de Pointes and ventricular fibrillation (red line).

Many patients with LQTS suffer from severe cardiac events, such as syncope and/or SCD, which are most often during physical exercise or emotional stress. However, a great number of patients with LQTS are asymptomatic, and diagnosis is usually incidental based on the ECG. There are some correlations between cardiac events and genotype. Cardiac events occur in LQT1 patients mainly during exercise (62%) being adrenergic stimulation a typical trigger of cardiac events in this LQTS type, and only in 3% of

cases they occur during sleep. The opposite pattern is shown in LQT3 carriers that display 39% of events during sleep and 13% during exercise. LQT3 carriers die mostly during low heart rate condition. LQT2 patients principally encounter events during emotional stress (49%) (Schwartz *et al.*, 2001).

Treatment

As most of cardiac events arise by an increment of sympathetic activity, anti-adrenergic treatments (beta-blockers and if necessary cardiac denervation) are recommended. Implantable cardioverter defibrillator (ICD) is indicated for patients with a high recurrence of cardiac events. However, responsiveness to pharmacotherapy also correlates with genotype, as beta-blocker seems to be less effective in LQT3 patients (Wehrens *et al.* 2002), while they are effective for LQT1 and LQT2 patients. In patients in which anti-adrenergic therapies are not effective genetic specific intervention may be adopted, for example sodium channel blockers assumption in LQT3 carriers or oral potassium supplement in LQT2 patients (Etheridge *et al.* 2003, Bloise *et al.* 2002).

Multiple mutations

Recently, molecular screenings showed that, within LQTS families, some individuals may carry more than a single mutation and the presence of compound mutations is more frequent than expected (Schwartz *et al.* 2003, Westenskow *et al.* 2004). These studies showed interesting genotype-phenotype correlations, being striking the differences in the clinical manifestations of the carriers of compound mutations and their family members carriers of a single mutation only. Symptoms as syncope and cardiac arrest are observed almost in all carriers of compound mutations but in only a small percentage of patients with only one mutation.

There is considerable variation in the clinical presentation of LQTS, ranging from no symptoms to cardiac arrest , even among members of the same family. Depending on the genetic defect, there are differences in the age of onset, severity of symptoms, and number of cardiac events and triggers. With advances in gene technology, it is now

feasible to perform genetic testing for LQTS, especially for those with family history. Identification of the mutations will lead to better management of symptoms and more targeted treatment, hopefully resulting in a reduction of mortality and cardiac events.

Brugada syndrome (reviewed in Shimizu 2005)

Brugada Syndrome (BrS) is responsible for 4% to 12% of all sudden cardiac deaths and nearly 20 % of deaths in patients with structurally normal heart. The incidence of the disease is on the order of 5 per 10,000 subjects and it is one of the leading cause of death of men under the age of 40 in regions (South Asia) where the syndrome is endemic (Antzelevitch *et al.* 2003).

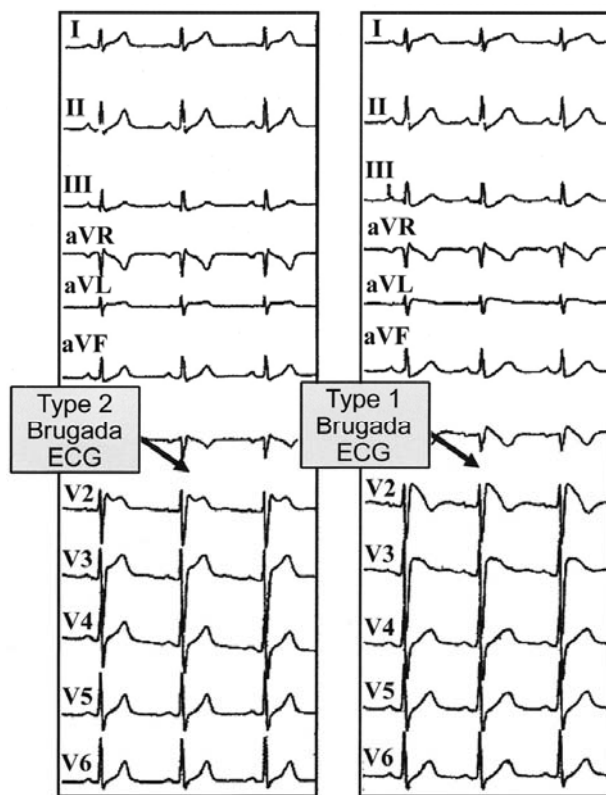


Figure 3.3: Type 2 ECG (not diagnostic) displaying a saddleback-type ST-segment elevation is observed in V2; diagnostic Type 1 ECG, which consists of a coved-type ST-segment elevation

Genetic Bases

In 1998, Chen and co-workers identified the first mutation leading to BrS in *SCN5A*, the gene encoding the alpha subunit of the Na⁺ channel (Chen *et al.*, 1998). *SCN5A* mutations account for only 18-30% of clinically diagnosed BrS patients at present, and more than 2/3 of BrS patients cannot be genotyped, suggesting the existing of genetic heterogeneity (Shimizu *et al.*, 2005). Recently, mutations in *GPD1-L* (London *et al.*, 2006), *CACNA1* and *CACNA2* gene have been discovered in BrS families

Phenotype

Brugada syndrome is characterized by ST-segment elevation in the right precordial leads (V₁-V₃) and episodes of ventricular fibrillation (VF) in absence of structural heart disease. Cardiac events due to VF often occur at night or during sleep as a form of sudden unexpected nocturnal death or syncope in approximately 70-80% of patients with BrS. Two specific types of ST segment elevation, coved and saddleback, are observed in this syndrome, the former of which is reported to relate to a higher incidence of VF and sudden cardiac death. However, the coved type ST segment elevation is more frequently recognized just before and after episodes of VF (Fig. 3.3).

Drug challenge

The electrocardiographic features of BrS are dynamic and often concealed. Sodium channel blockers amplify or unmask ST segment elevation, and are used as diagnostic tool in latent BrS with transient or no spontaneous ST segment elevation. Class IC sodium channel blockers (flecainide, pilsicainide, ecc.) and ajmaline (class IA) produce the most pronounced ST segment elevation. In addition to sodium channel blockers, many agents and conditions are reported or expected to unmask Brugada phenotype, a coved type ST segment elevation. As an example, calcium channel blockers (verapamil, etc.) decrease L-type calcium current (I_{CaL}) and are expected to induce BrS-type ST segment elevation. In addition, psychotropic agents, K⁺ channel openers, febrile state (hyperthermia), electrolyte disturbances, etc. are reported to amplify ST segment elevation.

Treatment

Among symptomatic patients, individuals experiencing aborted cardiac arrest are at high risk for recurrence (69%) while those who display spontaneous BrS electrocardiographic features and experience syncope have a recurrence of 19%. Asymptomatic patients at higher risk are those showing Brugada signs spontaneously, those in which BrS signs are provoked by drugs are at very low risk (Antzelevitch *et al.* 2003). ICDs are often recommended in patients experiencing cardiac arrest.

Na⁺ CHANNELOPATHIES (reviewed in Clancy and Kass 2005)

Voltage-gated Na⁺ channels cause the rapid depolarization that marks the rising phase of APs in the majority of excitable cells. At negative membrane potentials, channels typically reside in closed and available resting states that represent a nonconducting conformation. Depolarization results in activation of the voltage sensors and channel opening, allowing for ion passage. Subsequent to channel activation, channels enter inactivated states that are nonconducting and refractory. Repolarization is required to alleviate inactivation with isoform-specific time and voltage dependence.

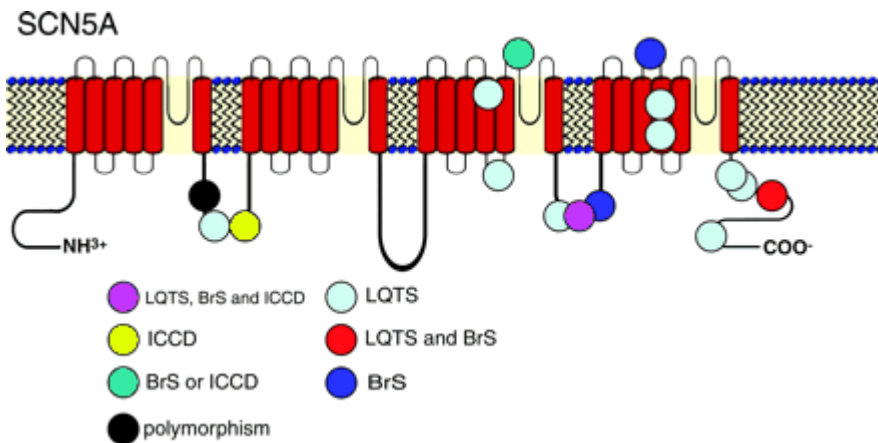


Figure 3.4. The cardiac Na⁺ channel is involved in multiple arrhythmogenic syndromes. Shown is a schematic representation of the voltage-gated cardiac Na⁺ channel (Na_v1.5), in which mutations can lead to the LQT3 form of long QT syndrome (LQTS), Brugada syndrome (BrS), and isolated cardiac conduction disorder (ICCD) or mixed combinations of disorders.

SCN5A encodes the cardiac isoform (Na_v1.5) of the voltage-gated Na⁺ channel, which is a heteromultimeric protein complex consisting of four heterologous domains, each containing six transmembrane spanning segments. Positive residues are clustered in the S4 segments and comprise the voltage sensor (Kontis and Goldin 1997, Stuhmer *et al.* 1989) (Fig. 3.4). The intracellular linker between domains three and four, DIII/DIV, includes a hydrophobic isoleucine-phenylalanine-methionine (IFM) motif, which acts as a blocking inactivation particle and occludes the channel pore, resulting

in channel inactivation subsequent to channel opening (Stuhmer *et al.* 1989). Recent studies also suggest a role for the COOH terminus in channel inactivation in brain and cardiac isoforms (Nav1.1 and Nav1.5, respectively) (Cormier *et al.* 2002, Mantegazza *et al.* 2001). The S5 and S6 transmembrane segments of each domain comprise the putative channel pore and associated ion selectivity filter (Sun *et al.* 1997).

There has been renewed interest in the study of voltage-gated Na⁺ channels since the recent realization that genetic defects in Na⁺ channels can underlie idiopathic clinical syndromes (Goldin 2001). Interestingly, all Na⁺ channel-linked syndromes are characterized by episodic attacks and heterogeneous phenotypic manifestations.

Many mutations in the cardiac voltage-gated Na⁺ channel isoform Nav1.5 have been shown to underlie several disease phenotypes including the Long QT Syndrome type 3 (LQT3), Brugada syndrome (BrS), and isolated cardiac conduction disease (ICCD). Mutations underlying these clinical syndromes are scattered throughout the channel, as shown in Figure 3.4.

Genetic defects in membrane ion channels can disrupt the delicate balance of dynamic interactions between the ion channels and the cellular environment, leading to altered cell function. As ion-channel defects are typically studied in isolated expression systems, away from the cellular environment where they function physiologically, a connection between molecular findings and the physiology and pathophysiology of the cell is rarely established. Computational modeling has proven useful to analyze the consequences of mutations on cardiac electrophysiology. Incorporating the results of electrophysiological characterization of mutant ion channels in a model makes it possible to investigate the alterations of channel kinetic properties due to genetic mutations. Computer models of the mutant currents allow to simulate the effects of mutations on the action potential morphology (Clancy *et al.*, 2002a; Clancy *et al.*, 2002b; Clancy *et al.*, 1999; Vecchietti *et al.*, 2007), in order to fill the gap between the genotype and the phenotype and to gain new insights into the underlying mechanisms of cardiac arrhythmias.

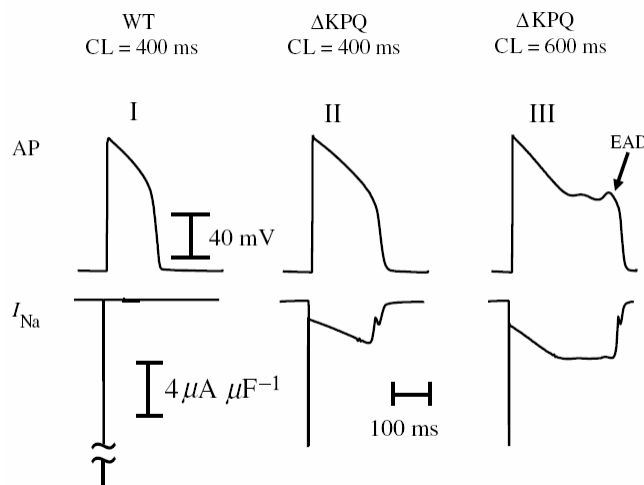


Figure 3.5. The effect of Δ KPQ mutation on the whole cell action potential. Wild-type (WT) Na⁺ channels activate and then rapidly enter nonconducting inactivation states where they remain throughout the action potential plateau (I). The Δ KPQ mutation results in a fraction of channels that transiently fail to inactivate resulting in persistent Na⁺ current (I_{Na}) during the action potential plateau (II), which prolongs the action potential duration (compare with WT on left). With slowing of the pacing rate, an EAD occurs (III). [Modified from Clancy and Rudy (1999).]

Long QT Syndrome

In general, Na⁺ channel-linked LQTS stems from mutation-induced disruption of channel inactivation, as was originally identified in the Δ KPQ mutation, a three-amino acid deletion in the intracellular linker between domains III and IV of NaV1.5. This motif is known to be critical for fast inactivation of the channel. Indeed, it was observed experimentally in expression systems that this structural defect leads to two modifications of channel function: 1) faster activation and recovery from inactivation, and 2) transient complete failure of inactivation in some of the channels; the mutation results in persistent noninactivating current (Chandra *et al.* 1998). The noninactivating component of I_{Na} acts to prolong the plateau of the AP and may allow for the development of arrhythmogenic triggered activity, referred to as early afterdepolarizations (EADs), as it was suggested by the simulation study of Clancy and Rudy (1999, Fig. 3.5). They simulated the modifications of Na⁺ channel gating by the

Δ KPQ mutation in a Markov model of I_{Na} , and they introduce the current model in the LRd ventricular cell model paced at various rate. During an AP the additive effects of channel reopenings in the background mode and bursting in the burst mode of Δ KPQ result in a late component of macroscopic current during the plateau phase. In the simulations, the APD of the mutant cell is markedly prolonged, and with slowing of the pacing rate, a secondary depolarization occurs before the completion of ventricular repolarization (EAD). In the context of arrhythmogenesis, regional delays of the repolarization process by AP prolongation and/or EADs can create spatial nonuniformities of excitability (“dispersion of repolarization”) that provide a substrate for the development of unidirectional block and reentry. Moreover, under certain conditions EADs can elicit an excitatory response that provides the trigger for arrhythmic activity.

While Δ KPQ is one example of altered gating, several recent studies suggest that mutation-induced gain of function in cardiac I_{Na} can exist in at least three distinct forms (Fig. 3.6). The most common is due to transient inactivation failure as in Δ KPQ, which underlies sustained Na⁺ channel activity over the plateau voltage range (Antzelevitch *et al.* 2000). A second is due to steady-state channel reopening called window current (Chandra *et al.* 1998), because reopening occurs over voltage ranges for which steady-state inactivation and activation overlap. A third original mechanism was demonstrated in channels containing the I1768V mutation, which does not result in an obvious gain of channel function (Clancy *et al.* 2003, Groenewegen *et al.* 2003). However, under nonequilibrium conditions during repolarization, channel reopening results from faster recovery from inactivation at membrane potentials that facilitate the activation transition (Clancy *et al.* 2003). Mutation-induced faster recovery from inactivation results in channels that reopen during repolarization, and the resulting current amplitude rivals that of bursting channels. Simulations have demonstrated that late current due to channel reopening causes severe prolongation of the AP plateau and arrhythmic triggers (Clancy *et al.* 2003).

Recently, several studies have focused on the role of the intracellular COOH terminus of the Na⁺ channel in voltage-gated Na⁺ channel inactivation. Notably, gene defects associated with LQT3 located in this region disrupt inactivation in a manner similar to mutations that affect the DIII/DIV linker inactivation gate. LQT3 mutations in this region (E1784K, 1795insD, Y1795C) evoke small, sustained currents similar to Δ KPQ (An *et al.*, 1998, Rivolta *et al.*, 2001, Veldkamp *et al.*, 2000).

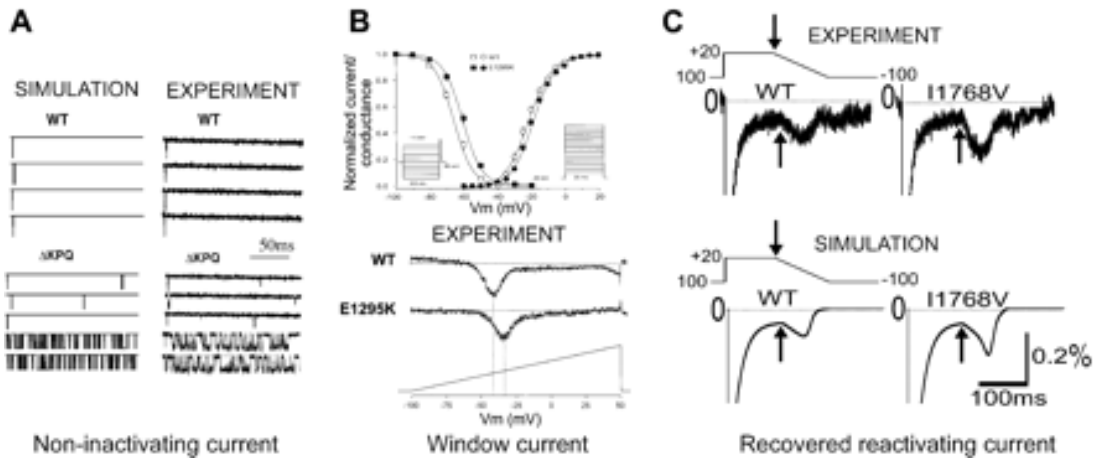


Figure 3.6: Na⁺ channel-linked LQTS mutations result in a gain of function and can stem from at least three distinct mechanisms. A: the most common is due to transient inactivation failure as in Δ KPQ, readily seen in the single-channel gating, which underlies sustained Na⁺ channel activity over the plateau voltage range. Wild-type (WT) and Δ KPQ mutant channels are shown in the top four and bottom five traces, respectively. Mutant channels exhibit two distinct forms of abnormal gating compared with WT. [From Clancy and Rudy 2001.] B: the E1295K mutation shifts the voltage dependence of steady-state channel reopening called window current into voltages relevant during the action potential plateau. Reopening occurs over voltage ranges for which steady-state inactivation and activation overlap (top). Window current is easily observable by implementing a slow positive voltage ramp. [From Abriel *et al.*, 2001.] C: a third original mechanism was demonstrated in channels containing the I1768V mutation, which does not result in an obvious gain of channel function. However, under nonequilibrium conditions during repolarization, channel recovery from inactivation states that occur subsequent to opening is faster at membrane potentials that facilitate the activation transition. Mutation induced faster recovery from inactivation results in channels that reopen during repolarization and that the resulting current amplitude rivals that of bursting channels. Figure from Clancy *et al.*, 2003.

Brugada Syndrome

Unlike LQTS that is associated with a gain of Na⁺ channel function, loss of Na⁺ channel function underlies the BrS phenotype. Mutations in Na_v1.5 have been linked to BrS and characteristically cause a reduction in I_{Na} (Grant *et al.*, 2002). This reduction in I_{Na} has been shown to occur by several mechanisms in BrS, including reduced rates of recovery from inactivation, faster inactivation subsequent to channel opening, and protein trafficking defects (Dumaine *et al.*, 1999; Rivolta *et al.*, 2001; Veldkamp *et al.*, 2000; Wang *et al.*, 2000).

Isolated Cardiac Conduction Disease

ICCD is observed on the ECG in a widening of the QRS complex, indicating delays in ventricular excitation (Grant *et al.* 2002). They are associated with bradycardia and may manifest as syncope. Mutations in NaV1.5 have been shown to cause ICCD and typically result from a depolarizing shift of the Na⁺ channel activation curve (Grant *et al.*, 2002). This shift most likely results from a reduction in the rate of channel activation or decreased channel sensitivity to the voltage required for activation. Mutant channels may require a greater amount of time to reach depolarized membrane potentials at which the maximum I_{Na} occurs. The lag in activation of ICCD mutant Na⁺ channels would result in a reduction of the AP upstroke velocity, a primary determinant of conduction velocity.

Mutations Can Result in Multiple Phenotypes

The relationship between genetic mutations and clinical syndromes is becoming increasingly complex as the revelation of novel mutations suggests paradoxical phenotypic overlap or exclusivity. Recently, at least four loci in the cardiac sodium channel have been identified where the same mutation can result in different disease phenotypes. An insertion of an aspartic acid residue (1795insD) in the COOH terminus of Na_v1.5 showed simultaneous LQT3-like and Brugada-like clinical manifestations in the same patients (Veldkamp *et al.*, 2000). Mutant 1795insD Na channels expressed in mammalian cells exhibit a shift in steady-state inactivation to negative potentials (with

unaltered activation), disrupted fast inactivation, persistent I_{Na}, augmented slow inactivation and delayed recovery from inactivation. The authors suggested that the net effect of both changes would be heart rate-dependent. At low frequencies, impaired fast inactivation and persistent I_{Na} outweigh the slowed recovery from inactivation because of long lasting diastolic intervals. This would favor AP prolongation consistent with LQT3 phenotype. However, at higher heart rates, the shorter recovery interval hindering complete Na⁺ channel recovery results in a reduction of Na⁺ channel availability and shortens AP duration. The consequent loss of Na⁺ channel function would then slow propagation and increase dispersion of repolarization, generally considered to underlie Brugada Syndrome. This dual scenario was also demonstrated by computational simulations that incorporate the measured altered Na⁺ channel gating properties (Fig. 3.7; Clancy and Rudy, 2002).

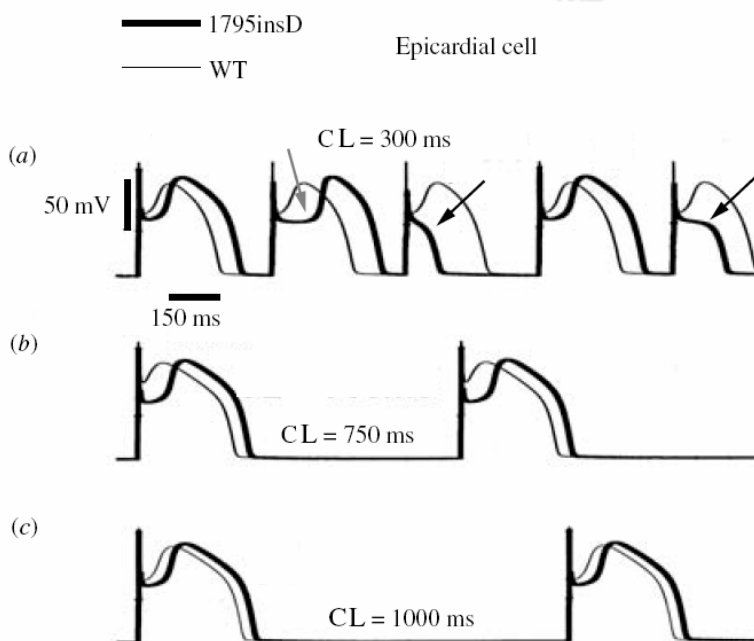


Figure 3.7: Rate-Dependent Effect of 1795insD on Epicardial Cell AP. At fast pacing (A) the AP morphology alternates between “loss of dome” (black arrows) and a prolonged notch (“coved dome”, gray arrow). At intermediate rate (B) the AP has a coved-dome morphology on every beat. At slow rate (C) WT and mutant AP morphologies are similar. Figure from Clancy & Rudy, 2002.

Additionally, mutation of the same residue to a histidine (Y1795H) or cysteine (Y1795C) results in BrS and LQTS, respectively, indicating the proximal region of the COOH terminus as a potentially important structure in Na⁺ channel function (Rivolta *et al.*, 2001). We investigated the effects of the two mutations by means of numerical modelling of ventricular action potential (Chapter 4, Vecchietti *et al.*, 2007). A Markov model capable of reproducing wild type as well as mutant I_{Na} was previously identified and was included into the Luo-Rudy ventricular cell model for AP simulation. Y1795C prolonged AP in a rate dependent manner and early afterdepolarizations (EADs) appeared during bradycardia. Y1795H resulted in minimal changes in the APs.

A mixed I_{Na} phenotype was reported in a mutant Na⁺ channel (Cormier *et al.*, 2002) with the C-terminal truncated at S1885 exhibiting negative shifted reduced channel availability (unchanged activation) and a tenfold increase in the fraction of channels that fail to inactivate (slowed inactivation).

The mutation of a glycine to arginine (G1406R) DIII-S5 linker region to DIII-S6 resulted in either BrS or ICCD in several families (Kyndt *et al.* 2001). Expression studies resulted in no current, although no trafficking errors were detected, suggesting a potential modifier gene or genes affecting NaV1.5 function.

The deletion of a lysine (Δ K1500) in the III-IV linker of NaV1.5 is associated with BrS, LQTS, and ICCD (Grant *et al.* 2002).

LQTS is typically associated with gain-of-function Na⁺ channel mutations while BrS and ICCD are typically associated with loss-of-function resulting in reduced I_{Na}. The fact that single mutations can underlie disparate phenotypes begs the question of underlying mechanisms. How can a single mutation simultaneously result in seemingly paradoxical syndromes (i.e., gain-of-function LQTs and loss-of-function BrS)?

The Heterogeneous Myocardial Substrate

One explanation may stem from the intrinsic heterogeneity of the underlying myocardial substrate with which mutant Na⁺ channels interact. The ventricular myocardium is comprised of at least three distinct cell types referred to as epicardial,

midmyocardial (M), and endocardial cells, which exhibit distinct electrophysiological properties (Liu *et al.* 1993). Epicardial cells display a characteristic spike and dome morphology due to large transient outward K⁺ current (I_{to}) and short APD resulting from a high density of the slowly activating component of the delayed rectifier K⁺ current (I_{Ks}) (Liu *et al.* 1993). Mutations that act to reduce I_{Na} in the presence of large repolarizing currents (I_{to} and I_{Ks}) may result in premature plateau repolarization (BrS phenotype) and APs with distinctive triangular morphology or in APs with prominent coved domes (Liu *et al.* 1993). I_{to} and I_{Ks} are smaller in M cells and are unable to overwhelm the mutation induced by reduced I_{Na}. Selective loss of the AP plateau in epicardial cells results in dispersion of plateau potentials across the ventricular wall. This gradient generates ST segment elevation on the ECG, which is a diagnostic indicator of BrS (Yan and Antzelevitch 1999). Clinically, ST segment elevation is observed in right precordial leads of BrS patients, consistent with the large I_{to} density in right ventricular epicardium (Yan and Antzelevitch 1999, Figure 3.7, left). In M cells, the noninactivating component of I_{Na}, in the presence of smaller repolarizing currents, acts to prolong the plateau of the AP and may allow for the development of arrhythmogenic EADs (LQT phenotype, Figure 3.7, right). APD prolongation is reflected in a prolonged QT interval on the ECG, indicative of the LQTS.

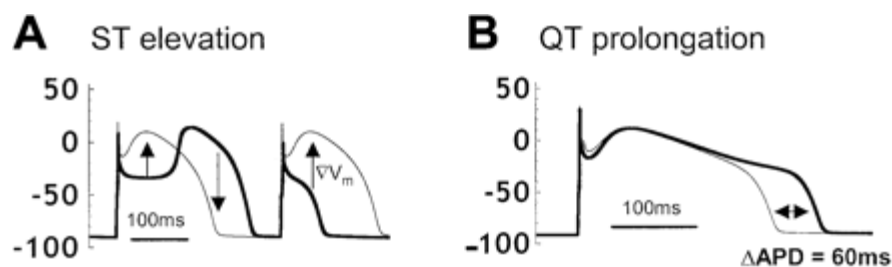


Figure 3.7. Cellular electrical abnormalities manifest as clinical syndromes. A: mutation-induced changes in epicardial action potential (AP) morphologies (thick line) cause dispersion of plateau potentials and a voltage gradient (∇V_m , arrows) (WT, thin line). This gradient will manifest on the ECG as ST segment elevation, indicative of BrS. B: mutations may prolong AP duration (APD) in myocardial (M) cells (thick line) compared with WT (thin line). The delay in repolarization ($\Delta APD = 60$ ms) is reflected as QT prolongation on the ECG, a hallmark of LQTS. (Modified from Clancy CE and Kass RS. *J Clin Invest* 110: 1075–1077, 2002).

Polymorphisms May Increase Susceptibility to Drug-Induced Arrhythmias

Within the context of arrhythmia, pharmacogenomic considerations are important to determine the potential for genetic heterogeneity to directly affect drug targets and interfere with drug interactions. Mutations or polymorphisms may directly interfere with drug binding or can result in a physiological substrate that increases predisposition to drug-induced arrhythmia.

Use-dependent block of voltage-gated Na⁺ channels results in preferential reduction of current at fast pacing rates (Liu et al 2002). This property is potentially useful in reducing runaway excitation by reducing Na⁺ current and thereby decreasing the likelihood of reexcitation. The unpredictable outcomes of pharmacological intervention with mutant channels must be investigated to develop appropriate treatments, since a Na⁺ channel blocker may be ineffective, or overly effective, in interacting with mutant channels.

Genetic mutations or polymorphisms may affect drug binding by altering the length of time that a channel resides in a particular state. For example, the epilepsy associated R1648H mutation in Na_v1.1 reduces the likelihood that a mutant channel will inactivate and increases the channel open probability (Lossin *et al.* 2002). Hence, an anticonvulsant that interacts with open channels will have increased efficacy, while one that interacts with inactivation states may have reduced efficacy. However, even this type of analysis may not predict actual drug-receptor interactions (Liu *et al.* 2002). The I1768V mutation increases the cardiac Na⁺ channel isoform propensity for opening, suggesting that an open channel blocker would be more effective, but in fact, the mutation is in close proximity to the drug-binding site, which may render open channel blockers nontherapeutic (Liu *et al.* 2002).

Local anesthetic molecules such as lidocaine and flecainide block Na⁺ channels and have been used therapeutically to manage cardiac arrhythmias. Despite the prospective therapeutic value of the inherent voltage- and use-dependent properties of channel block by these drugs in the treatment of tachyarrhythmias, their potential has been

overshadowed by toxic side effects. However, Na⁺ channel blockers have proven useful as a diagnostic tool and in treatment of BrS and LQT3 (Brugada *et al.* 2000). Na⁺ channel blockade by flecainide is of particular interest as it had been shown to reduce QT prolongation in carriers of some LQT3 mutations and to evoke ST segment elevation, a hallmark of the BrS, in patients with a predisposition to the disease (Brugada *et al.* 2000). Thus, in the case of LQT3, flecainide has a potential therapeutic application, whereas for BrS it has proven useful as a diagnostic tool. However, in some cases, flecainide has been reported to provoke BrS symptoms (ST segment elevation) in patients carrying LQT3 mutations (Priori *et al.* 2000). Investigation of the drug interaction with these and other LQT3 and BrS linked mutations may indicate the usefulness of flecainide in the detection and management of these disorders and determine whether or not it is reasonable to use this drug to identify potential disease-specific mutations.

In the present study (Chapter 4) the administration of two class IC antiarrhythmic drugs (flecainide and mexiletine) on WT and mutant (Y1795C and Y1795H) was simulated. Flecainide and Mexiletine shortened AP and abolished EADs. Flecainide but not Mexiletine induced APs heterogeneity across the ventricular wall that accounts for the ST segment elevation induced by Flecainide in Y1795H carriers (Vecchietti *et al.*, 2007).

Recent findings revealed the differential properties of certain drugs on mutant and wild-type cardiac Na⁺ channels. One such example is the preferential blockade by flecainide of persistent I_{Na} in the ΔKPQ Na⁺ channel mutant (Nagatomo *et al.* 2000). It was also shown that some LQT-associated mutations were more sensitive to blockade by mexilitene, a drug with similar properties to lidocaine, than wild-type channels (Wang *et al.* 1997). In three mutations, ΔKPQ, N1325S, and R1644H, mexilitene displayed a higher potency for blocking late Na⁺ current than peak Na⁺ current (Wang *et al.* 1997).

Liu *et al.* (2002) found that flecainide, but not lidocaine, showed a more potent interaction with a COOH-terminal D1790G LQT3 mutant than with wild-type channels and a correction of the disease phenotype. The precise mechanism underlying these differences is unclear. Lidocaine has a pKa of 7.6–8.0 and thus may be up to 50% neutral at physiological pH. In contrast, flecainide has a pKa of ~9.3, leaving <1% neutral at pH 7.4. Thus one possibility underlying differences in the voltage dependence of flecainide- and lidocaine-induced modulation of cardiac Na⁺ channels is restricted access to a common site that is caused by the ionized group of flecainide. Another possibility is that distinctive inactivation gating defects in the D1790G channel may underlie these selective pharmacological effects. Indeed, Liu *et al.* recently found mutations that promote inactivation (shift channel availability in the hyperpolarizing direction) enhance flecainide block. Interestingly, their data also showed that flecainide sensitivity is mutation, but not disease, specific (Liu *et al.* 2002).

These studies are important in the demonstration that effects of flecainide segregate in a mutation-specific manner that is not correlated with disease phenotype, suggesting that it may not be an effective agent for diagnosing or treating genetically based disease. The nature of the interaction between pharmacological agents and wild-type cardiac Na⁺ channels has been extensively investigated. However, the new findings of drug action on mutant channels in LQTS and BrS have stimulated a renewed interest in a more detailed understanding of the molecular determinants of drug action, with the specific aim of developing precise, disease-specific therapy for patients with inherited arrhythmias.

4 In silico assessment of Na⁺ channelopathies

Cardiac sodium channel gene (*SCN5A*) mutations are associated with two inherited arrhythmogenic disorders, Long QT syndrome type 3 (LQT3) and Brugada syndrome (BrS). Both syndromes predispose to life threatening ventricular arrhythmias and sudden death that most often occurring during sleep or at rest (Priori *et al.*, 2000; Brugada and Brugada, 1992; Schwartz *et al.*, 2001). However, they present distinctive ECG phenotypes: the hallmark of LQT3 is the prolongation of QT interval (Schwartz *et al.*, 2000a; Priori *et al.*, 2003) whereas BrS typically shows an ST segment elevation in the right precordial leads, often accompanied by right bundle branch block (Brugada and Brugada, 1992). The response to Class I antiarrhythmic drugs in the two diseases is also remarkably different. In BrS Flecainide (Brugada and Brugada, 1992) but not Mexiletine (Shimizu *et al.*, 2000) allows unmasking an overt phenotype, while in LQT3 both Mexiletine (Priori *et al.*, 1996; Schwartz *et al.*, 1995) and Flecainide (Benhorin *et al.*, 2000; Priori *et al.*, 2000) may shorten the QT interval. Functional characterization of mutants has demonstrated that LQT3 is associated with a gain of function mainly caused by a defective current inactivation, while BrS mutations produce a loss of function through a variety of different biophysical mechanisms (Priori *et al.*, 2003). So far, expressions studies in heterologous cell lines have provided critical information for the understanding of the biophysical consequences of mutation at the channel/current level, but they have given little insights into the arrhythmogenic mechanisms that initiate and sustain arrhythmias. In the recent years computer modelling of cardiac excitability has emerged as a most valuable tool to study the effects of mutations on ventricular action potential (Viswanathan and Rudy, 1999; Clancy and Rudy, 1999; Clancy and Rudy, 2001; Clancy and Rudy, 2002).

Here we report the results of in silico experiments concerning two *SCN5A* mutants that have been identified in families with LQT3 (Y1795C) and BrS (Y1795H) (Fig.

4.1). Extensive in vitro characterization of both allelic variants had been previously carried out (Rivolta *et al.*, 2001). The Y1795C mutation exhibited a significant sustained current when expressed in heterologous cell lines. A light maintained current was also observed in Y1795H. In addition, both mutations caused a significant shift of the inactivation process towards negative potentials. In a previous study performed by our research group (Vecchietti *et al.*, 2006), a nine state Markov model was identified to simulate the Na⁺ current in wild-type Na⁺ cardiac channel and the current alterations observed in Y1795C and Y1795H mutant channels. In this model-based study, we analyzed the simulated mutation-dependent AP shape and duration abnormalities and the effects of mexiletine and flecainide on wild-type and mutant APs, in order to gather insights on the electrophysiologic mechanisms underlying the ECG phenotypes and the responses to these drugs observed in LQT3 and BrS patients.

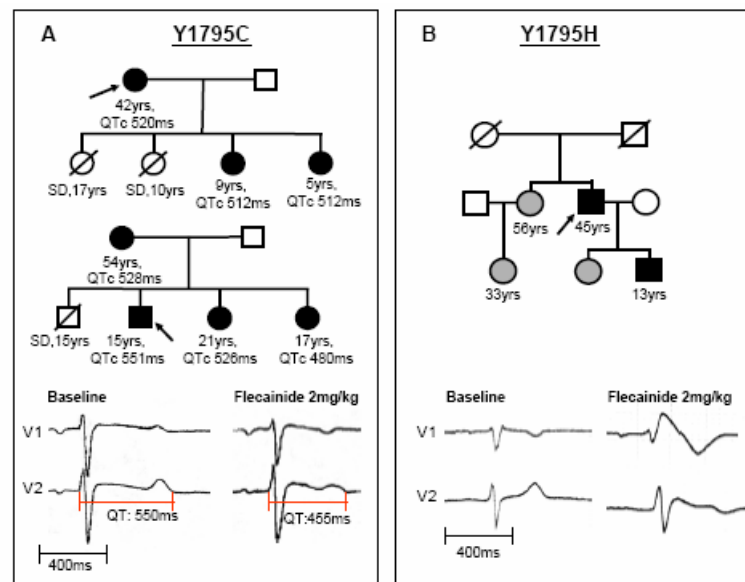


Figure 4.1: Pedigrees and representative ECGs of the Y1795C (panel A) and Y1795H (panel B) families. Filled symbols represent genetically and clinically affected individuals (black) or silent mutation carriers (grey). The effect of Flecainide intravenous administration is depicted at the bottom. QTc (QT interval corrected for heart rate, Bazett's formula) shortening was observed in the Y1795C ECG (from 530 ms to 470 ms) while 2 mm ST segment elevation was elicited by this drug in Y1795H. Figure from Vecchietti *et al.*, 2007.

Materials and Methods

Markov model of the Na⁺ current

The cardiac I_{Na} was modelled by a nine state Markov chain (Fig. 4.2) already proposed by Clancy and Rudy (Clancy and Rudy, 2002). The model included three distinct closed states, a conducting open state, and five inactivation states (one fast-, two intermediate- and two closed-inactivation). The expression of transition rates are reported in Tab. 4.1. The parameters of transition rates were previously identified as extensively reported in (Vecchietti *et al.*, 2006) to reproduce by the Markov model the whole-cell current measured by Rivolta et al (Rivolta *et al.*, 2001) in WT and mutant channels expressed in HEK293 cells.

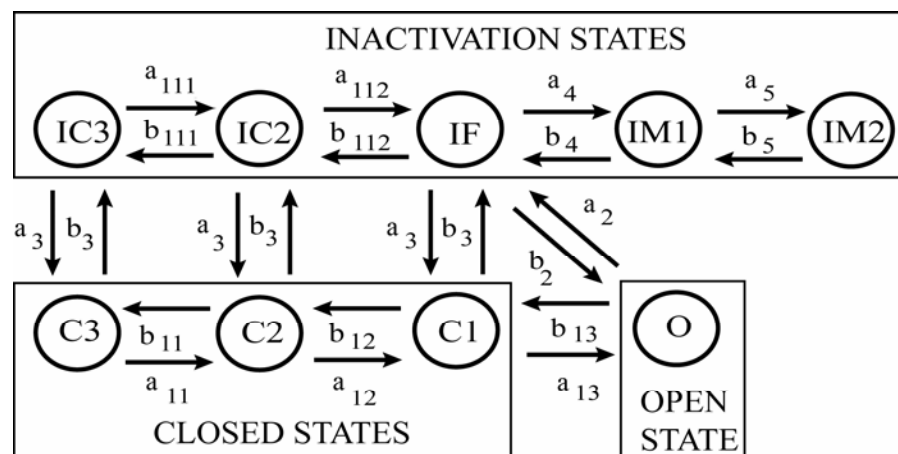


Figure 4.2: Diagram of the nine state Markov Model of the cardiac Na⁺ current. The model includes three closed states (C1, C2, C3), a conducting open state (O), two closed inactivation states (IC3, IC2), one fast inactivation state (IF) and two intermediate inactivation states (IM1, IM2). The expressions of the transition rates and the assignment of the parameters for WT and mutant channels are reported in Tab 4.1 and 4.2. Figure from Vecchietti *et al.*, 2007.

Ventricular cell computer model

The ventricular AP simulator was based on the Luo-Rudy (LRd) model (Chapter 2) that was implemented in Simulink 5 (The MathWorks. Inc- Natick, Mass; USA). Intra- and extra-cellular ion concentrations were set to constant values ($[K^+]_o = 4.5$ mmol/L, $[K^+]_i = 141.2$ mmol/L, $[Na^+]_o = 140$ mmol/L, $[Na^+]_i = 10$ mmol/L and $[Ca^{2+}]_o = 1.2$

mmol/L), except for intracellular Ca²⁺ concentration for which dynamic changes were simulated.

Table 4.1 - Transition rate expressions (ms⁻¹).

Transition rates
$a_{11}=(\alpha \exp(-V/17)+\beta \exp(-V /150))^{-1}$
$a_{12}=(\alpha \exp(-V /15)+\beta \exp(-V /150))^{-1}$
$a_{13}=(\alpha \exp(-V /12)+\beta \exp(-V /150))^{-1}$
$b_{11}=\varepsilon \exp(-V /20.3)$
$b_{12}=\zeta \exp(-V /20.3)$
$b_{13}=\eta \exp(-V /20.3)$
$a_{111}=(\theta \exp(-V /17)+\omega \exp(-V /150))^{-1}$
$a_{112}=(\theta \exp(-V /15)+\omega \exp(-V /150))^{-1}$
$b_{111}=\varphi \exp(-V /20.3)$
$b_{112}=\kappa \exp(-V /20.3)$
$a_3=\lambda \exp(-V / \mu)$
$b_3=v (8.4 \cdot 10^{-3}+2.0 \cdot 10^{-5} V)$
$a_2=(\xi \exp(-V /16.5)+\upsilon \exp(-V /200))^{-1}$
$b_2=a_{13} a_2 a_3/b_{13} b_3$
$a_4=\pi a_2$
$b_4=\rho a_3$
$a_5=\sigma a_2$
$b_5=\tau \exp(-V / 7.7)$

The transient outward current (I_{T_o}) was modelled according to Dumaine et al (Dumaine *et al.*, 1999). The original formulation of the I_{Na} current was replaced with the nine-state Markov model. In order to reproduce the heterozygous condition of Y1795C and Y1795H patients 50% mutant and 50% WT channels were simulated. The maximum Na⁺ conductance (G_{Na}) was set to 16 mS/ μ F for WT, in agreement with Faber and Rudy (Faber and Rudy, 2000). G_{Na} was set to 29.46 mS/ μ F for Y1795C and 5.96 mS/ μ F for Y1795H in order to account for the experimentally measured ratios (mutants vs WT) of I_{Na} current peaks (Rivolta *et al.*, 2001). All the kinetic rates were normalized to 37°C with a Q10 of 2.1 (Benndorf and Nilius, 1987; Schwarz, 1986).

Transmural heterogeneity (Liu *et al.*, 1993; Sicouri *et al.*, 1996) (epicardium, endocardium and midmyocardium -cells) of the AP was modelled by setting the I_{T0} expression level (Clancy and Rudy, 2002) and the density ratio between slow and rapid components of the delayed-rectifier potassium current (I_{Ks}/I_{Kr}) (Liu and Antzelevitch, 1995). In epicardial (Epi) cells the maximal I_{T0} conductance (G_{T0}) was set to 1.1 mS/μF and the I_{Ks} / I_{Kr} density ratio was set to 63. In midmyocardial (M) cells, G_{T0} 0.5 mS/μF and I_{Ks}/ I_{Kr} 23.3. In endocardial (Endo) cells, G_{T0} 0.05 mS/μF and I_{Ks}/ I_{Kr} 29.6.

Table 4.2 - Na channel model parameters for WT and mutant channels

Parameters	Y1795H	WT	Y1795C (40 bpm)	Y1795C (115 bpm)
A	0.0141	0.0378	0.0077	0.0196
β	0.0345	0.0925	0.2663	0.168
ε	0.5751	0.2492	0.3962	0.4409
ζ	0.7676	0.3326	0.5287	0.5885
η	1.0801	0.4681	0.7442	0.8281
θ	0.0313	0.1093	0.0240	0.0435
ω	0.0558	0.1949	0.7617	0.3684
φ	0.5751	0.1917	0.1278	0.4409
κ	0.7676	0.2559	0.1705	0.5885
λ	1.1380 10 ⁻⁶	3.7933 10 ⁻⁷	4.0000 10 ⁻⁷	13.800 10 ⁻⁷
μ	7.6029	6.1839	7.1839	7.1839
ν	3.0000	1.0000	0.6667	2.3000
ξ	0.0133	0.0159	4.0661 10 ⁻⁶	0.0024
υ	0.0607	0.0722	0.1275	0.0676
π	4.8000 10 ⁻⁴	0.0022	0.0001	0.0009
ρ	0.2400	0.1000	0.1125	0.1000
σ	0.1737 10 ⁻⁴	0.0924 10 ⁻⁴	0.0024 10 ⁻⁴	0.1053 10 ⁻⁴
τ	0.4097 10 ⁻⁷	0.0854 10 ⁻⁷	0.0004 10 ⁻⁷	0.1133 10 ⁻⁷

This setting allowed a numerical reconstruction of Epi, M and Endo cells APs. The maximum conductance of the L-Type calcium current was decreased by 20% with respect to the original LRd formulation in all cells (Banyasz *et al.*, 2003), in accordance with (Dumaine *et al.*, 1999).

Pacing was simulated by a 1 ms pulse train of 50 A/F in amplitude with frequency of 40, 70 and 115 bpm. Rosenbrock variable step algorithm (max step 10 μ s) was used to numerically solve the model equations (Shampine and Reichelt, 1997). In order to ensure a steady state condition, 180 s long simulations were performed; all the data shown refer to the last beat. AP duration was measured at 90% of repolarization (APD₉₀).

Table 4.3 – Percentage of current blocking used to mimic Flecainide and Mexiletine administration. In parentheses the bibliographic references are indicated.

Current	Blocking (%)	
	Flecainide	Mexiletine
I _{Na}	50 ((Liu <i>et al.</i> , 2002))	50 ((Hering <i>et al.</i> , 1983))
I _{CaL}	45 ((Hatem <i>et al.</i> , 1992))(Hancox and Convery, 1997)	25 ((Ono <i>et al.</i> , 1986))(Mitcheson and Hancox, 1997)
I _{To}	10 ((Akar <i>et al.</i> , 2004; Slawsky and Castle, 1994))	-
I _{Kr}	10 ((Follmer <i>et al.</i> , 1992))(Wang <i>et al.</i> , 1996; Paul <i>et al.</i> , 2002)	-

Table 4.4 - Modification of the parameters of kinetic rate $a_3 = \lambda \exp(-V / \mu)$ to reproduce the negative shift of availability curve induced by Flecainide (10 μ M). The parameter μ was set to 6.0773 in all cases.

	Λ
WT	7.021 10 ⁻⁸
Y1795C (40 bpm)	1.388 10 ⁻⁸
Y1795C (115 bpm)	2.916 10 ⁻⁸
Y1795H	1.112 10 ⁻⁸

Flecainide and Mexiletine Simulation

The effects of Flecainide and Mexiletine were mimicked by reducing the maximal conductance of I_{Na}, I_{CaL}, I_{To} and I_{Kr} currents (Tab. 4.3).

According to our experimental data (not shown), Flecainide-induces mild negative shift of the availability curve of the I_{Na} current (WT: 3 mV, Y1795C: 7 mV, Y1795H: 8

mV). The parameter assignment for the kinetic rate a_3 in the Markov model was modified accordingly (see Tab. 4.4).

Results

Simulated WT action potential

When the WT I_{Na} Markov model was included in the ventricular cell model, the simulated APs shape resembled the typical reported waveforms (Antzelevitch and Fish, 2001) for the three cell types (Fig. 4.3 left panels). The AP durations at 70 bpm were Endo: 162 ms, Epi: 157 ms, M: 181 ms. The AP durations at 40 and 115 bpm are reported in Table 4.5. AP morphology did not vary with changes in pacing frequency (40 up to 115 bpm).

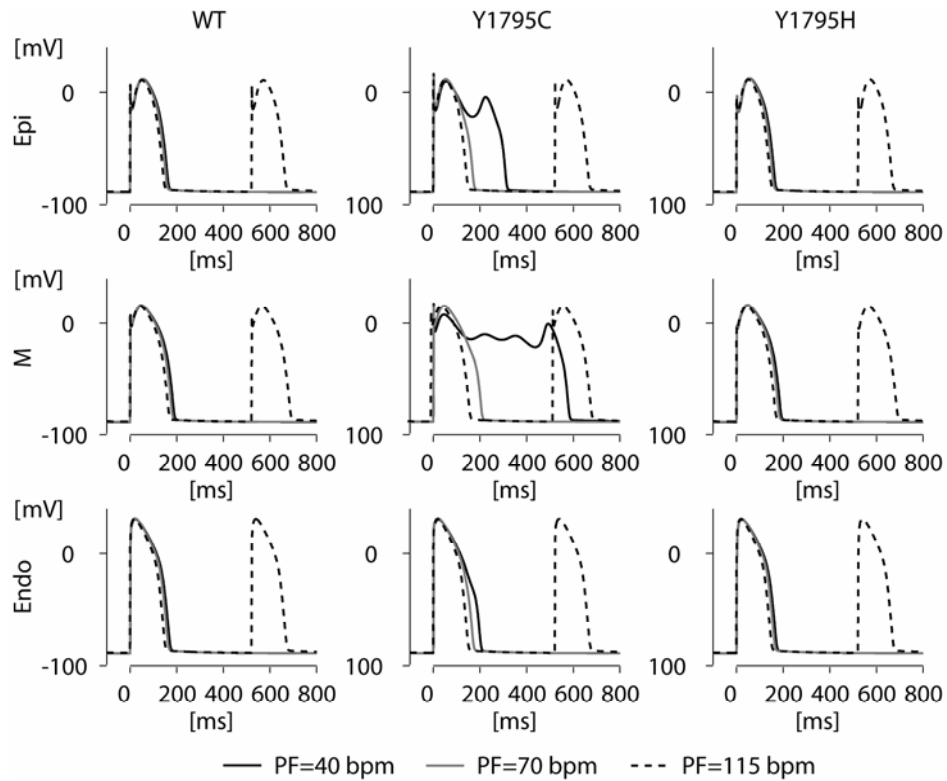


Figure 4.3: Y1795C mutation (middle panels) affects AP of the three cells composing the ventricular wall (epicardial, M and endocardial cells) in a rate dependent manner. The major effect is shown at the pacing frequency of 40 bpm when EADs appear in epicardial and M cell AP. Y1795H mutation (right panels) has not remarkable effects on the AP of the three myocardial layers. Figure from Vecchietti *et al.*, 2007.

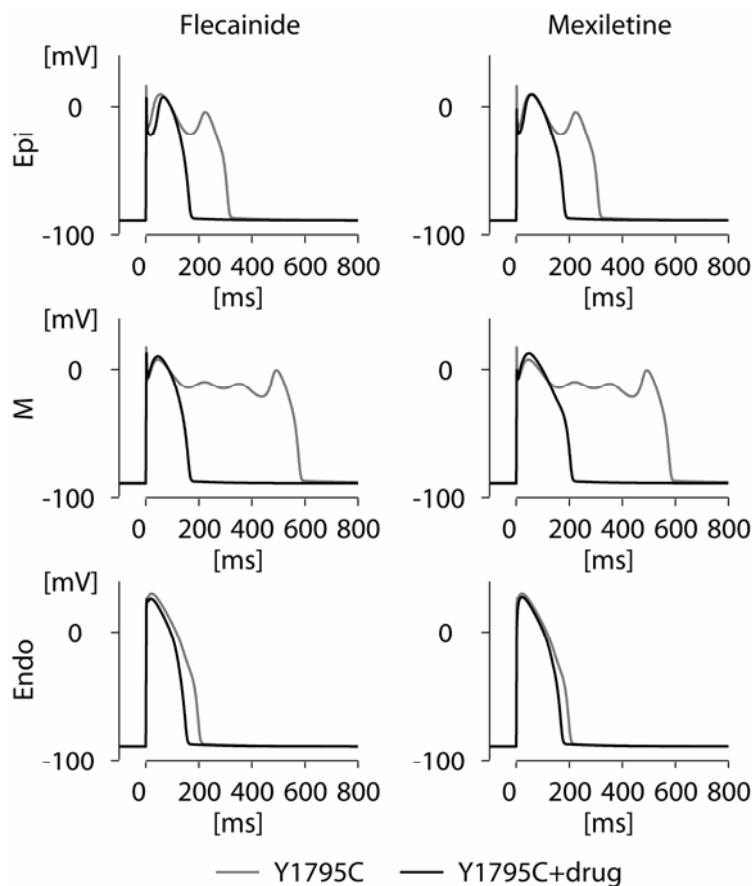


Figure 4.4: Effect of Flecainide (left panels) and Mexiletine (right panels) on ventricular cell AP in presence of Y1795C mutation at the pacing rate of 40 bpm. Both drugs reduce APD in endocardial cell and suppress EADs in epicardial and M cell. Figure from Vecchiotti *et al.*, 2007.

Effects of Y1795C mutation on action potential

The simulated Y1795C APs were longer as compared with WT in all cell layers (Endo: 6%, Epi: 10%, M: 16% at a pacing rate of 70 bpm), and showed remarkable increase of the APD sensitivity of to heart rate (Fig. 4.3 and Table 4.5). This effect was more prominent in Epi and in M cells, in which early afterdepolarizations (EADs) appeared at 40 bpm (Fig. 4.3, middle panel).

Effects of Y1795H mutation on action potential

The heterozygous condition for the Y1795H mutant channel only slightly changed the AP morphology (Fig. 4.3, right panels) and duration (Table 4.5) with respect to the

WT. Albeit in vitro characterization show that Y1795H induce a small sustained Na⁺ current (Rivolta *et al.*, 2001), the resulting AP prolongation was negligible in all cell types (Endo: 1.2%, Epi: 1.5%, M: 1.7% at a pacing rate of 70 bpm). The reduced current availability of the Y1795H channel resulted in a mild reduction of the AP upstroke amplitude (10%in Epi cell) as compared to the WT.

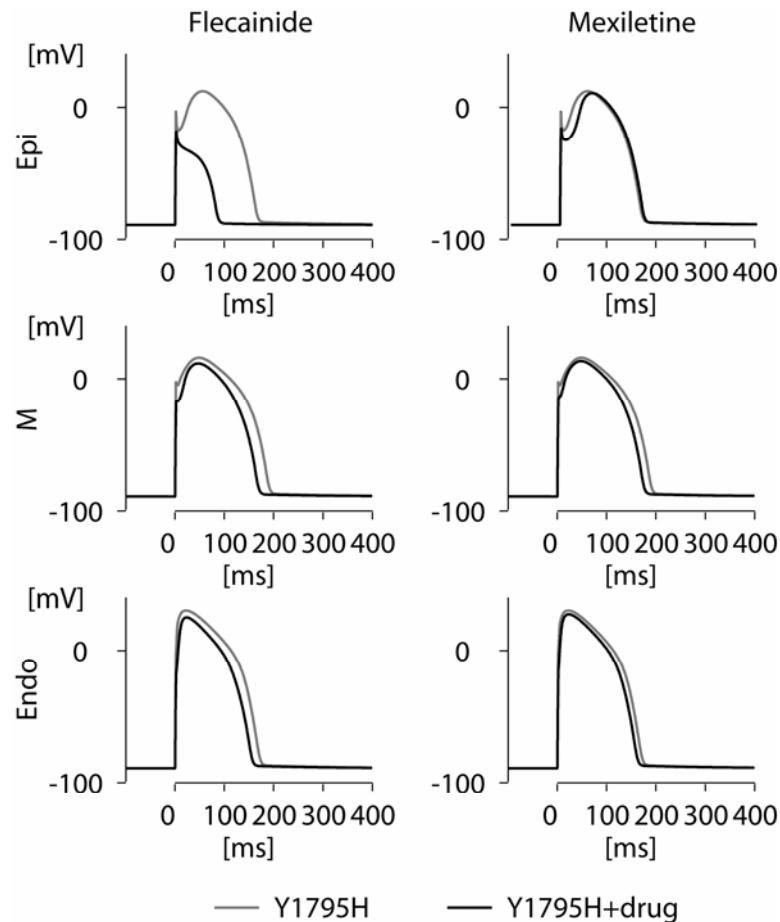


Figure 4.5 Effect of Flecainide (left panels) and Mexiletine (right panels) on ventricular cell AP in presence of Y1795H mutation at the pacing rate of 40 bpm. Flecainide but not Mexiletine causes the appearance of a domeless AP in epicardial cell. Figure from Vecchietti *et al.*, 2007.

Effects of Flecainide and Mexiletine on the WT action potential

The in silico simulation of Flecainide induced a transmural opposite response in WT APD (Table 4.5). At 40 bpm: 13% prolongation of the APD₉₀ in Epi and 11% shortening of APD₉₀ (Tab. 4.5) in Endo. This finding is in agreement with experimental

results (Krishnan and Antzelevitch, 1991). Mexiletine slightly shortened APD₉₀ both in Epi and in Endo cells (Epi: 2%, Endo: 6% at 40 bpm). Both drugs caused an AP shortening in M cell (Flecainide: 15%, Mexiletine: 10% at 40 bpm).

Effects of Flecainide and Mexiletine on the Y1795C action potential

In bradycardia Flecainide and Mexiletine caused APD₉₀ to shorten in the Y1795C mutant cell but with a stronger effect in the case of Flecainide (Table 4.5): -22.5% vs. -13.5% in Endo cell at 40 bpm. Notably, both drugs inhibit the onset of EADs in Epi and M cells (Fig. 4.4). As already shown for WT, at 115 bpm Flecainide caused the lengthening of APD in the Epi cell (see Table 4.5).

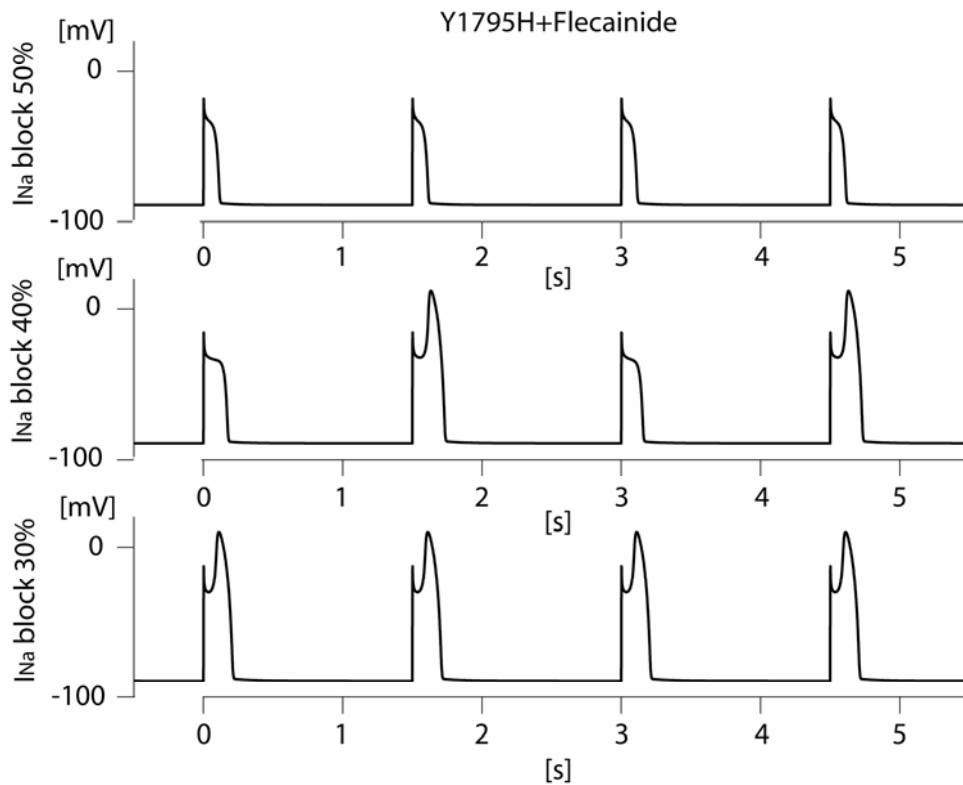


Figure 4.6: AP morphology changes due to different levels of Flecainide-induced I_{Na} blockade in epicardial cell in presence of Y1795H mutation. At a blocking level of 40% an alternation of prolonged and domeless AP appeared; the AP dome was stably restored at 30% I_{Na} reduction. Figure from Vecchiotti *et al.*, 2007.

Effects of Flecainide and Mexiletine on the Y1795H action potential

Flecainide also elicited a myocardial layer-specific response in the case of Y1795H mutant (Fig. 4.5, left panels). Flecainide reduced APD in Endo and M cells (Table 4.5); in Epi cell a striking complete loss of the AP dome occurred at 40 bpm (APD₉₀: from 166 ms to 116 ms) whereas at 115 bpm an alternating pattern appeared (see Table 4.5). Conversely, Mexiletine caused modest AP changes (Fig. 4.5, right panels and Table 4.5) with APD decreasing in M and Endo cells and increasing in Epi cell.

Interestingly, the effect of Flecainide on AP morphology of the Epi cell was dependent upon the amount of I_{Na} blockade (Fig. 4.6). For a 40% block, domeless APs alternatively separated by long APs were predicted (Fig. 4.6, middle panel). The oscillatory pattern was stable overtime. For a 30% current reduction, oscillations in the APD disappeared and a stable pattern of long markedly notched APs was reproduced (Fig. 4.6, lower panel). Similar transitions through different AP waveforms were observed when raising the pacing frequency up to 115 bpm by maintaining the 50% of I_{Na} blockade (Table 4.5).

Since the different response elicited by Flecainide and Mexiletine on the Epi cell AP (Fig. 4.5) was obtained by simulating the same (50%) I_{Na} reduction for the two drugs, the simultaneous different block of the other ion currents (Tab. 4.3) seems to take part in differentiating drug-induced AP alterations. To investigate the role of each current we analysed the AP sensitivity to different levels of I_{CaL}, I_{To} and I_{Kr} block (Fig. 4.7). The loss of the AP dome in Epi cell, characterizing the Flecainide simulation (Fig. 4.7, BL1 curve), persisted also when I_{Kr} was either completely blocked (data not shown) or not blocked at all (Fig. 4.7, BL2 curve) If I_{Kr} and I_{To} were not blocked (Fig. 4.7, BL3 curve) the AP duration was further reduced. The AP was still dome-less when the I_{CaL} blockade was reduced from 45% to 35% (Fig. 4.7, BL4 curve). In a condition of 35% I_{CaL} blocking, the 10% I_{To} blockade caused the appearance of the AP dome with a markedly pronounced notch (Fig. 4.7, BL5 curve). Without the block of I_{Kr} and I_{To}, the restoring of the AP morphology with dome occurred when a 25% I_{CaL} blockade was

simulated (Fig. 4.7, BL6 curve). The last condition corresponds to the simulation of Mexiletine. Notably, the abrupt changes in AP morphology with respect to the degree of block enlightens on the “all or none” nature of this phenomenon.

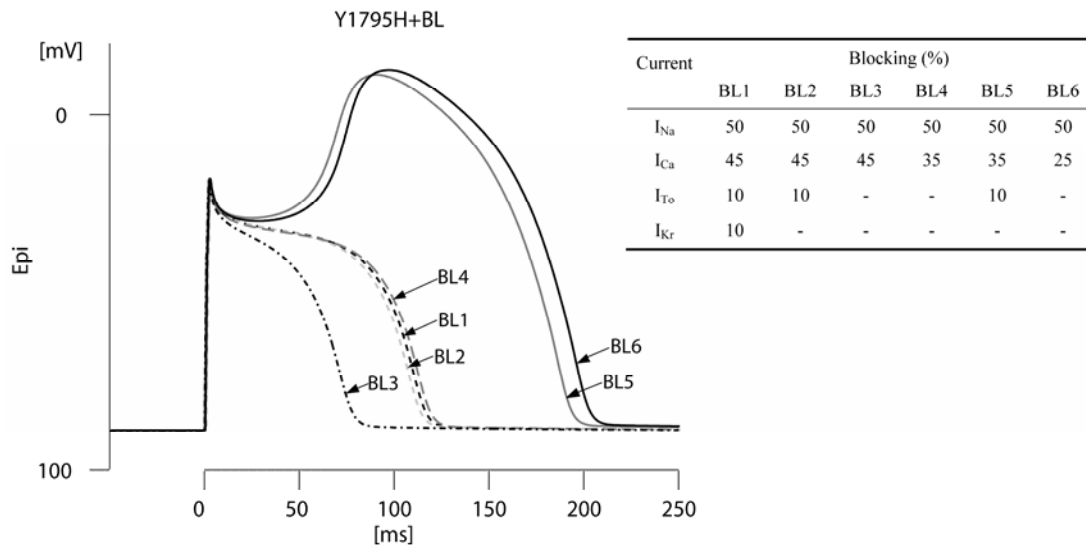


Figure 4.7: AP morphology changes induced by different levels of I_{Na}, I_{CaL}, I_{To} and I_{Kr} blocking in presence of Y1795H mutation (Epi cell, 40 bpm). Figure from Vecchietti *et al.*, 2007.

Discussion

In the present study we investigated with numerical experiments the effect of two mutations of residue 1795 (Y1795C and Y1795H) of the cardiac sodium channel protein that cause LQT3 and BrS respectively. The heterologous expression of both mutants demonstrated that they modify the biophysical properties of the I_{Na} current (Rivolta *et al.*, 2001). Specifically, Y1795C leads to a residual sustained inward Na⁺ current that is consistent with the LQT3 phenotype while Y1795H accelerates inactivation thus reducing current availability.

Here we numerically reproduced the biophysical properties of WT and mutant sodium channels by a Markov model of I_{Na} and we implemented these data in the Luo-Rudy ventricular action potential model (Faber and Rudy, 2000; Dumaine *et al.*, 1999) in order to assess: 1) the mutation-dependent AP abnormalities in Epi, Endo and M cells and 2) the response to sodium channel blocking drugs known to modify the ECG

in LQT3 and BrS patients. On the basis of such analyses we show how the mutation-dependent AP alterations account for the patients’ electrocardiographic phenotype and provide clues for the understanding of arrhythmogenic mechanisms associated with these mutations.

Table 4.5 - APD90 values (ms) in the different cell types with and without drugs resulting from simulations with the pacing rate of 40 bpm and 115 bpm.

		40 bpm			115 bpm		
		Epi	M	Endo	Epi	M	Endo
No drug	WT	161	185	167	146	163	148
	LQTS	EADs	EADs	201	150	167	150
	BrS	166	187	170	151	169	151
Flecainide	WT	182	157	149	168	155	141
	LQTS	180	165	156	187	155	141
	BrS	116	165	156	(*)	158	144
Mexiletine	WT	158	167	157	146	158	144
	LQTS	180	205	174	147	158	143
	BrS	168	172	168	153	159	145

(*) Alternating pattern: a long epicardial AP (APD90= 227 ms) was followed by two shorter activations (loss of dome) of different duration (97 ms and 125 ms), and by another long-short AP sequence (APD90= 225 ms and APD90=97 ms).

Effects of Y1795C and Y1795H on AP in the three myocardial layers

We took advantage from previously published data (Sicouri *et al.*, 1996) to simulate the transmural heterogeneity of the AP by modulating the amount of the transient outward current (I_{To}) and the ratio between the slow (I_{Ks}) and the rapid (I_{Kr}) components of the delayed-rectifier current (Clancy and Rudy, 2002; Liu *et al.*, 1993; Liu and Antzelevitch, 1995). We then characterized the alterations induced by each of the mutants on the AP of epicardial, endocardial and midmyocardial cells at different pacing rates.

Numerical simulation confirmed the observation made by Clancy *et al.* (Clancy *et al.*, 2002) in their model of endocardial cells that bradycardia accentuates the APD

prolongation as a consequence of an increased sustained I_{Na} current at slower rates (Fig. 4.3). In addition, we showed that the effect of the late I_{Na} current during bradycardia was more pronounced in Epi/M cells than in Endo cell. While Y1795C induced in the Endo cell model only APD prolongation (Clancy *et al.*, 2002), in the Epi and M cell models the mutation also induced EADs (Fig. 4.3, middle panels). In Epi cell EADs developed despite of a shorter basal AP in this cell type with respect to Endo cell. This is due to the presence of a larger I_{To} in this layer. The prominent notch in AP phase 1 of the Epi cells due to the I_{To} determines a different balance of currents in the subsequent phases of the action potential, allowing the sustained I_{Na} to trigger EADs. In fact, we did not find EADs by simulating Y1795C Epi cell with G_{Ito}=50 S/F (as Endo cell, data not shown). These results are in agreement with the LQT3 phenotype observed in the Y1795C carriers and with the fact that three life-threatening events (three sudden deaths and one cardiac arrest) occurred during sleep (Fig. 1).

At variance with Y1795C, the Y1795H mutation induced only negligible changes of AP morphology in the three myocardial layers, in agreement with the clinical findings that the Brugada Syndrome phenotype observed in the carriers of the mutation was only evident upon pharmacological challenge with Flecainide (Fig. 1).

Response of mutants to sodium channel blockers

The Y1795C model displayed a reduction of Endo APD by 22% with Flecainide and by 13% with Mexiletine. Interestingly in the clinical setting Flecainide administration (2 mg/Kg) reduced the QT interval to the same extent (Priori *et al.*, 1996; Benhorin *et al.*, 2000) (Fig 1). These data are consistent with what shown in LQT3 patients in whom class I antiarrhythmic drugs clearly shortened QT interval (Schwartz *et al.*, 1995). In our simulations both drugs suppressed the EADs in M and Epi cells. The efficacy of the two drugs in suppressing EADs is consistent with the observation made in a mouse model of LQT3 (Tian *et al.*, 2004) and provides a mechanistic explanation for the prevention of lethal arrhythmias observed over 5 year follow up in a 5-year old

LQT3 patients who experienced a cardiac arrest on beta-blockers but was subsequently protected by mexiletine treatment (Schwartz *et al.*, 2000b).

The simulation of Flecainide administration in the case of Y1795H experiments induced shortening of the APD in Endo and in M cells, while in Epi cells AP alterations of both duration and morphology were observed (see Fig. 4.5, left panels, and Fig. 4.6). The beat to beat action potential alteration shown in Fig. 4.6 (middle panel) could be the cellular counterpart of T wave alternans (TWA) (Morita *et al.*, 2006). In fact, TWA have been reported in BrS patients upon class Ic drug administration (Ohkubo *et al.*, 2003) and they may be a marker of electrical instability (Morita *et al.*, 2002). Thus, our finding support the pro-arrhythmic potential of class Ic drug administration in BrS patients.

In the Epi cells the action potential showed a loss of the AP dome: this phenomenon has been suggested as the substrate for the ST segment elevation observed in Brugada Syndrome. Accordingly, our in silico analysis predicts that carriers of the Y1795H mutation would have minimal ECG changes at baseline but would respond to Flecainide with a prominent ST segment elevation and electrical instability. Once again this is in agreement with the clinical findings showing a “coved type” ST segment elevation only after Flecainide administration (Fig 1). Antzelevitch and coworkers (Yan and Antzelevitch, 1999) suggested that the strong I_{T_o} current of epicardial cells in the presence of a reduced inward current is responsible for the loss of AP dome. Coherently with this hypothesis we observed prompt AP morphology normalization when I_{T_o} was decreased by 50%. At variance with Flecainide, Mexiletine induced only a slight APD reduction with no loss of the AP dome. This is in agreement with clinical observations by Shimizu et al (Shimizu *et al.*, 2000) who showed that Mexiletine did not elicit ST segment elevation in BrS patients.

As of today, a conclusive explanation of the differential effect of Flecainide and Mexiletine in the BrS patients is not available. Our data suggest that Flecainide but not Mexiletine unmasked BrS silent mutation mainly because of their differential blocking

effect on the inward current (greater extent the I_{CaL} current block). Thus, we suggest that in presence of sodium channel blockers the balance between I_{CaL} and I_{To} currents has to be crucially important for unmasking the arrhythmogenic substrate in BrS patients. This hypothesis is in accordance with the experimental findings of Fish and Antzelevitch (Fish and Antzelevitch, 2004), whose data suggested that combined calcium channel block may be more effective than sodium channel block alone in unmasking the Brugada syndrome and that pharmacological agents that inhibit I_{To} may be useful in preventing arrhythmias in BrS patients.

Study limitations

We used a computer model based on the well-established LRd model that has been already used to assess the impact of mutations on AP in patients with inherited arrhythmogenic disorders (Clancy and Rudy, 2002; Clancy and Rudy, 2001; Clancy and Rudy, 1999; Gima and Rudy, 2002). Qualities and limitations of this model, which is mostly based on guinea pig experimental data, have been extensively discussed (Luo and Rudy, 1994a; Clancy and Rudy, 1999; ten Tusscher *et al.*, 2004). It is worth to note that for the present analysis we considered as control the APs computed by model with the WT human cardiac Na channel and we focused on the impact of mutations on the AP with respect to this condition. Thus, the dependence of the results from the model setting should be limited. Nevertheless, models of human ventricular cells recently published (ten Tusscher *et al.*, 2004) (Iyer *et al.*, 2004) should be used in further investigations.

The present simulation analysis assumes the existence of transmural heterogeneity of repolarization to an extent similar to that observed in animal studies (Antzelevitch and Fish, 2001). It is fair to note that the role of transmural dispersion of repolarization in the human heart is still under debate (Drouin *et al.*, 1995). Our simulation results support the hypothesis that transmural heterogeneity can play a crucial role in the ECG phenotype of I_{Na} mutations.

We did not consider the rate-dependent Na channel binding properties of Flecainide

and Mexiletine. In fact, the recovery from drug block is rapid with mexiletine and slow for flecainide. Liu *et al.* (Liu *et al.*, 2002) showed a 10% increase of Flecainide-induced blocking when pacing rate was changed in a physiologic range from 1 to 2 Hz. A lower variation of the blocking degree is expected for Mexiletine. In spite of the variations of drug blocking due to heart rate changes are modest, they could influence AP morphology and duration.

The assignment of current blocking is not without uncertainties because of the lack of consistent experimental data assessing the effects of the two drugs. However, the sensitivity analysis reported in Fig. 4.7 makes the assignment less critical demonstrating that the loss of AP dome kept on also when limited block extents were tested.

Conclusion

In this study we investigated by computer simulation the effects of two *SCN5A* mutations on the action potential of endocardial, epicardial and midmyocardial cells and we mimicked their response to Flecainide and Mexiletine. We demonstrate that there is a remarkable agreement between the cellular abnormalities and the electrocardiographic manifestations observed in the carriers of the two genetic defects. Furthermore, we show that a “gain of function” mutation of *SCN5A* induces bradycardia-dependent APD prolongation in epicardial and midmyocardial cells leading to development of EADs. In this framework, both Mexiletine and Flecainide reverse the APD prolongation and prevent the EADs. This effect is likely to be a direct consequence of the blockade of the late sodium current. Interestingly, our data show for the first time that a loss of function *SCN5A* mutation may induce only minimal effect on the shape of the APD across the myocardium and is therefore consistent with a normal ECG. It is only in the presence of selective perturbation of other currents that it is possible to reveal such a concealed arrhythmogenic syndrome. This evidence accounts for the variability of the ST segment elevation at ECG and for the paroxysmal nature of the arrhythmic events in Brugada Syndrome.

5 CaMKII effects on the Na⁺ channel gating

Ca/Calmodulin-dependent protein kinase II

Intracellular Ca²⁺ is the central second messenger in the translation of electrical signals (i.e. action potentials) into mechanical activity of the heart (i.e. contractions). Recently it has become clear that several Ca²⁺ dependent proteins contribute to the fine tuning of this highly coordinated process of excitation/contraction coupling. One of these intracellular proteins is the Ca/Calmodulin-dependent protein kinase (CaMK) of which CaMKII is the predominant isoform in the heart.

CaMKII is one of the targets for calmodulin (CaM) binding. CaMKII is a multifunctional CaMK, because it can phosphorylate and alter the function of a variety of substrates. After CaMKII was initially identified in the nervous system, CaMKII has been found to exist in almost all tissue types, including heart (Jett *et al.*, 1987; Edman and Schulman, 1994; Uemura *et al.*, 1995). CaMKII is a particularly interesting enzyme in the heart, where Ca²⁺ is the key regulator of cardiac contraction. In fact, this signaling pathway regulates cardiac myocyte excitability and contractility in a very complex way affecting many different targets (Maier and Bers, 2002). CaMKII δ is the predominant isoform in the heart (Edman and Schulman, 1994). In human heart failure (HF) and in an animal HF model, expression and activity of CaMKII are enhanced 2-3 fold (Kirchhefer *et al.*, 1999; Hoch *et al.*, 1999). It has been shown that transgenic overexpression of the cytosolic isoform CaMKII δ_C induces dilated cardiomyopathy and HF (Zhang *et al.*, 2003; Maier *et al.*, 2003). Inhibition of CaMKII was shown to prevent remodeling after myocardial infarction and excessive beta-adrenergic stimulation (Zhang *et al.*, 2005). CaMKII has also been linked to VT in a mouse model of hypertrophy (Wu *et al.*, 2002).

CaMKII phosphorylates several proteins in the heart in response to Ca signals, including Ca transport proteins such as RyR (Witcher *et al.*, 1991; Hain *et al.*, 1995) and phospholamban (PLB) (Davis *et al.*, 1983; Simmerman *et al.*, 1986). CaMKII stimulates the L-type calcium channels and under disease conditions marked by a high risk for arrhythmic sudden death, CaMKII activity and Ca²⁺ channel openings are increased (Anderson 2004). In addition, novel data suggest that non-Ca²⁺ transporters, such as

sarcolemmal Na⁺ (Wagner *et al.*, 2006) and K⁺ channels (fast component of the transient outward current I_{to,f} and inward rectifier I_{K1}, Li *et al.*, 2006) may be regulated by CaMKII and thus be sensitive to Ca²⁺ handling properties and also influence them via electrophysiological effects.

Structure and function

There are four distinct but closely related CaMKII genes (α , β , γ , δ) (Braun and Schulman, 1995). The α and β isoforms are restricted to nervous tissue, whereas γ and δ are more ubiquitous, with δ as the predominant isoform in heart (Edman and Schulman, 1994). Distinct splice variants of the δ isoform have different intracellular localization: subcellular localizations of CaMKII δ were found with δ_B being specifically compartmentalized to the nucleus due to an eleven amino acid nuclear localization sequence (NLS) and with δ_C being the cytosolic isoform without NLS.

The multimeric CaMKII holoenzyme consists of homo- or heteromultimers of 6-12 kinase subunits (Braun and Schulman, 1995) forming a wheel-like structure (Fig. 5.1). Each CaMKII monomer contains an amino-terminal catalytic domain, a central regulatory domain (containing partially overlapping autoinhibitory and CaM binding regions) and a carboxy-terminal association domain responsible for oligomerization (Fig. 5.1, Braun and Schulman, 1995). The autoinhibitory region close to the active site of the catalytic domain sterically blocks access to substrates. During CaMKII activation (when [Ca²⁺]_i increases, as during systole), Ca-CaM displaces the auto-inhibitory domain on CaMKII by wrapping around it and thereby activating the enzyme. The kinase can then lock itself into the activated state by auto-phosphorylation on the conserved Thr-286 on the auto-inhibitory segment of an adjacent CaMKII monomer. Auto-phosphorylation is thus critical in creating memory in CaMKII and maintaining the enzyme active after [Ca]_i declines (e.g. during diastole). Phosphorylation of Thr-286 is not essential for kinase activity, but it does have important consequences, i.e. by increasing the affinity of the kinase- CaM complex. This effect traps CaM on the autophosphorylated subunit. At high [Ca], the affinity of CaM to CaMKII increases ~700 fold (from an affinity of 45 nM to 60 pM). Even when [Ca]_i declines to resting levels, CaM is still trapped on the kinase for several seconds. As a result, the kinase retains 100% activity as long as CaM is trapped, regardless of the [Ca]_i level. Furthermore, autophosphorylation is itself sufficient to

disrupt the autoinhibitory domain, and the kinase remains partially active (20-80%) even after CaM dissociates from this autonomous state. For complete inactivation to occur, autophosphorylated CaMKII can be dephosphorylated by protein phosphatases (PP1, PP2A and PP2C). Several CaMKII inhibitors have been used in heart cells, including the organic inhibitors KN62 and KN93 which competitively inhibit CaM binding to CaMKII (K_i~370 nM) and are quite selective. Unfortunately, some of these agents appear to have direct ion channel effects that may be independent of CaMKII actions. Peptide inhibitors are not known to directly alter ion channels. Some useful examples include autocamtide-2 related inhibitory peptide (AIP) and autocamtide-2 inhibitory peptide (AC3-I).

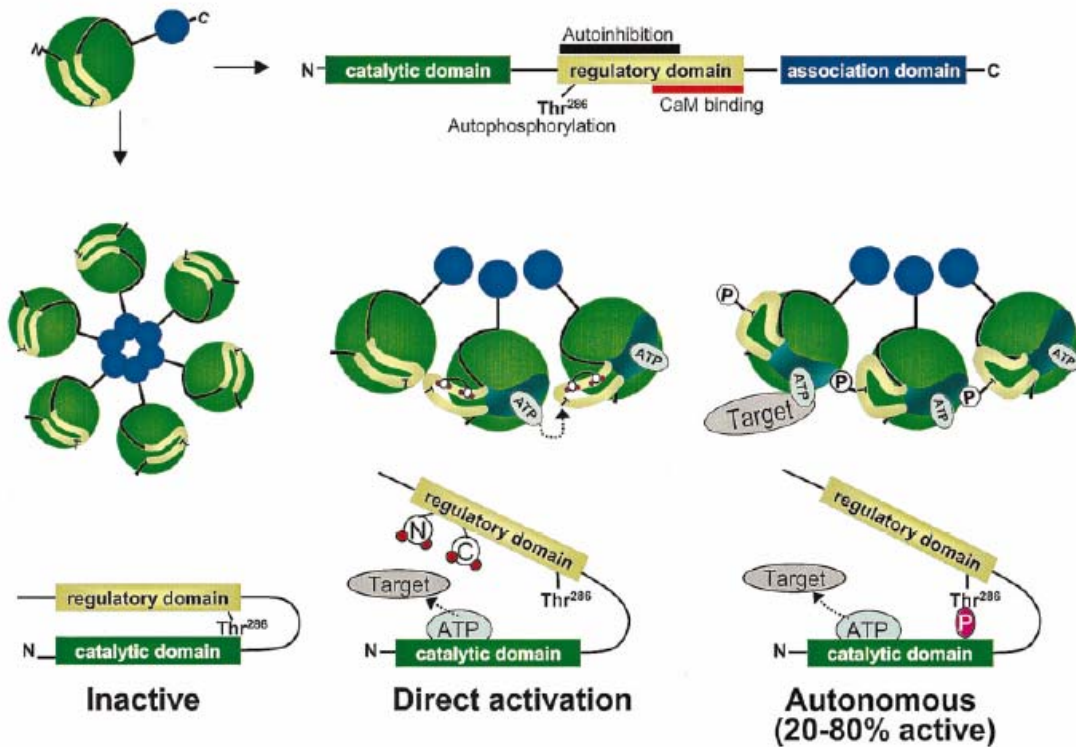


Figure 5.1: Domain layout and oligomeric organization of CaMKII. The three main domains of the CaMKII monomer are indicated in cartoon and linear layout (top). Middle left shows that CaMKII forms homo- or heteromultimers (6-12 monomers) in wheel-like structures (a second one may sit on top of the one shown, forming a double wheel). Lower middle and right panels show activation of CaMKII by Ca-CaM binding and subsequent autophosphorylation at Thr286 (P). CaM binding is sufficient to activate CaMKII so the active site (ATP) can interact and phosphorylate target proteins, but autophosphorylation makes CaMKII active (20-80%) even after CaM dissociates. Figure from Maier and Bers, 2002 (adapted from a Figure by Braun and Schulman, 1995).

CaMKII regulates cardiac Na⁺ channels

Many ion channels use CaM as their constitutive or transient Ca²⁺-sensing partner, and Ca²⁺ clearly plays a crucial role in regulation of cardiac excitability and contraction (Maier and Bers 2002). It is known that calmodulin regulates Na⁺ channel gating through binding to an IQ-like motif at the C-terminus (Tan *et al.*, 2002). Downstream signaling through Ca/CaM-dependent protein kinase II (CaMKII) may be of relevance.

Recently, the role of CaMKII δ_C (the predominant isoform in the heart) on Na channel function was explored using two models. First, Na⁺ channel function and expression were assessed in CaMKII δ_C overexpressing-transgenic (Tg) mice (which develop HF). Second, acute CaMKII δ_C overexpression (rabbit myocytes, compared to myocytes transfected with β Gal as control) was investigated to avoid developmental changes in transgenic animals and unspecific adaptations occurring in HF. Wagner *et al.* (2006a) showed that CaMKII δ_C regulates Na channel gating and [Na⁺]_i which may have an implication in HF. These results are here summarized.

Steady-state inactivation and activation

Figure 5.2 shows the development of steady state inactivation as a function of membrane potential in rabbit myocytes ([Na⁺]_o=10mM). CaMKII δ_C overexpression (vs.

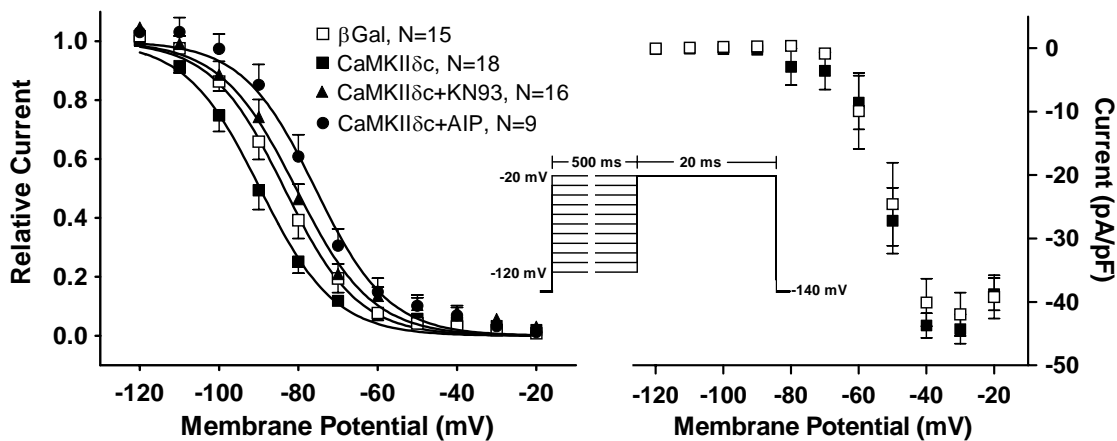


Figure 5.2: CaMKII δ_C enhances steady-state inactivation of Na⁺ channels in rabbit myocytes (10 mmol/l [Na⁺]_o). Mean data acquired using the depicted protocol (inset). Left, in CaMKII δ_C myocytes there was a significant leftward shift vs. β Gal ($P < 0.05$) which could be reversed by CaMKII-inhibition using KN93 ($P < 0.05$) or AIP ($P < 0.05$). Right, mean data for the voltage-current relation corresponding to the pre-pulses are shown for CaMKII δ_C vs. β Gal. Figure from Wagner *et al.* (2006a).

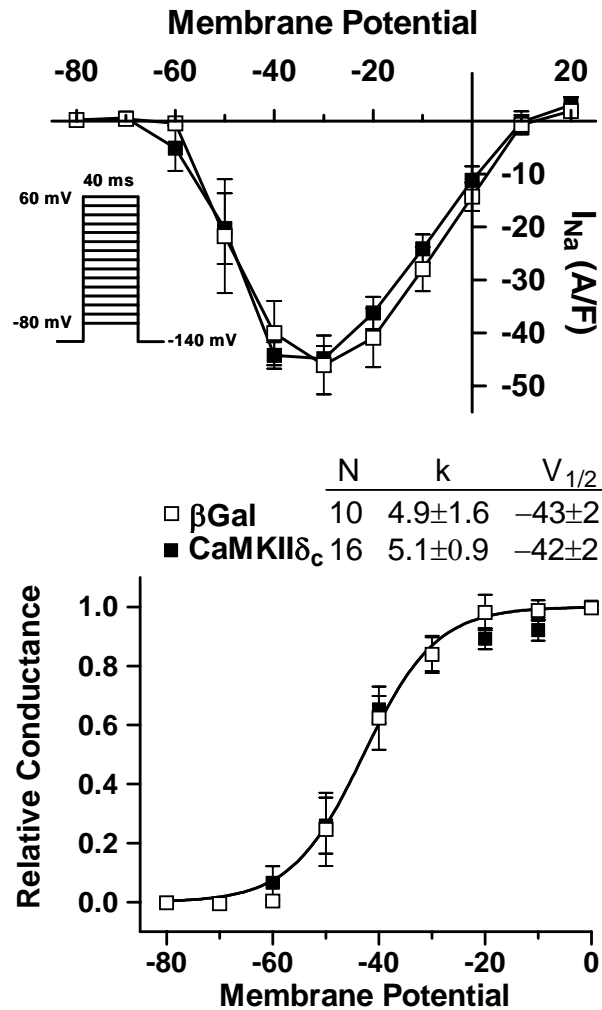


Figure 5.3: Voltage dependence of activation in rabbit myocytes (10 mmol/l $[Na^+]_o$). Above, analysis of voltage-current (I-V) relation using the indicated pulse protocol (inset) for CaMKII δ_c myocytes vs. control (β Gal). Below, relative channel conductance derived from the I-V relation. Figure from Wagner *et al.* (2006a).

β Gal) caused a negative voltage shift in I_{Na} availability, which reduces the fraction of available Na⁺ channels at a given membrane voltage. This effect was clearly Ca-dependent. When $[Ca]_i$ was increased to 500 nmol/l, $V_{1/2}$ was significantly shifted towards more negative potentials. All effects were reversed using CaMKII inhibitors KN93 (1 μ mol/l) or AIP (100 nmol/l) (Fig 5.2). Similar results were observed using more physiologic $[Na^+]_o$ and when investigating CaMKII δ_c transgenic mice.

The current-voltage (I-V) relation of Na channels in CaMKII δ_c overexpressing myocytes was assessed (Fig 5.3). There was no difference in maximal current density. Analyzing the voltage-dependence of channel conductance G, there was no difference for

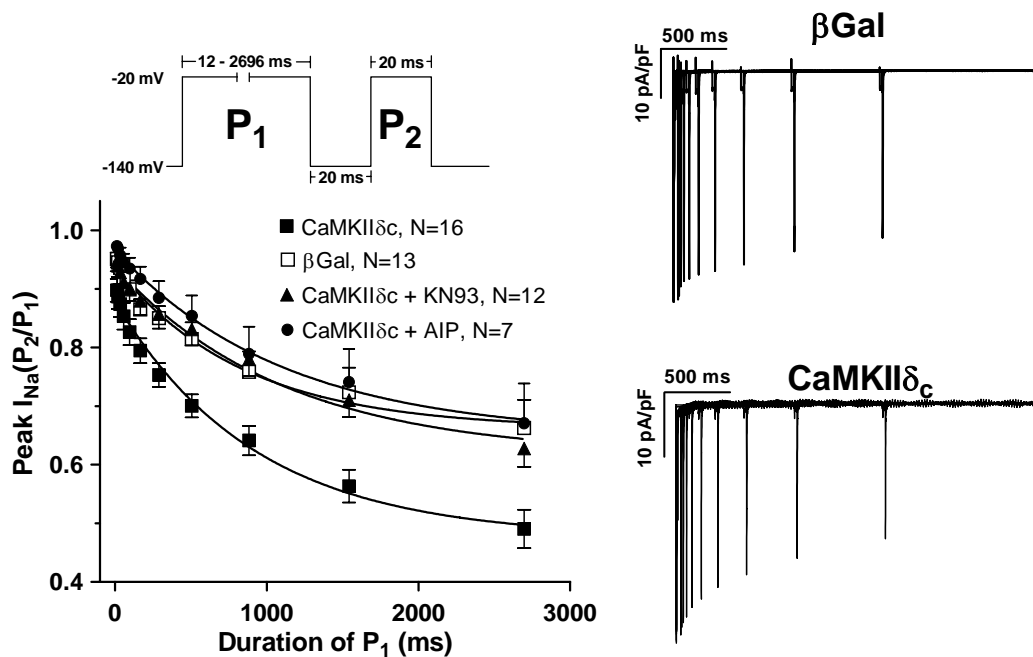


Figure 5.4: CaMKII δ c increases intermediate inactivation (I_{IM}) of Na⁺ channels in rabbit myocytes (10 mmol/l [Na⁺]_o). (Left) Data was acquired using a two pulse protocol (above). Increasing durations of the conditioning pulse (P1) resulted in progressively reduced peak I_{Na} assessed with a second pulse (P2) consistent with intermediate inactivation of a small fraction of Na⁺ channels (mean data, below). This fraction was significantly increased when CaMKII δ c was overexpressed ($P < 0.05$ vs. β Gal) and could be reduced by KN93 ($P < 0.05$) or AIP ($P < 0.05$). (Right) Original traces show with increasing duration of P1 peak I_{Na} upon P2 was progressively reduced. Compared to control (β Gal, above), this reduction was markedly enhanced when CaMKII δ c was overexpressed (below). Figure from Wagner *et al.* (2006a).

the relative conductance at any given membrane voltage, suggesting that Na⁺ channel activation is not altered by CaMKII. Therefore, the differences in steady-state inactivation are almost exclusively ascribable to altered inactivation.

Intermediate inactivation and recovery from inactivation

Intermediate inactivation (I_{IM}), a form of Na⁺ channel inactivation that accumulates over a few hundred milliseconds (after fast inactivation, I_{fast}) and recovers much more slowly at negative E_m than I_{fast} , was additionally investigated. Enhanced I_{IM} has been implicated in Brugada syndrome (Wang *et al.*, 2000) and has been suggested to be a consequence of CaM-dependent Na⁺ channel regulation (Tan *et al.*, 2002). I_{IM} was measured using depolarizations of variable duration (P1) followed by a 20-ms recovery period at -140 mV, allowing for recovery from fast inactivation but not from I_{IM} . The following test pulse (P2) to -20 mV activated all channels not in I_{IM} (Figure 5.4).

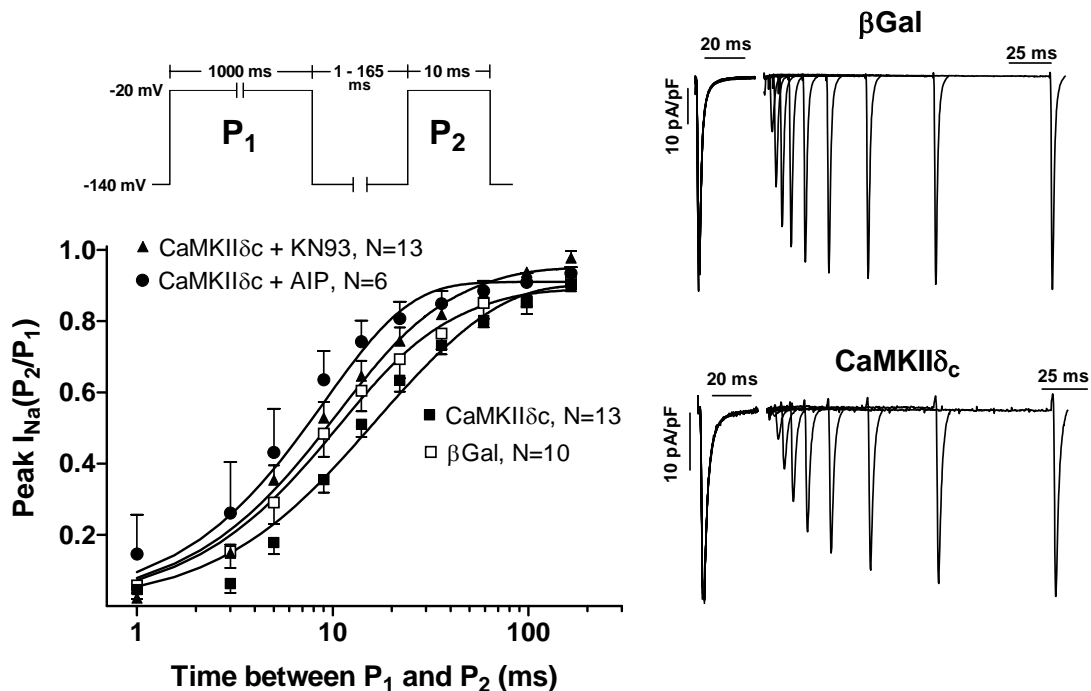


Figure 5.5: CaMKII δ_c slows the recovery from inactivation in rabbit myocytes (10 mmol/l $[\text{Na}^+]_o$). (Left) Mean data acquired using the two pulse protocol (above). Increasing durations of the recovery interval between the conditioning pulse (P_1) generating Na⁺ channel inactivation and the test pulse (P_2) measuring Na⁺ channel activity resulted in a progressively increased peak current upon the test pulse. This is consistent with the progressive recovery of Na⁺ channel activity after inactivation was established. Compared to control (β Gal), this recovery was significantly prolonged in CaMKII δ_c myocytes ($P < 0.05$) and could be enhanced back to control values upon CaMKII δ_c inhibition (KN93, $P < 0.05$, AIP, $P < 0.05$). (Right) Original traces of I_{Na} show with increasing duration of the recovery interval between P_1 and P_2 peak I_{Na} upon P_2 was progressively increased. Compared to control (β Gal, above), this increase was markedly slowed when CaMKII δ_c was overexpressed (below). Figure from Wagner *et al.* (2006a).

Physiologically, only a small fraction of Na⁺ channels undergo I_{IM} and reduce the amount of channels available for the second excitation. Figure 5.4 shows that CaMKII δ_c overexpression significantly increased the fraction of channels undergoing I_{IM} . Again, this effect was Ca²⁺ dependent. At high $[\text{Ca}^{2+}]_i$ (500 nM), the amplitude of I_{IM} was significantly increased. All effects were reversible with the CaMKII inhibitors KN93 or AIP. A similarly enhanced I_{IM} was observed using a more physiologic $[\text{Na}^+]_o$ and in CaMKII δ_c transgenics.

Recovery from inactivation was investigated using a sustained depolarization at a time scale that initiates fast and I_{IM} (1,000 ms), followed by recovery intervals of increasing durations and a subsequent test pulse (Figure 5.5). In comparison to that of control, recovery from inactivation was slowed in CaMKII δ_c myocytes (Figure 5.5). The effect of

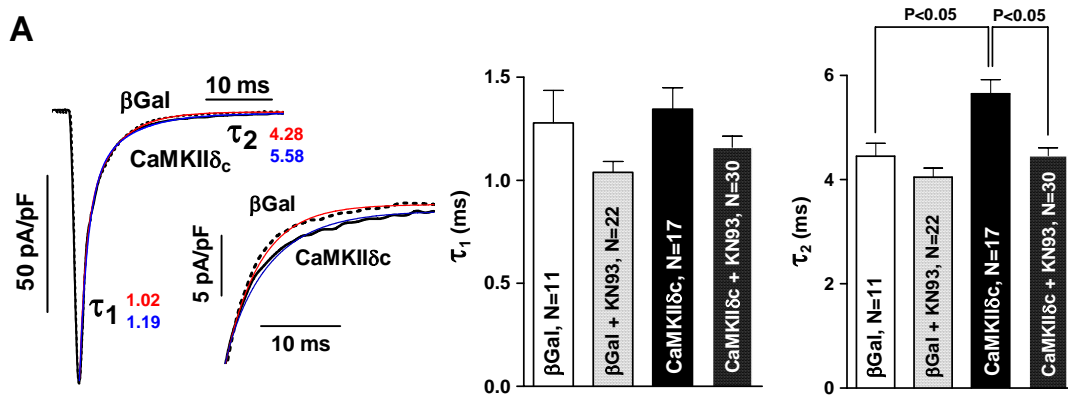


Figure 5.6: CaMKII δ_c slows fast decay of I_{Na} . As evident from the original trace and its magnification (inset), CaMKII δ_c slows fast Na channel inactivation in rabbit CaMKII δ_c myocytes compared to β Gal. The Na⁺ current decay (first 50 ms) was fitted with a double exponential function. Fits to the original traces and corresponding parameters τ_1 and τ_2 (ms) are shown in red (β Gal) and blue (CaMKII δ_c). The deceleration of current decay was most prominent in the late component (right). τ_2 was significantly longer compared to control, whereas τ_1 appeared to be unchanged. In the presence of KN93, the late component of Na⁺ channel decay could be accelerated back to control values. Interestingly, KN93 also significantly hastened current decay in β Gal. Figure from Wagner *et al.* (2006a).

CaMKII δ_c on recovery from inactivation was Ca²⁺ dependent. These results indicate that CaMKII δ_c activity substantially slows I_{Na} recovery from inactivation. This may reflect, in part, slower recovery from I_{IM} , as there was more I_{IM} in the cases where recovery was prolonged. The slower I_{Na} recovery could also limit I_{Na} availability, especially at high heart rates. The CaMKII δ_c -dependent slowing of Na⁺ channel recovery was also seen in physiologic $[Na^+]_o$, and the effect could be measured in CaMKII transgenics. Consistently, the effect of CaMKII δ_c overexpression was completely reversible with CaMKII inhibition.

Fast, open-state inactivation and $[Na^+]_i$

When Na⁺ channels open, they close very rapidly, within 10–20 ms, a process called fast or open-state inactivation. In contrast to I_{IM} , for which no structural correlate has been found yet, the cytoplasmic linker between domains III and IV and the C terminus of the Na⁺ channel protein has been suggested to underlie I_{fast} . Mutations in these regions are known to disrupt this process, leading to LQT3. Since the putative target of CaMKII-dependent regulation could be located there, the authors investigated the effect of CaMKII δ_c on fast I_{Na} decay. Acute CaMKII δ_c overexpression significantly slowed the late component of fast I_{Na} inactivation (see τ_2 , Figure 5.6), which was sensitive to KN93.

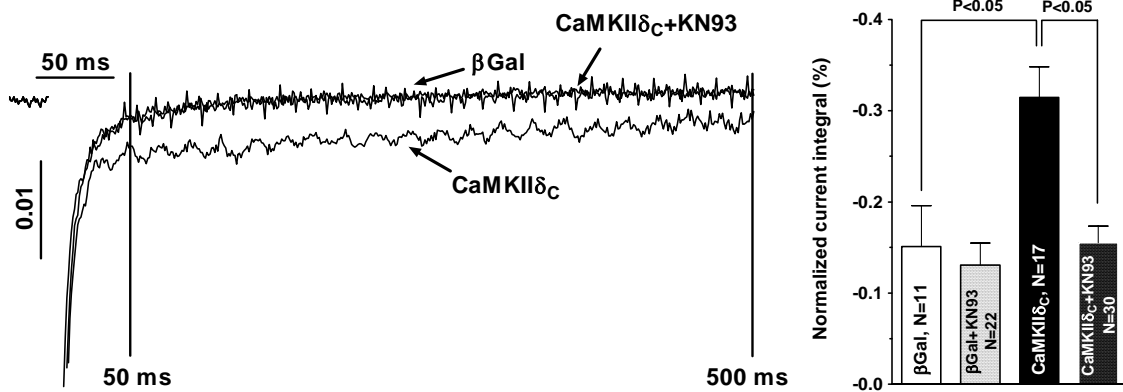


Figure 5.7: CaMKII δ_c enhances late I_{Na} . Currents were elicited at -20 mV (from -140 mV resting potential, duration 1000 ms), leakage subtracted and normalized to peak current. The current integral was calculated between 50 and 500 ms and displayed relative to the I_{Na} integral if no inactivation had occurred. Left, original traces. Right, mean data of the normalized current integral. Compared to control, adenovirus-mediated CaMKII δ_c overexpression resulted in a significantly increased late I_{Na} which could be restored back to control using KN93. Figure from Wagner *et al.* (2006a).

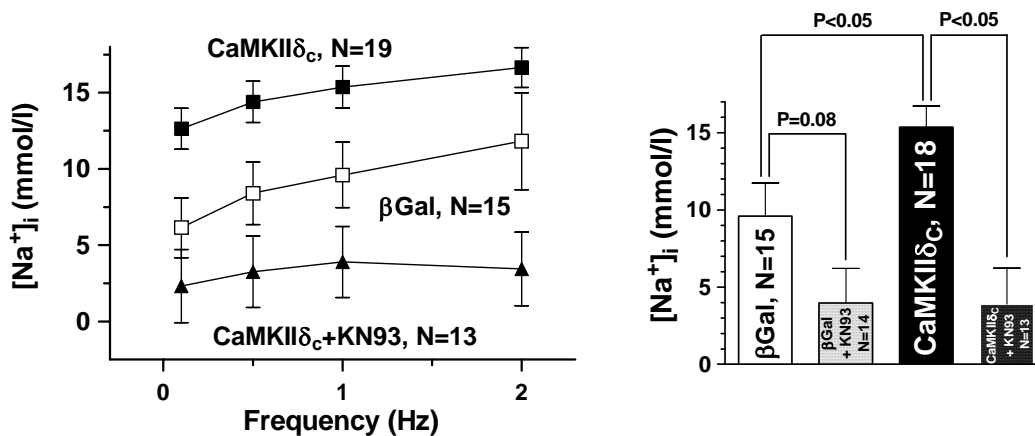


Figure 5.8: Mean data for $[Na^+]_i$ at different stimulation frequencies (left) and at 1 Hz (right) in rabbit myocytes. CaMKII δ_c overexpressing myocytes displayed a higher $[Na^+]_i$ at all stimulation frequencies ($P < 0.05$) that could be reduced using KN93 ($P < 0.05$). There was a trend towards a lower $[Na^+]_i$ in β Gal-transfected myocytes upon CaMKII-inhibition (KN93). Figure from Wagner *et al.* (2006a).

Incomplete I_{Na} inactivation during the AP can influence AP duration and $[Na^+]_i$ and can also be arrhythmogenic. A distinct persistent I_{Na} component was recorded in both acute (Figure 5.7) and chronic CaMKII overexpression, whereas it was not seen in β -gal rabbit or WT mouse myocytes. Again, KN93 prevented this persistent I_{Na} in CaMKII δ_c rabbit myocytes.

To assess the impact of these alterations in late I_{Na} on Na⁺ influx, the late I_{Na} (50–500 ms) was integrated and normalized to the cytosolic volume. Interestingly, the increased amount of Na⁺ influx upon CaMKII overexpression strikingly resembles the TTX-sensitive Na⁺ entry suggested to cause elevated $[Na^+]_i$ in an HF model with increased CaMKII activity (Despa *et al.*, 2002; Hoch *et al.*, 1999).

To assess whether the CaMKII-dependent alterations in I_{Na} gating cause increased $[Na^+]_i$, $[Na^+]_i$ was measured in field-stimulated myocytes. In CaMKII δ_C -overexpressing rabbit myocytes, $[Na^+]_i$ was significantly increased at all stimulation frequencies compared with that in control. This increase was completely reversed by KN93 (Figure 5.8).

CaMKII and arrhythmias

To test whether CaMKII δ_C mice were prone to VT, electrophysiological measurements *in vivo* were performed (Figure 5.9). Application of 2 consecutive premature beats via programmed electrical stimulation induced monomorphic and polymorphic VT. In addition, 1 Tg mouse died because of spontaneous ventricular fibrillation immediately after recordings were started. In contrast, no arrhythmias were observed in WT mice (Figure 8, A and C). In separate experiments, application of isoproterenol increased heart rate in WT mice, but no arrhythmias were observed (Figure 5.9, B and C). In contrast, in Tg mice, isoproterenol infusion induced monomorphic VT. Analysis of resting ECG parameters (Figure 5.9D) revealed that the corrected QT (QTc) interval and QRS duration were significantly prolonged in Tg versus WT mice. Interestingly, the PR interval was significantly shortened in Tg mice. CaMKII has been previously implicated in AV nodal conduction (Li *et al.*, 1998). To assess whether CaMKII δ_C overexpression alters AP duration depending on the heart rate, monophasic APs (MAPs) were recorded in isolated perfused hearts. After AV node ablation, Tg hearts had higher intrinsic ventricular heart rates. At high pacing frequencies (BCL, 100 ms), MAP duration was not significantly different for Tg versus WT hearts (Figure 5.9, E and F). It is possible that enhanced steady-state Na⁺ channel inactivation and disturbed open-state inactivation may counterbalance each other. At lower pacing frequencies physiological for mice, MAP duration was significantly prolonged in Tg hearts. This was

not reversible by CaMK inhibition, suggesting that other effects, possibly related to adaptation or HF, also affect repolarization in the chronic CaMKII expression model.

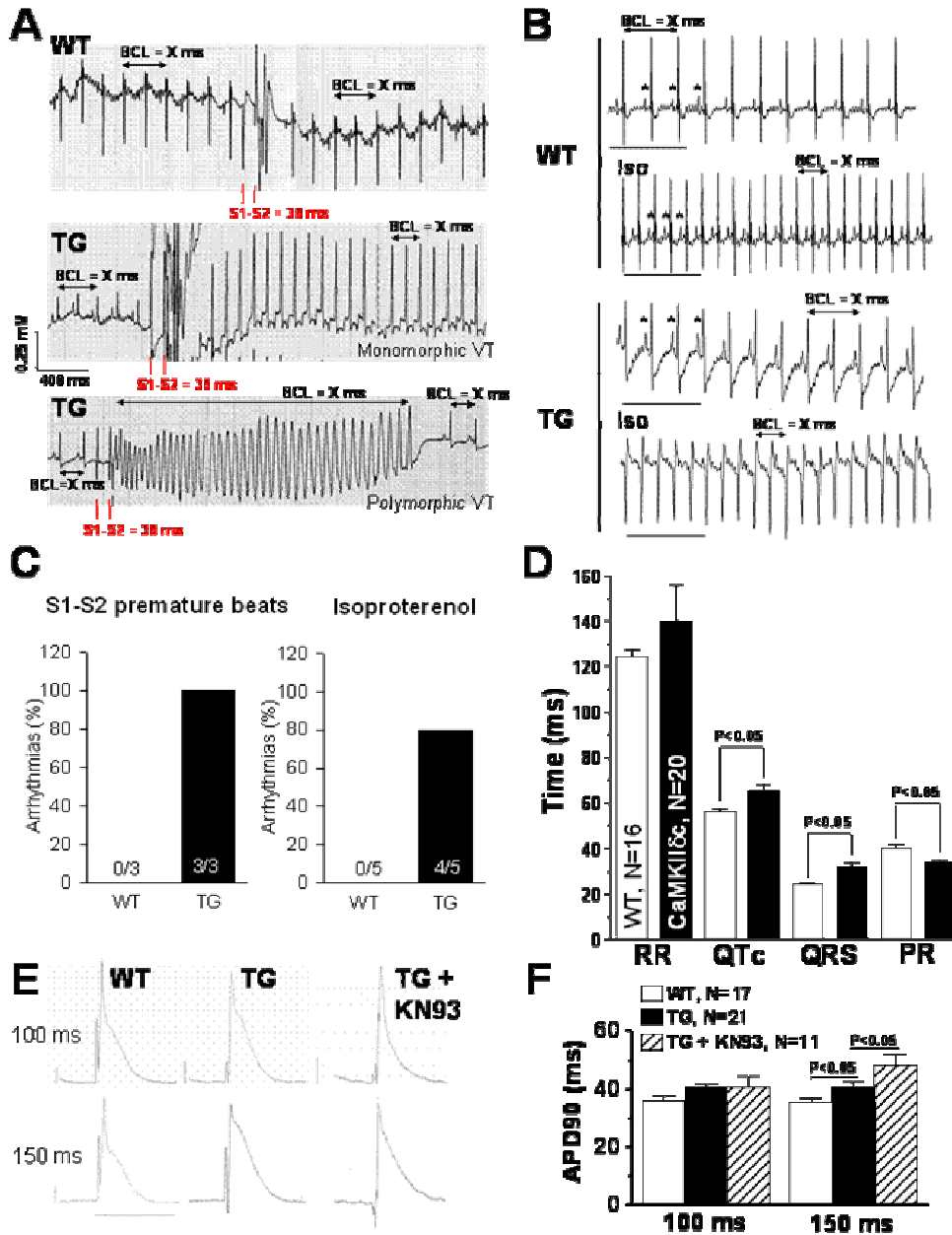


Figure 5.9: Arrhythmias in CaMKII δ_C -transgenic mice. (A) Programmed electrical stimulation in vivo; original ECG-traces are shown. (B) Representative ECG-traces are shown before (left) and after isoproterenol (Iso) administration. (C) Frequency of arrhythmia induction for programmed electrical stimulation (left) and isoproterenol (right). (D) Summary of resting ECG parameter data (RR interval, QTc interval, QRS duration and PR interval). (E) Original recordings of right ventricular monophasic action potentials (MAP) from hearts paced at cycle lengths of 100 (above) and 150 ms (below) for WT (left), TG (middle) and TG+KN93 (right). Bars reflect 1 mV and 100 ms. (F) Mean MAP durations at 90% repolarization (APD90). Figure from Wagner *et al.* (2006a).

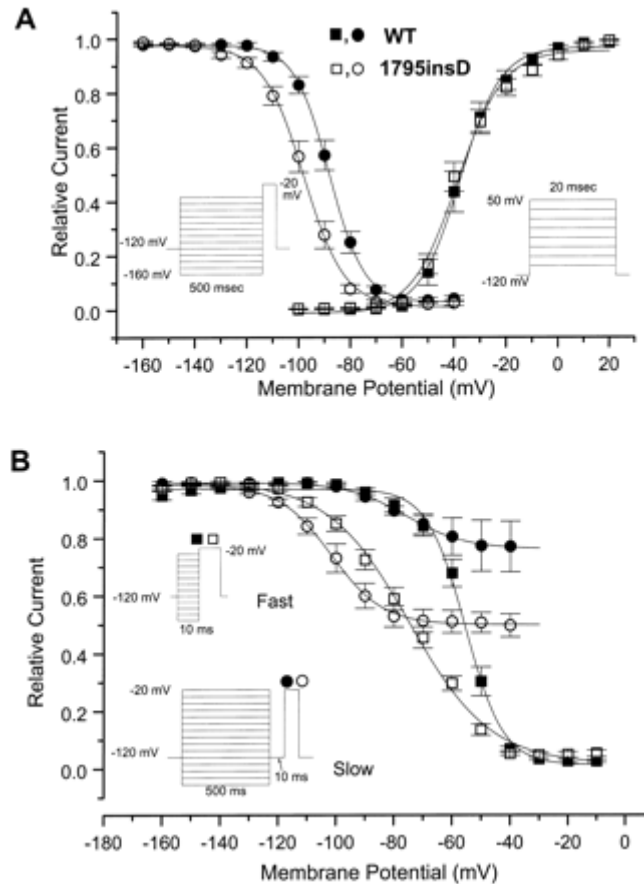


Figure 5.10: Voltage-dependent properties of 1795insD channel gating. A, Voltage dependence of activation and inactivation. The mutation caused a negative shift in the voltage dependence of inactivation but did not alter activation. B, Separation of steady-state inactivation into fast and slow inactivation using the voltage-clamp protocols inset. A larger fraction of channels underwent slow inactivation when depolarized. Figure from Veldkamp *et al.*, 2000.

The effective refractory period (ERP) was decreased in Tg hearts, resulting in progressive encroachment of excitation, a scenario known to cause VT (Wagner *et al.*, 2003).

Discussion

Wagner *et al.* (2006a) showed that acute CaMKII δ_C overexpression slows I_{Na} inactivation (both fast and slow phases), increases $[Na^+]_i$, enhances intermediate I_{Na} inactivation and slows recovery there from, shifts steady-state inactivation of Na⁺ channels to more negative E_m in a Ca²⁺-dependent manner, and all of these effects could be reversed with CaMKII inhibition. Overall, these CaMKII δ_C effects tend to prolong Na⁺ influx during depolarization (which may explain the enhanced $[Na^+]_i$), but increase steady-state inactivation of Na⁺ channels at shorter diastolic intervals. This combination

of effects could be particularly arrhythmogenic, and since CaMKII is elevated in HF (Kirchhefer et

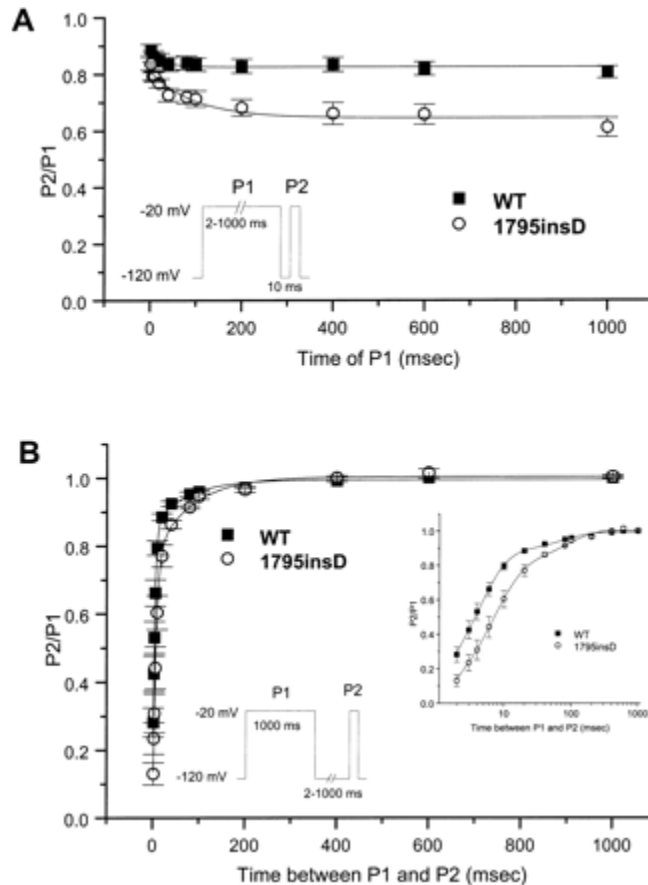


Figure 5.11: Enhanced slow kinetic component of inactivation for 1795insD. A, Development of slow inactivation was evaluated using the voltage-clamp protocol inset. B, Recovery from inactivation was also examined in the same cells using the protocol inset. Figure from Veldkamp *et al.*, 2000.

al., 1999; Hoch *et al.*, 1999), these effects could cause an acquired form of arrhythmogenesis. CaMKII δ_C enhances intermediate inactivation and reduces availability, while at the same time impairing fast inactivation and enhancing persistent I_{Na} . These divergent alterations of Na⁺ channel function cause a paradoxical phenotypic overlap of LQT3 (where I_{Na} inactivation is slowed or incomplete) and Brugada syndrome (where available I_{Na} is reduced), both thought to underlie arrhythmias. Indeed, the altered Na channel phenotype caused by CaMKII is very similar to that caused by 1795InsD mutation in human Nav1.5 that is linked with simultaneous LQT3 and Brugada syndrome features (Veldkamp *et al.* 2000, see chapter 3). As already discussed in chapter 3, the mutation disrupts fast inactivation, causing sustained Na⁺ current throughout the action

potential plateau and prolonging cardiac repolarization at slow heart rates (Figures 5.10 and 5.12). At the same time, 1795insD augments slow inactivation, delaying recovery of Na⁺ channel availability between stimuli and reducing the Na⁺ current at rapid heart rates (Figures 5.11 and 5.12). Therefore, it is conceivable that increased CaMKII δ_C activity in HF (Kirchhefer *et al.*, 1999; Hoch *et al.*, 1999) may alter Na⁺ channel gating thereby generating the substrate for life-threatening VT. In fact, the study shows that Tg mice are prone to VT. Surrogate parameters of the propensity for VT such as reduced effective refractory period, slowed intraventricular conduction and disturbed repolarization affirm these findings, albeit the underlying arrhythmic mechanisms remains to be elucidated.

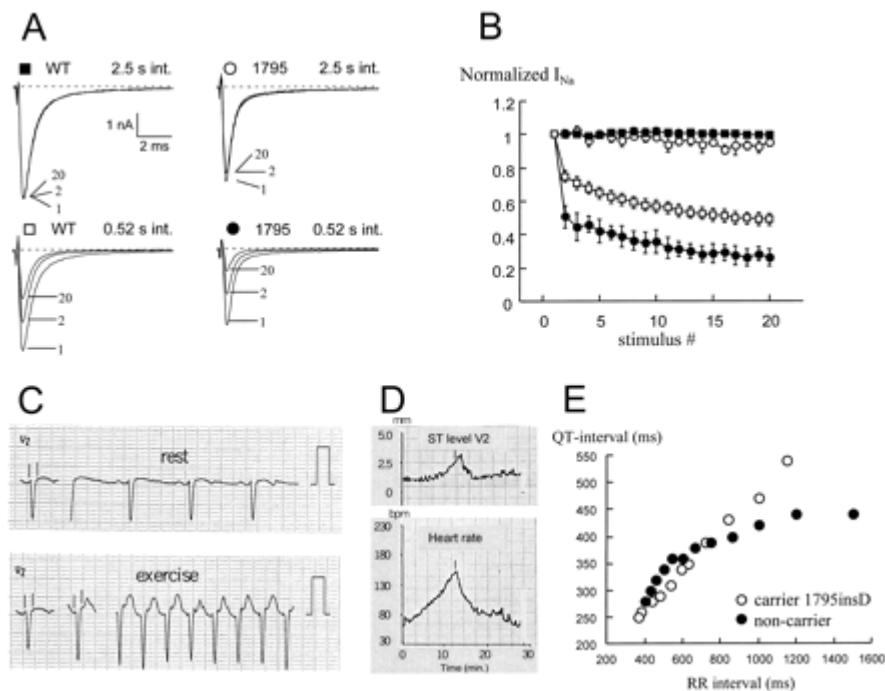


Figure 5.12: Rate-dependent changes in I_{Na} availability and the ECG phenotype. A, Wild-type (left) and mutant (right) I_{Na} recorded during the 1st, 2nd, and 20th depolarizations in a train of 0.5-second depolarizing pulses from -100 to 0 mV, at cycle lengths of 2.5 seconds (top) and 0.52 second (bottom). B, Plot shows normalized wild-type and mutant peak I_{Na} as a function of stimulus number for the rapid (0.52 second) and slow (2.5 seconds) stimulus rates. Currents were normalized to the first stimulus. C, ECG recorded during rest (top) and during an exercise test (bottom). Note the marked increase in ST-segment elevation during exercise. ST-segment elevation was measured at the J point (second vertical marker) with respect to the isoelectric line (indicated by the first vertical marker). Velocity was 25 mm/s, and the scale bars indicate 1 mV. D, Plot shows changes in ST-segment elevation (top) and heart rate (bottom) over time in response to exercise. E, QT interval is plotted against heart rate in the carrier and a family member of the same gender and similar age who does not carry the mutant allele. The QT interval was measured by hand in lead V2 at 1-minute intervals during the same exercise test as in panels C and D. In the carrier, at the longest R-R intervals, the QT interval is markedly prolonged (QT interval/[R-R interval] $>0.5 > 450$ ms). Figure from Veldkamp *et al.*, 2000.

6 Cardiac I_{Na} Markov Model Identification

Introduction

Mathematical models have been widely used to reproduce the voltage-dependent gating of ion channels. Modeling the results of electrophysiological characterization of ion channels allows the investigation of the effects of alterations of channel kinetic properties on the cell electrical activity by incorporating the current formulation in a comprehensive model of the cardiac action potential (Clancy *et al.*, 2002; Clancy and Rudy, 2002; Clancy and Rudy, 1999; Vecchietti *et al.*, 2005; Vecchietti *et al.*, 2006).

In order to obtain a Na^+ current model suited to analyze the effects of CaMKII δ_C overexpression at the action potential level, we used a Markov model structure, which has been proposed by Clancy (Clancy *et al.*, 2002; Clancy and Rudy, 2002), to reproduce the electrophysiologic characteristics of the Na^+ current measured in β Gal as well as in CaMKII δ_C overexpressing rabbit myocytes. Experimental data from Wagner *et al.*, 2006 (presented in the previous Chapter) were used to identify the transition rates between the states of the Markov model.

A description and the results of the model parameter identification are provided in the present Chapter. Then, the effects of the CaMKII δ_C -altered I_{Na} current on action potential and intracellular Na^+ concentration were assessed by incorporating the Markov model in the Shannon model of the rabbit ventricular myocyte described in Chapter 2.

Methods

The Markov model of I_{Na} is shown in Figure 6.1. The model contains two possible modes of gating, a background mode and a burst mode. The background mode reflects the normal sequence of activation and inactivation that most of the channels undergoes after voltage stimulation, whereas the burst mode reflects a small population of channels that transiently fail to inactivate. The background mode includes the upper nine states, consisting of three closed states (UC3, UC2, UC1), a conducting open state (UO), a fast inactivation state (UIF), and two intermediate inactivation states (UIM1 and UIM2) that are required to reproduce the complex fast and slow recovery features of inactivation. The UIM1 state acts as a channel “sink” in which the majority of channels reside but are

unable to recover and reopen during depolarization. Channels enter the UIM2 state via slow transitions. Channel closed-state inactivation is achieved via the inclusion of two closed-inactivation states (UIC2 and UIC3).

Since I_{Na} activation is a cooperative process (Chanda, Asamoah & Bezanilla, 2004) (activation of a voltage sensor in one domain influences activation in the other domains), three closed states, each representing a putative channel conformation are used, rather than modeling the activation of voltage sensors in each domain separately. Fast inactivation takes place preferentially from the open state reflecting its dependence on channel activation (Armstrong & Bezanilla, 1977; Bezanilla & Armstrong, 1977). Inactivation can then be stabilized by a transition from IF to an intermediate inactivated state IM1, which reflects participation of the C-terminus (Veldkamp *et al.*, 2000), and channels that are slowly inactivated reside in IM2. Finally, closed-state inactivation has been included by movement from C3 and C2 into the inactivated tier (IC3 and IC2) to correctly simulate channel availability (Clancy and Rudy, 2002).

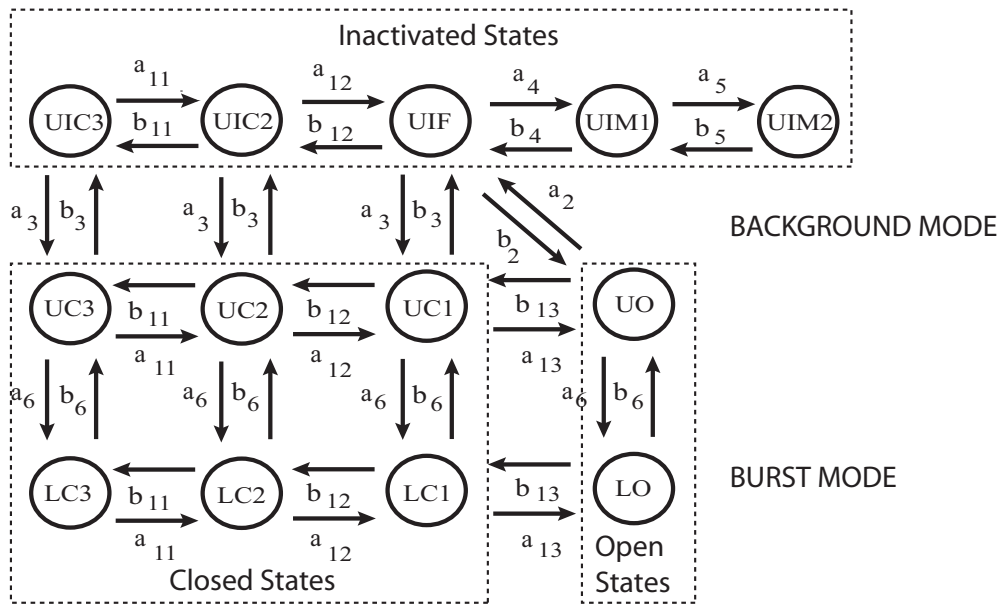


Figure 6.1: Markov model of the cardiac Na^+ channel. The channel model contains background (upper nine states) and burst (lower four states) gating modes. The burst mode reflects a population of channels that transiently fail to inactivate.

The lower four states in Figure 6.1 (prefixed with “L,” denoting “lower”) correspond to a burst mode of gating of channels that lack inactivation. Single channel experiments suggest that transitions between these modes are voltage independent since bursting may

persist through a series of pulses, depolarizing to -30 mV (over a period of 100 milliseconds) and repolarizing to -120 mV (over a period of 400 milliseconds). Hence transition rates between upper and lower states represent a probability of transition between the two modes of gating.

All the other transition rates depend on the membrane potential in a non-linear fashion. A full list of transition rates is reported in Table 6.1. They have been slightly changed with respect to the original Clancy's formulation (Clancy *et al.*, 2002; Clancy and Rudy, 2002).

Table 6.1 - Transition rate expressions (ms^{-1}).

Transition rates
$a_{11} = (P_{1a1}/(P_{2a1} \exp(-V/17)+0.20 \exp(-V/150)))$
$a_{12} = (P_{1a1}/(P_{2a1} \exp(-V/15)+0.23 \exp(-V/150)))$
$a_{13} = (P_{1a1}/(P_{2a1} \exp(-V/12)+0.25 \exp(-V/150)))$
$b_{11} = P_{1b1} \exp(-V/P_{2b1})$
$b_{12} = P_{1b12} \exp(-(V-P_{2b12})/(P_{2b1}))$
$b_{13} = (P_{1b13} \exp(-(V-P_{2b13})/(P_{2b1})))$
$a_3 = P_{1a3} \exp(-V/P_{2a3})$
$b_3 = (P_{1b3} + P_{2b3} V)$
$a_2 = (P_{1a2} \exp(V/P_{2a2}))$
$b_2 = (a_{13} a_2 a_3)/(b_{13} b_3)$
$a_4 = a_2/P_{1a4}$
$b_4 = a_3$
$a_5 = (P_{1a5} \exp(V/P_{2a5}))$
$b_5 = P_{1b5} \exp(-V/P_{2b5})$
$a_6 = 4.7e^{-7}$ for βGal ; $a_6 = 11.75e^{-7}$ for CaMKII
$b_6 = 9.5e^{-4}$

Macroscopic current density is given by:

$$I_{Na} = G_{Na} \cdot P_o \cdot (V - E_{Na}) \quad \text{where } G_{Na} = \sigma \cdot g_{Na}$$

The variable P_o is the sum of all channel open probabilities ($P_{UO} + P_{LO}$), V is the membrane potential, and E_{Na} is the Na reversal potential. G_{Na} is the maximum membrane conductance: channel density (σ) times the unitary channel conductance (g_{Na}). The changes in channel state probabilities are described by first order differential equations.

Table 6.2 - Transition rates maximally influencing each voltage clamp protocol.

Protocol	Transition rates
Activation; Tau	a ₂
Inactivation	a ₃ /b ₃
Recovery from Inactivation	a ₄ /b ₄ , a ₅ /b ₅
Late current	a ₆ /b ₆
Intermediate Inactivation	a ₄ /b ₄ , a ₅ /b ₅

Table 6.3 – Na⁺ channel model parameters for βGal and CaMKII channels

Parameters	βGal	CaMKII
P _{1a1}		3.802
P _{2a1}		0.1027
P _{1a2}		9.178
P _{2a2}		25
P _{1a3}		3.7933e ⁻⁷
P _{2a3}		7.7
P _{1b1}		0.1917
P _{2b1}		20.3
P _{1b12}		0.2
P _{2b12}		5
P _{1b13}		0.22
P _{2b13}		10
P _{1b3}	0.0042	0.0067
P _{2b3}		2e ⁻⁶
P _{1a4}		100
P _{1a5}	0.3543e ⁻³	0.6377 e ⁻³
P _{2a5}		23.2696
P _{1b5}	0.2868e ⁻³	4.57e ⁻⁵
P _{2b5}		35.9898

Assuming N discrete channel states (N=13 in the present model), the probability of the channel residing in a particular state P_i at any time satisfies:

$$\frac{dP_i}{dt} = \sum_{j=1}^N [k_{ji} \cdot P_j(t, V)] - \sum_{j=1}^N [k_{ij} \cdot P_i(t, V)]$$

for $i = 1, 2, \dots, N - 1; i \neq j$ and $\sum_{j=1}^N P_i = 1$

The voltage-dependent (V-dependent) rate constants k_{ij} describe the transition from state i to state j . Initial conditions are obtained by finding values for state probabilities from the steady-state equation:

$$\frac{dP_i}{dt} = 0$$

Microscopic reversibility is ensured by fixing the products of the forward and reverse transition rates of closed loops in the model.

Parameters, which appear in the expressions of transition rates listed in Table 6.1, were identified by a fitting procedure to reproduce with the Markov model the results of the electrophysiological characterization of cardiac Na^+ cardiac channel in β Gal and in CaMKII δ_C overexpressing rabbit myocytes. Experimental voltage-clamp data used in the present study have been reported in Wagner *et al.* (Wagner *et al.*, 2006) and summarized in the previous Chapter. The following voltage-clamp protocols were considered for parameter identification: steady-state activation, steady-state inactivation, intermediate inactivation, recovery from inactivation, late current and fast and slow time constants of current decay. Each voltage-clamp protocol, briefly described in the Results section as well as in the previous Chapter, was simulated. Afterwards, the representative curves for each protocol were obtained from the simulated currents as well as from the experimental ones. Simulated data were interpolated to obtain continuous curves and compared with the experimental data. A preliminary sensitivity analysis was performed to establish the transition rates that maximally influence the simulated data for each voltage-clamp protocol (Table 6.2). Then, the parameters of the transition rates were identified with an automatic procedure considering for each protocol only the group of transition rates disclosed by the sensitivity analysis. The Nelder-Mead simplex direct algorithm (Lagarias *et al.*, 1998) was used to find the parameter values minimizing the sum of the least-square errors between model predictions and experimental data. The parameters of the transition rates, that influence more than one protocol (see Table 6.2), were then manually tuned to have a good fitting on all the experimental data under analysis. The parameter values proposed by Clancy and Rudy (Clancy and Rudy 2002) were chosen as initial guesses in the minimization procedure to identify the transition rate parameters that allowed the best fitting of our β Gal data. The identified β Gal set (Table 6.3) was

subsequently used as initial guess to identify the CaMKII δ_C channel parameters. A full list of the parameters is reported in Table 6.3. Matlab R2006a and Simulink (The MathWorks Inc.- Natick, Mass) were used for all the numerical computations.

Results

In Chapter 5, the voltage clamp protocols assessing steady-state inactivation, activation, recovery from inactivation and intermediate were applied to the cells by using an extracellular solution containing 10 mM extracellular Na^+ . The parameter identification presented in this section is based on the data collected with a physiological extracellular Na^+ concentration of 140 mM (squares in Fig. 6). At this concentration, the activation curve is not available because the huge Na^+ currents evoked at 140 mM external Na^+ led to the loss of voltage control and thus to unreliable data. To overcome such limitation, the activation curve was fitted on experimental and simulated data available in the literature (Shannon *et al.*, 2004; Clancy and Rudy, 2002).

G_{Na} was set to 9 pA/pF to fit the value of I_{Na} peak amplitude.

Steady-state inactivation and activation

To assess the voltage dependence of steady state inactivation, current were measured upon test pulses to -20 mV (20 ms) after pre-pulses (500 ms) to -120:-20 mV (10 mV increment). According to experimental results, CaMKII δ_C overexpression shifts the inactivation curve to more negative potentials with respect to β Gal (see Fig. 6.2A).

Steady-state activation was assessed by stimulating the cell with 40 ms long voltage steps from a holding potential of -140 mV to -80:+60 mV (10 mV increment). The relative channel conductance was calculated by dividing peak current at a given membrane voltage by the driving force ($V_m - E_{Na}$). The resulting conductance was normalized to the maximal chord conductance. In accordance with the experimental data, simulated CaMKII δ_C overexpression does not affect channel activation with respect to β Gal (see Fig. 6.2B, β Gal and CaMKII δ_C traces are superimposed).

Recovery from inactivation

Recovery from inactivation was investigated using a sustained depolarization at a time scale that initiates fast and intermediate inactivation (1000 ms) followed by a recovery interval of incremental duration and a consecutive test pulse. CaMKII δ_C slows the

recovery from inactivation in our simulations, as well as in the experimental results (see Fig. 6.2C).

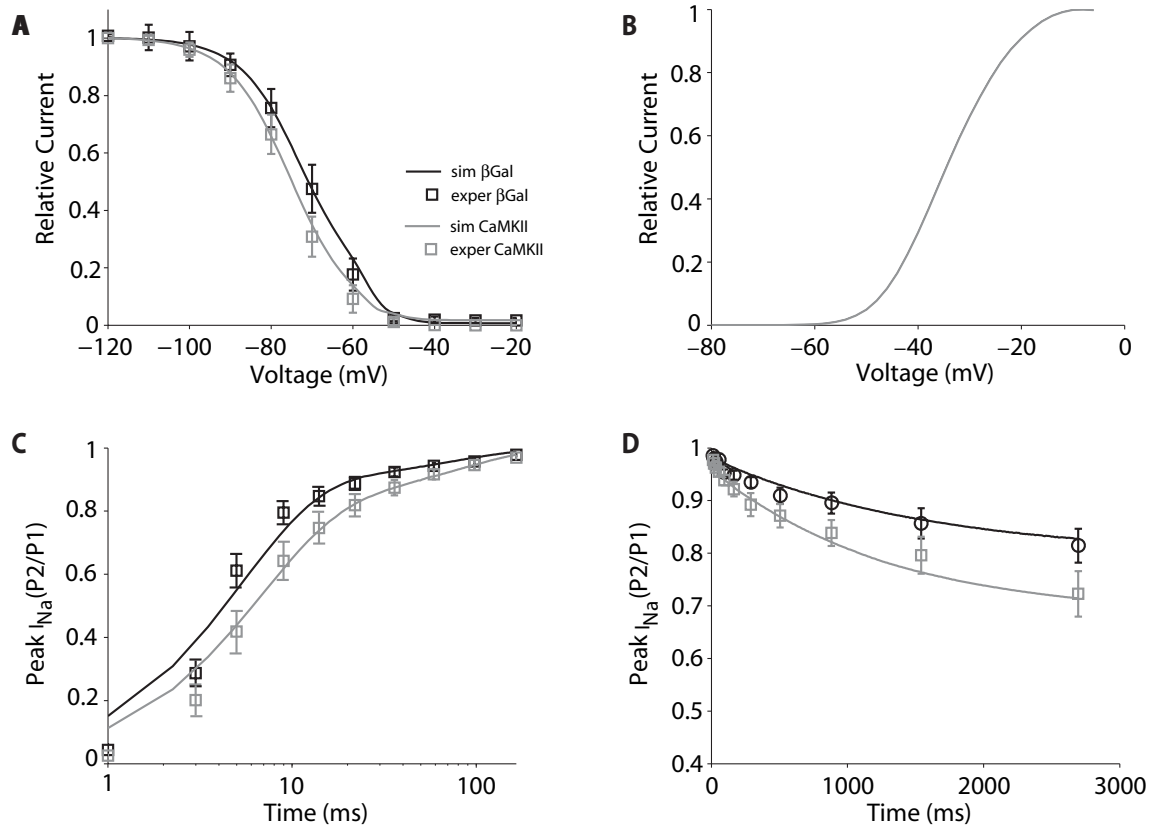


Figure 6.2: Experimental (squares) and simulated (solid lines) data at 140 mM external Na^+ concentration. A) Steady-state inactivation. CaMKII δ_C overexpression shifts the availability curve towards negative potentials. B) Activation. Na^+ channel activation is not affected by CaMKII δ_C overexpression (traces are superimposed). CaMKII δ_C slows the recovery from inactivation (C) and enhances the Intermediate Inactivation (D).

Intermediate inactivation

I_{IM} was measured using depolarizations of variable duration (P_1) followed by a 20 ms recovery period at -140 mV making all Na^+ channels that are not in I_{IM} available at the test pulse P_2 to -20 mV. In the computer simulation I_M is enhanced in CaMKII δ_C model (see Fig. 6.2D).

Fast and slow time constants of current decay

As evident from the simulated traces (Fig. 6.3A), CaMKII δ_C slows fast Na^+ channel inactivation in rabbit CaMKII δ_C myocytes compared to β Gal. The Na^+ current decay (first 50 ms) was fitted with a double exponential function. Fits (dotted lines) to the simulated traces (solid lines) and corresponding parameters τ_1 and τ_2 (ms) are shown in

black (β Gal) and grey (CaMKII δ_c). The deceleration of current decay was most prominent in the late component (right). τ_2 was longer compared to control (7.8 vs. 5.6 ms), whereas τ_1 appeared to be unchanged (1.3 ms). These data are in accordance with experimental results published by Wagner *et al.* (2006) and illustrated in Chapter 5 (compare with Fig. 5.6).

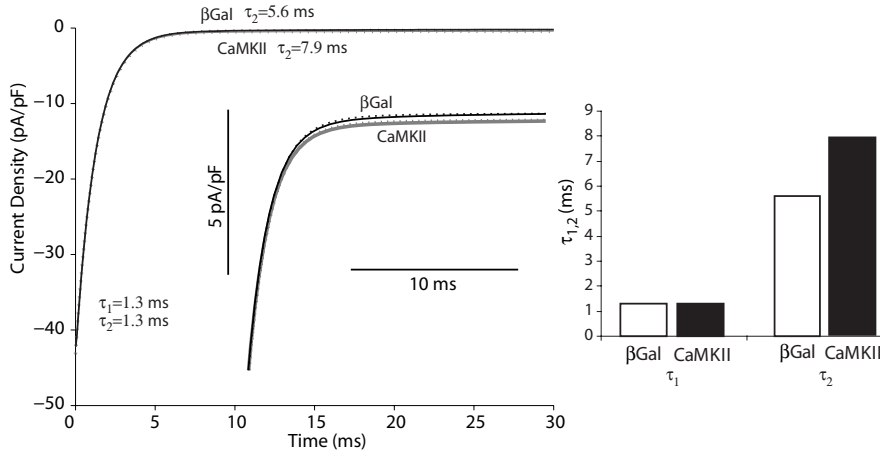


Figure 6.3: Fast and slow time constants of I_{Na} decay. Acute CaMKII δ_c overexpression slows the late component of fast I_{Na} inactivation.

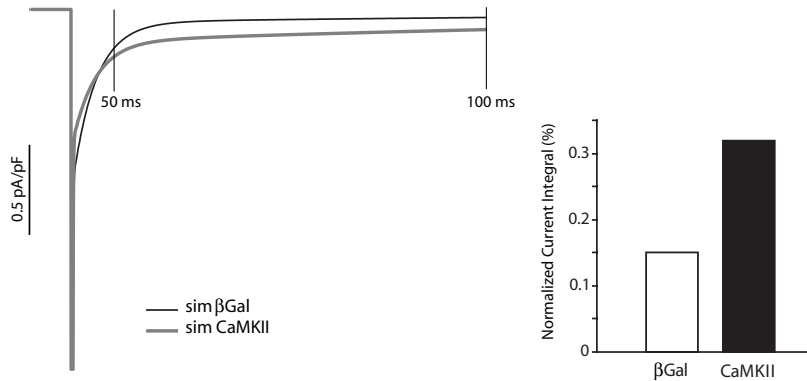


Figure 6.4: Late I_{Na} is enhanced by CaMKII δ_c overexpression. Left, simulated traces. Right, normalized current integral.

Late current

CaMKII δ_c enhances late I_{Na} . Currents were elicited at -20 mV (from -140 mV resting potential, duration 1000 ms), and normalized to peak current. The current integral was calculated between 50 and 500 ms (see Fig. 6.4) and displayed relative to the I_{Na} integral if no inactivation had occurred. As shown in Fig. 6.4, compared to control, adenovirus-mediated CaMKII δ_c overexpression resulted in a larger late I_{Na} . These results fit the experimental data shown in Chapter 5 (compare with Fig. 5.7, Wagner *et al.*, 2006)

Discussion

In this study we used a hidden Markov model to analyze the Na^+ current measured using whole-cell patch-clamp procedures in both β Gal and CaMKII δ_C overexpressing rabbit cardiomyocytes (Wagner *et al.*, 2006). The effects of CaMKII δ_C overexpression on the Na^+ current were accounted by assigning different values to model parameters with respect to the β Gal Na^+ channel.

Even if there is little experimental evidence for the existence of these distinct sodium channel states, the model proposed by Clancy and Rudy has been successfully used to simulate several Na^+ current features (Clancy *et al.*, 2002; Clancy and Rudy, 2002; Bondarenko *et al.*, 2004; Rivolta *et al.*, 2002). Irvine *et al.* (Irvine *et al.*, 1999) proposed a more sophisticated Na^+ channel model, which explicitly takes into account the influence of temperature. Clancy and Rudy (2002) used the nine state model only for the WT Na^+ channel, whereas they proposed a modified structure in which a ‘burst mode’ was introduced for Y1795C channels (Clancy *et al.*, 2002). Such modification was based on their observation that a very small Y1795C channel population (less than 0.02% (Tateyama *et al.*, 2003)) transiently fails to inactivate giving rise to single channel currents with very long mean open time (2.5 s (Clancy *et al.*, 2002)). To depict this behavior of Y1795C mutant channels they introduced in the model a second (long-lasting and non-inactivating) open state. This behavior (long-lasting bursts) has been shown to cause a whole-cell persistent current in presence of mutant cardiac Na^+ channels (Dumaine *et al.*, 1996). Thus the burst layer was incorporated both in β Gal and CaMKII δ_C Na^+ channel models. The transition rate a_6 (from the background to the burst level) has been set smaller in β Gal than in CaMKII δ_C to reproduce a smaller late current. The resulting model satisfactorily reproduces the main dynamic characteristics highlighted by standard whole-cell electrophysiology protocols and seems suited to analyze the effects of CaMKII δ_C overexpression at the action potential level.

Conclusions

The Markov model structure presented in this study, with different assignment of transition rates, is able to reproduce the main electrophysiological features characterizing cardiac Na^+ current in case of β Gal and CaMKII δ_C overexpression respectively. In particular, the model reproduces the enhanced sustained current as well as the

enhancement of fast and intermediate inactivation shown by the CaMKII δ_C overexpression. The proposed model can be a useful tool to analyze the effects of CaMKII δ_C -induced altered currents on action potential and Na⁺ influx, even if the effects of this protein on other transporters have to be taken into account.

7 Effects of CaMKII over-expression on cardiac excitability

Na⁺ Current

The Markov model of I_{Na} was incorporated in a comprehensive action potential model to investigate the consequences of the altered Na⁺ channel gating on myocyte electrical activity. The effects on the AP morphology and duration, as well as the alteration in the intracellular sodium concentration ($[Na^+]_i$) were investigated.

Methods

The ventricular AP was simulated by using the Shannon model of rabbit ventricular myocyte (Shannon *et al.*, 2004) implemented in Matlab R2006a (The MathWorks. Inc-Natick, Mass; USA).

The model was adjusted to correctly describe the ratio between slow and fast component of I_{To} to reproduce the experimental APD adaptation to the pacing rate observed in rabbit myocytes (Podgwozd *et al.*, 2001). To this purpose, the conductances of $I_{To,fast}$ and $I_{To,slow}$ were set to 0.02 and 0.06 mS/ μ F respectively.

The original formulation of the I_{Na} current was replaced with the Markov model. The maximal conductance G_{Na} at 37°C was calculated as 16.5 mS/ μ F both for β Gal and CaMKII ($Q_{10}=1.5$ (Milburn *et al.*, 1995; Correa *et al.*, 1991) for Na⁺ channel conductance). However, Wagner *et al.* collected data from cultured myocytes (the culture is necessary to overexpress CaMKII) rather than from freshly isolated myocytes. It is well known that the culture conditions lead to a reduction of the number of t-tubules and thus of the Na⁺ channel density (that are located on the t-tubules). A reduction of the peak I_{Na} by 40-50% is reported in cultured myocytes. To simulate the condition of freshly isolated myocytes, the maximal conductance G_{Na} was set to 23 mS/ μ F. All the kinetic rates were normalized to 37°C with a Q_{10} of 2.1. (Maltsev and Undrovinas, 2006).

Pacing was obtained by a current pulse train (pulses of 5 ms in duration) of 9.5 A/F in amplitude with different pacing rates. A variable order solver (ode15s) based on the numerical differentiation formulas (NDFs) was used to numerically solve the model equations (Shampine and Reichelt, 1997; Shampine *et al.*, 1999). The digital cell was

paced until a steady AP was reached. The APD was assessed at 90% of repolarization (APD₉₀).

Table 7.1 – Simulated APDs for β Gal and CaMKII δ_C overexpression at different pacing rates.

	APD ₉₀ (ms)	
	β Gal	CaMKII
0.25 Hz	326	583
0.5 Hz	310	474
1 Hz	262	323
2 Hz	203	213
3 Hz	175	179

Results

The ventricular cell computer model was used to analyze the effects of CaMKII δ_C -modulated Na⁺ channels on action potential morphology and duration and on the intracellular Na⁺ concentration. The effects of the Na⁺ channel kinetic alterations due to CaMKII overexpression on the ventricular action potential are shown in 7.1 for three pacing rates of 3 Hz (A), 1 Hz (B), and 0.25 Hz (C). The CaMKII mutant channel did not induce significant changes in AP morphology with respect to β Gal. The β Gal AP (black line) exhibits a characteristic spike-and-dome morphology and durations of 175, 262 and 326 ms respectively. In contrast, the CaMKII APs (grey line) exhibit distinctive rate-dependent durations. At fast rates (3 Hz), the CaMKII is completely superimposable with the control (Figure 7A, APD₉₀=179 ms). At slower rates (1 [Figure 7B] and 0.25 Hz [Figure 7C]), cell APs exhibit a significant prolongation that is enhanced as pacing is slowed (APD₉₀=323 ms at 1 Hz and APD₉₀=583 ms at 3 Hz). At low frequencies, impaired fast inactivation and persistent I_{Na} outweigh the slowed recovery from inactivation because of long lasting diastolic intervals. This favors AP prolongation. The CaMKII δ_C -induced AP prolongation is due to the presence of a larger inward late Na⁺ current during phases 2 and 3 of the AP (also β Gal induced a sustained Na⁺ current that is smaller than in the CaMKII δ_C case). However, at higher heart rates, the shorter recovery interval preventing complete Na⁺ channel recovery results in a reduction of Na⁺ channel availability (loss of function), that reduces the peak and abolishes the sustained current without evident effects on the AP duration. Indeed, the reduced availability of the Na⁺

channel is reflected in the decreased velocity of the AP upstroke (Figure 7.1A, inset). In Table 7.1 the APD₉₀ at pacing rate of 0.25, 0.5, 1, 2 and 3 Hz are summarized.

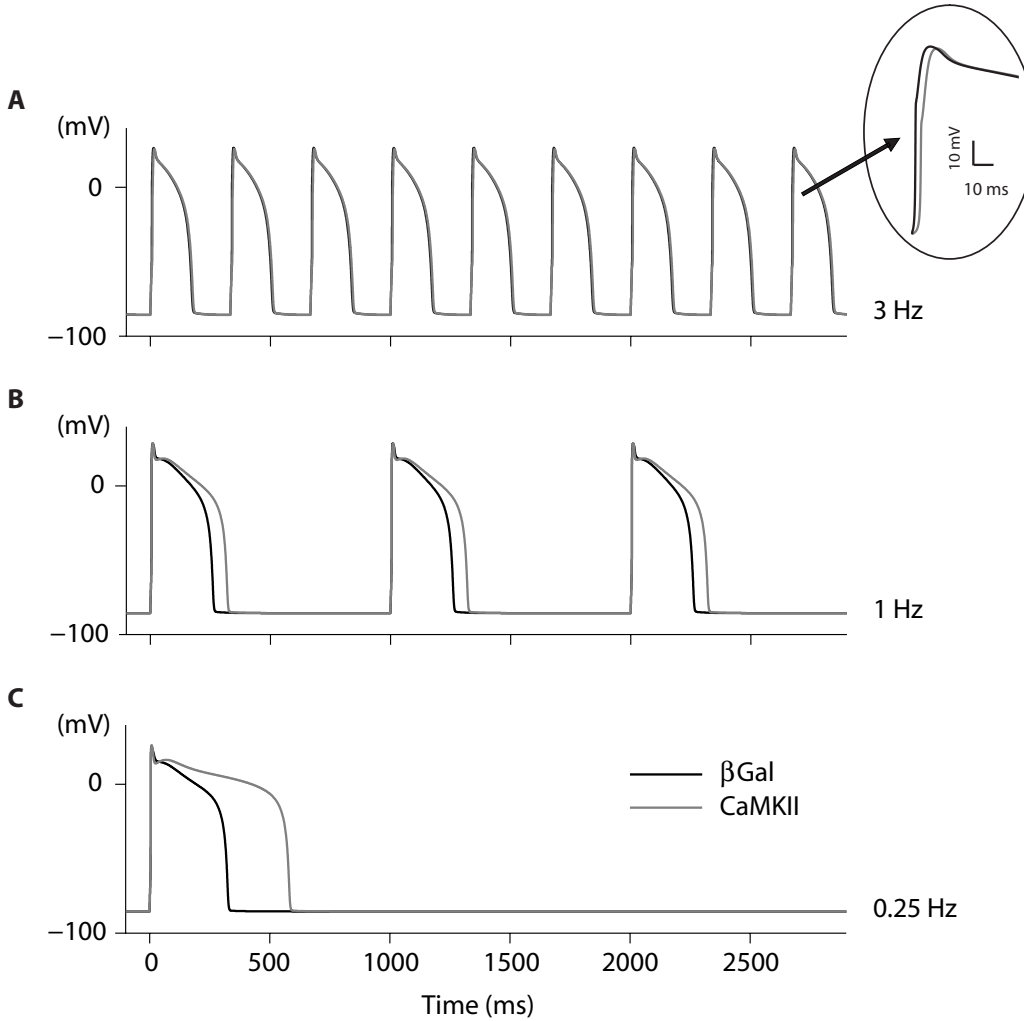


Figure 7.1: CaMKII effects on Na⁺ channel gating affects AP in a rate-dependent manner. At lower heart rates, the enhanced late I_{Na} prolongs the AP (B, C); this effect is completely blunted at higher rates (A), where the reduced channel availability slows down the AP upstroke (inset).

In Table 7.2, the influence of CaMKII δ_C overexpression on Na⁺ influx is shown. The higher sustained Na⁺ current in CaMKII δ_C myocytes leads to an increase in the intracellular Na⁺ concentration for low frequencies (where there is a significant contribution of the sustained Na⁺ current), whereas no differences are predicted at high frequencies. In addition, the observed increase is very small with respect to the higher [Na⁺]_i observed by Wagner *et al.* (2006a) in CaMKII overexpressing rabbit myocytes (Chapter 5, Figure 5).

Discussion

CaMKII δ_C enhances intermediate inactivation and reduces availability, while at the same time impairing fast inactivation and enhancing persistent I_{Na} . These divergent alterations of Na^+ channel function cause a paradoxical phenotypic overlap of Long QT type 3 (LQT3, where I_{Na} inactivation is slowed or incomplete) and Brugada syndrome (where available I_{Na} is reduced), both thought to underlie arrhythmias. Indeed, the altered Na^+ channel phenotype caused by CaMKII is very similar to that caused by 1795InsD mutation in human Nav1.5 that is linked with simultaneous LQT3 and Brugada syndrome features (Veldkamp *et al.*, 2000). The mutation disrupts fast inactivation, causing sustained Na^+ current throughout the action potential plateau and prolonging cardiac repolarization at slow heart rates. At the same time, 1795insD augments slow inactivation, delaying recovery of Na channel availability between stimuli and reducing the Na current at rapid heart rates (Clancy and Rudy, 2002; Veldkamp 2000).

Table 7.2 – Simulated intracellular Na^+ concentrations for β Gal and CaMKII δ_C overexpression at different pacing rates.

	[Na^+] _i (mM)	
	β Gal	CaMKII δ_C
0.25 Hz	7.2	7.8
0.5 Hz	8.0	8.7
1 Hz	9	9.4
2 Hz	10.5	10.5
3 Hz	11.6	11.6

Similarly, the effects of CaMKII on the Na^+ channel gating have a differential impact on the AP depending on the pacing rate. At low frequencies the simulations show a gain of function of the Na^+ current, with the presence of a late current that prolongs the repolarization. The sustained current decreases with the increase in the pacing rate, where a loss of function (reduced peak current) is predicted. This loss of Na^+ channel function, due to the reduction in the channel availability, would slow propagation and increase dispersion of repolarization. The intriguing thing with respect to CaMKII is that CaMKII-dependent I_{Na} regulation due to upregulated CaMKII in heart failure could constitute a common acquired form of arrhythmia (combined Long QT and Brugada syndrome), in

otherwise normal Na⁺ channels. Such an acquired Na⁺ channel disfunction may contribute to arrhythmia under conditions where CaMKII effects are enhanced, as in HF. Interestingly, CaMKII has already been linked to casually to ventricular arrhythmias in a mouse model of cardiac hypertrophy and failure by Anderson's group (Wu *et al.*, 2002; Zhang *et al.*, 2005).

However, increased levels of CaMKII in HF may target several proteins in the ventricle (Maier and Bers, 2006). As already discussed (Chapter 5), CaMKII phosphorylates Ca²⁺ transport proteins such as phospholamban, ryanodine receptors and L-type calcium channels. In addition, other ion channels, including sarcolemmal Na⁺ and K⁺ channels are regulated by this CaMKII.

The further step of the study (see next sections) was then to incorporate the reported effects of CaMKII on the other sarcolemmal targets: the L-type channels (responsible for the L-type Ca²⁺ current I_{CaL}) and the K⁺ channels K_V1.4 and K_V4.3 (respectively responsible for slow and fast component the transient outward K current I_{To}).

The model excludes the possibility that the alteration reported by Wagner on Na⁺ channel gating might account for the higher Na⁺ concentration in CaMKII overexpressing rabbit myocytes. Further experiments should be performed (e.g. using the specific Na channel blocker tetrodotoxin, TTX) to assess whether a window current at diastolic membrane potentials, accounting for a persistent sodium influx at the physiological resting potential, may occur. Another possibility is that additional Na⁺ transportes, other than the voltage-dependent sodium channel, may be involved in the CaMKII-mediated increase in [Na⁺]_i, even if a role of the Na⁺/K⁺ pump, the primary responsible of Na⁺ extrusion form the cell, has been previously ruled out (Despa *et al.*, 2001).

L-type Ca²⁺ and K⁺ Transient Outward Current

CaMKII modulates voltage gated L type Ca²⁺ channels and thereby Ca²⁺ current (I_{CaL}). Several groups independently demonstrated that Ca-dependent I_{CaL} facilitation (positive staircase of I_{CaL} with repeated depolarizations) is mediated by CaMKII-dependent phosphorylation (Anderson *et al.* 1994; Yuan and Bers, 1994). By overexpressing CaMKII δ_C in adenovirus-mediated rabbit ventricular myocytes I_{CaL} amplitude was increased and inactivation was slowed (Kohlhaas *et al.* 2006).

Table 7.3 – Parameter changes for I_{CaL} and I_{To}. [Ca²⁺]_c is the Ca concentration in the actual compartment (either subsarcolemma or junction).

	βGal	CaMKII
I _{CaL}		
G _{CaL}	100%	115%
df _{Ca} /dt	1.7 [Ca ²⁺] _c (1-f _{Ca})-11.9e ⁻³ f _{Ca}	1.2 [Ca ²⁺] _c (1-f _{Ca})-11.9e ⁻³ f _{Ca}
I _{to,slow}		
G _{To,slow}	0.06 mS/ μ F	0.09 mS/ μ F
X _{To,slow}		1/(1+exp(-(V+3)/15))
Y _{To,slow}		1/(1+exp((V+33.5)/10))
R _{To,slow}		1/(1+exp((V+33.5)/10))
TauX _{To}		9/(1+exp((V+3)/15))+0.5
TauY _{To}	182 /(1+exp((V+33.5)/10))+1	15 /(1+exp((V+33.5)/10))+1
TauR _{To}	8085 /(1+exp((V+33.5)/10))+ 313	3600 /(1+exp((V+33.5)/10))+ 500
I _{to,fast}		unchanged

I_{To} currents are generally classified in two different types, "fast" (I_{To,f}) and "slow" (I_{To,s}), with different recovery from inactivation time constants. A general consensus exists that whereas I_{To,f} is mediated by Kv4.2 and/or Kv4.3 channels, I_{To,s} is generated primarily by Kv1.4 channels. Several signaling systems have been shown to modulate I_{To}, including some using CaMKII. In preliminary studies in rabbit ventricular myocytes acutely overexpressing CaMKII, Wagner *et al.* (Wagner *et al.* 2006b) found a CaMKII-dependent enhancement of I_{To} consistent with increased Kv1.4 function and AP shortening.

The modulation of I_{CaL} (larger current amplitude and slower inactivation) and I_{To} by CaMKII (enhancement of the slow component and faster recovery from inactivation) was

incorporated in the model of rabbit ventricular AP to investigate the impact these CaMKII effects on the AP (that was expected to be prolonged by the sole effect of I_{Na}).

Methods

The L-type Ca^{2+} current was modified to reproduce the effects of CaMKII as follow: the channel maximal conductance was increased by 15% and the Ca^{2+} dependent inactivation was modified as shown in Table 7.3.

The formulations (Table 7.3) of the slow and fast component of I_{T0} were adapted to account for the increased expression levels of Kv1.4 channels ($G_{T0,slow}$ was increased by 50%) and for the enhanced recovery from inactivation in CaMKII overexpressing rabbit myocytes (the time constants of inactivation were modified accordingly).

The AP simulations and APD measurements were performed as previously described in this chapter.

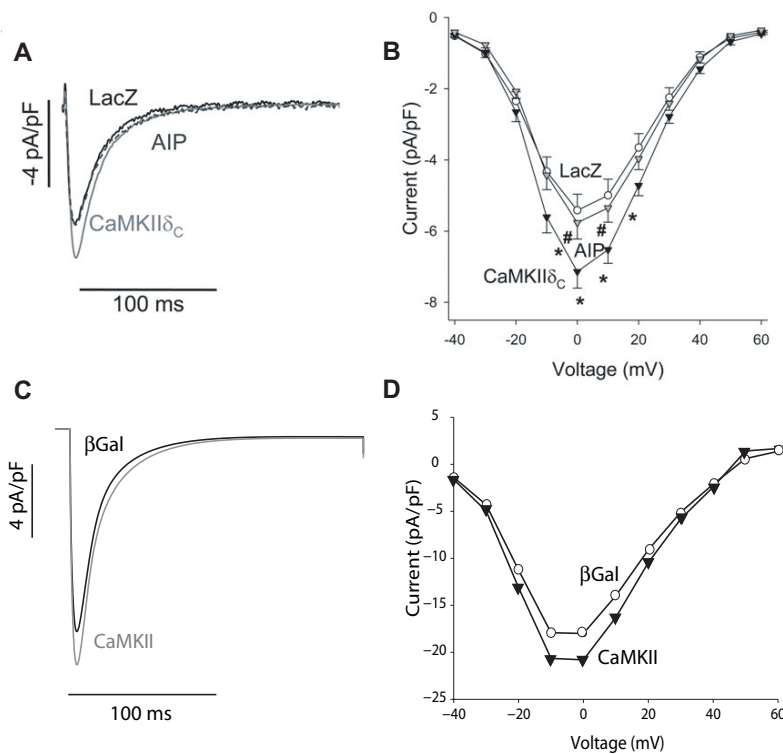


Figure 7.2: CaMKII effects on I_{CaL} . Experimental (A) and simulated (C) traces recorded upon a depolarization pulse. Experimental (B) and simulated (D) I-V relations. I_{CaL} is significantly increased in CaMKII δ_C vs control (LacZ). Inactivation is slowed by CaMKII δ_C . Experimental data (upper panel) are from Kohlhaas *et al.*, 2006.

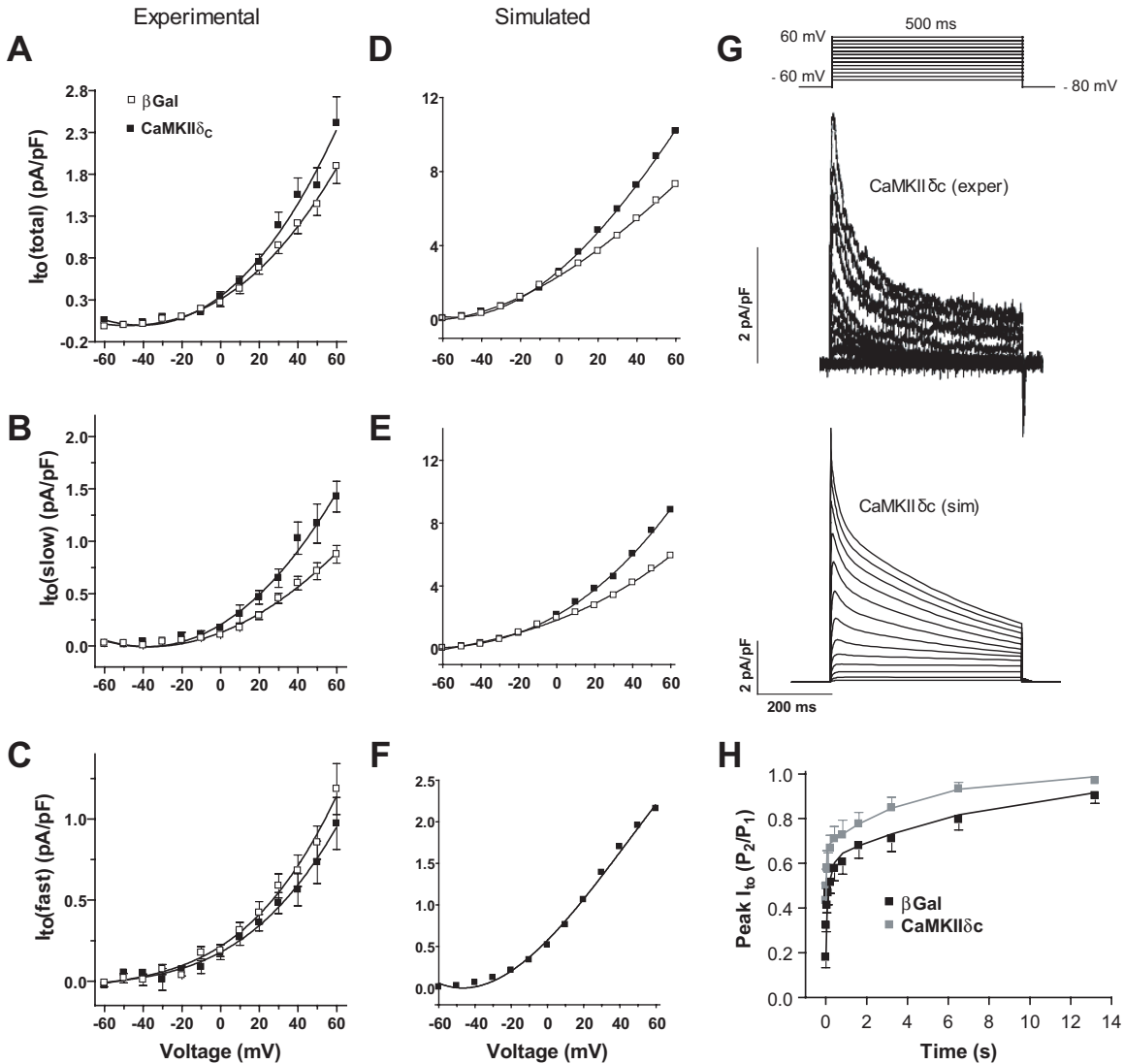


Figure 7.3: CaMKII effects on I_{T0} . Experimental (left) and simulated (middle panel) I-V relations for total (A, D), slow (B, E) and fast (C, F) I_{T0} . CaMKII δ_C (close symbols) mediated increase of the total current is mainly due to CaMKII δ_C effects on the slow component. G) Representative current traces during under voltage clamp activation protocol for experimental (upper) and simulated (lower) CaMKII mediated I_{T0} . H) Recovery from inactivation was investigated using a 500 ms depolarization pulse (from -80 mV holding potential to +50 mV) followed by recovery intervals of increasing durations and a subsequent test pulse. Recovery from inactivation is significantly increased by CaMKII δ_C . Symbols represent experimental data, lines represent simulation results for β Gal (black) and CaMKII (grey). Experimental data are from Wagner *et al.* (unpublished).

Results

I_{CaL}

Figure 7.2 shows experimental and simulated *I_{CaL}*-voltage relationships, where peak *I_{CaL}* is increased in CaMKII δ_C versus control. Also, the *I_{CaL}* decay time constant was prolonged in CaMKII δ_C versus control myocytes.

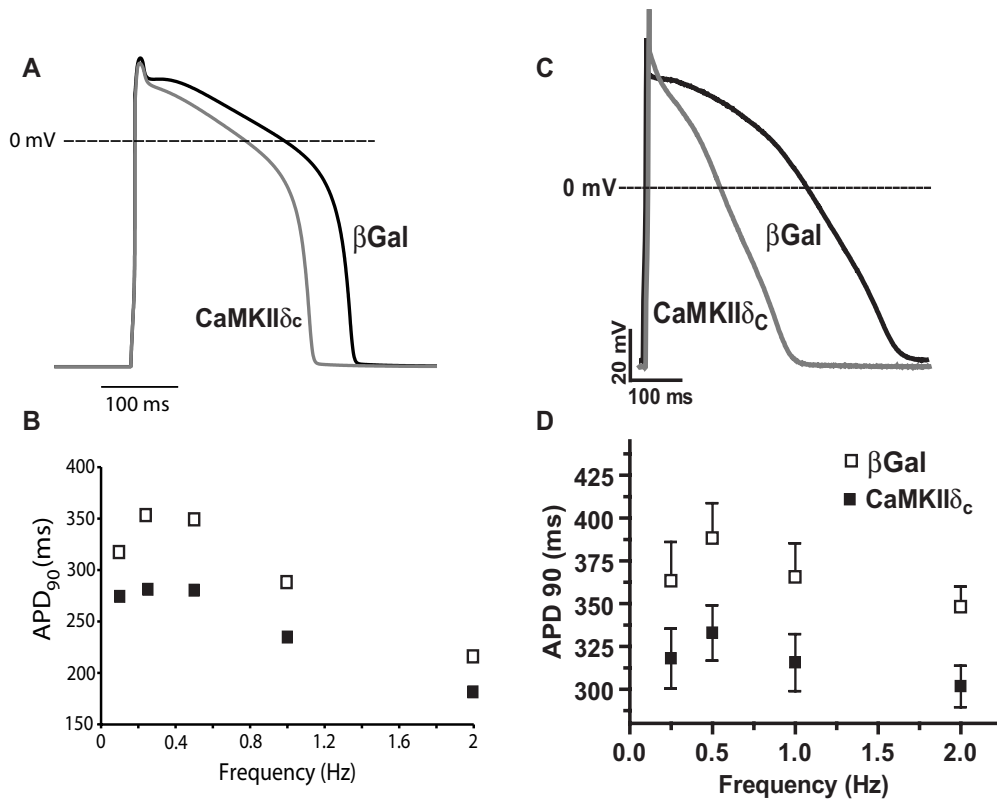


Figure 7.4: Simulated (A, B) and experimental (C, D) action potentials and APD-frequency relations in β Gal and CaMKII δ_C overexpressing cardiac myocytes.

The APD shows the typical dependence on the pacing frequency in rabbit myocytes, with an ascending phase to 0.25-0.5 Hz and a descending phase to higher frequencies.

I_{T0}

The agreement between the simulated and experimental transient outward currents is shown in Figure 7.3. The total *I_{T0}* current was significantly larger in rabbit myocytes overexpressing CaMKII δ_C both in experimental and simulated data (Figure 7.3 A, D). The increase of total *I_{T0}* appears to be mainly due to a significant increase of *I_{T0,slow}* (Figure 7.3 B, E), whereas CaMKII δ_C overexpression does not significantly alter *I_{T0,fast}* (Figure 7.3 C, F). Representative traces of total *I_{T0}* are shown in Figure 7.3 (G) for

experimental and simulated CaMKII δ_C overexpression. Recovery from inactivation was significantly enhanced in CaMKII δ_C overexpressing rabbit myocytes (Figure 7.3 H).

Action Potential Simulations

The effects of the Na⁺, Ca²⁺ and K⁺ current alterations due to CaMKII overexpression on the ventricular action potential are shown in 7.4 for the pacing rate of 1 Hz (A), as well as the APD dependence on pacing frequency (B). Experimental data from Wagner *et al.* (unpublished) are also shown for comparison (C, D). The combination of CaMKII δ_C effects on the sarcolemmal currents leads to the shortening of the AP, in accordance with the APs recorded from CaMKII δ_C overexpressing rabbit myocytes.

The CaMKII-dependent enhancement in the repolarizing current I_{To} (in particular its slow inactivating component) is shown to counterbalance and reverse the effects of AP prolongation that would occur if only the depolarizing currents I_{Na} and I_{CaL} were affected.

Concluding remarks

The present study aimed to show the contribution of mathematical modelling and numerical simulation in the understanding of the interplay among the several factors playing a role in cardiac cell excitability. The attention was focused on the cardiac sodium (Na^+) channel that controls cardiac excitability and the velocity of impulse propagation by initiating the action potential (AP). Different disorders in heart excitability have been related to derangements of the cardiac Na^+ channel due to either genetic mutations or acquired diseases, such as heart failure (HF). These disorders are characterized by enhanced arrhythmia susceptibility. A number of inherited diseases associated to mutations in *SCN5A*, the gene encoding the alpha subunit of the cardiac Na channel, have been discovered and linked to Long QT type 3 (LQT3) and Brugada (BrS) syndromes, conduction diseases and structural defects. Notably, mutations showing overlapping phenotypes have been characterized. As an example, 1795InsD mutation in human *SCN5A* is linked with simultaneous LQT3 and BrS features.

A 9-state Markov model of the cardiac Na^+ current was used to investigate two mutations in the C-terminus of the Na^+ channel associated to LQT3 and BrS (Y1795C and Y1795H respectively). The dynamic Luo-Rudy model of the ventricular AP was used to analyse their influence on action potential and the administration of sodium channel blockers (flecainide and mexiletine) was simulated. The model predicted that the Na^+ current alteration induced by Y1796C mutation prolonged the action potential in a cell type and frequency dependent fashion, confirming the higher susceptibility of M cells and the dangerousness of bradycardia for LQT3 patients.

Conversely, Na^+ current alteration induced by Y1795H mutation, associated to BrS, did not alter action potential morphology in agreement with mild electrocardiographic manifestations at baseline of the patients harbouring this mutation.

Flecainide and Mexiletine are antiarrhythmic drugs used to restore physiological QT interval duration in LQT3 subjects, while Flecainide but not Mexiletine unmask BrS carriers in which ST segment elevation is not evident. In agreement with clinical

CONCLUDING REMARKS

observation, the model predicted that both Flecainide and Mexiletine shorten action potential in LQT3 cells, but only Flecainide caused an ‘all or none’ AP in BrS epicardial cell that may be responsible of the ST segment displacement observed in BrS patients after the administration of Flecainide. The study also suggests that Flecainide is able to unmasked concealed BrS patients as it blocks more markedly the L-Type calcium current (I_{CaL}) than Mexiletine.

Na^+ channel gating modifications have been recently linked also to acquired diseases, such as drug-induced Long QT syndrome, cardiac ischemia and HF. It has recently been shown that the calcium/calmodulin-dependent protein kinase II (CaMKII) regulates Na channel gating, which may underlie the propensity to arrhythmia in HF where CaMKII expression is increased. Interestingly, the modulation of Na^+ current upon CaMKII overexpression shows striking similarities with the alterations in the kinetic properties of the Na^+ channel caused by the 1795InsD mutation (overlapping LQT3 and BrS).

To assess whether its effects on the Na^+ channel may participate to a proarrhythmic substrate, a 13-state model of the Na^+ current was implemented to isolate the sole impact of Na channel gating alterations on the action potential morphology and duration in HF. CaMKII δ_C enhances intermediate inactivation and reduces availability, while at the same time impairing fast inactivation and enhancing persistent I_{Na} . These divergent alterations of Na^+ channel function cause a paradoxical phenotypic overlap of LQT3 (where I_{Na} inactivation is slowed or incomplete) and Brugada syndrome (where available I_{Na} is reduced): the effects of CaMKII on the Na^+ channel gating have a differential impact on the AP depending on the pacing rate. At low frequencies the simulations show a gain of function of the Na^+ current, with the presence of a late current that prolongs the repolarization (Long QT-like). With the increase in the pacing rate a loss of function (reduced peak current) is predicted. This loss of Na^+ channel function, due to the reduction in the channel availability, would slow propagation and increase dispersion of repolarization (BrS-like). The intriguing thing with respect to CaMKII is that CaMKII-dependent I_{Na} regulation due to upregulated CaMKII in heart failure could constitute a common acquired form of arrhythmia (combined Long QT and Brugada syndrome), in otherwise normal Na^+ channels. Such an acquired Na^+ channel disfunction may contribute to arrhythmia under conditions where CaMKII effects are enhanced, as in HF.

CONCLUDING REMARKS

The increased levels of CaMKII in HF may target several proteins in the ventricle: Ca^{2+} transporter, such as ryanodine receptors, phospholamban and L-type calcium channels, but also non- Ca^{2+} transporters, such as sarcolemmal Na^+ and K^+ channels. The effects of CaMKII on the other sarcolemmal targets were incorporated into the model: the L-type channels (responsible for the L-type Ca^{2+} current I_{CaL}) and the K^+ channels $\text{K}_{\text{V}1.4}$ and $\text{K}_{\text{V}4.3}$ (respectively responsible for slow and fast component the transient outward K current I_{To}). The model showed that a gain of function of $I_{\text{To,slow}}$ due to $\text{CaMKII}\delta_{\text{C}}$ overexpression is sufficient to explain the AP shortening observed in $\text{CaMKII}\delta_{\text{C}}$ overexpressing rabbit cardiomyocytes.

On the basis of such analyses the present thesis shows how a mathematical approach is suitable to provide clues for understanding arrhythmogenic mechanisms associated with mutation-dependent or acquired channelopathies.

References

- Abriel H, Cabo C, Wehrens XHT, Rivolta I, Motoike HK, Memmi M, Napolitano C, Priori SG, and Kass RS. 2001. Novel arrhythmogenic mechanism revealed by a long-QT syndrome mutation in the cardiac Na⁺ channel. *Circ Res* 88: 740–745
- Abriel H, Kamynina E, Horisberger JD and Staub O. 2000. Regulation of the cardiac voltage-gated Na⁺ channel (H1) by the ubiquitin-protein ligase Nedd4, *FEBS Lett* 466: 377–380.
- Abriel H and Kass RS. 2005. Regulation of the voltage-gated cardiac sodium channel Nav1.5 by interacting proteins. *Trends in Cardiovascular Medicine* 15(1): 35-40 Review.
- Akar FG, Wu RC, Deschenes I, Armoundas AA, Piacentino V III, Houser SR, and Tomaselli GF. 2004. Phenotypic differences in transient outward K⁺ current of human and canine ventricular myocytes: insights into molecular composition of ventricular Ito. *Am J Physiol Heart Circ Physiol*. 286: H602-H609.
- An RH, Wang XL, Kerem B, Benhorin J, Medina A, Goldmit M, and Kass RS. 1998. Novel LQT-3 mutation affects Na⁺ channel activity through interactions between alpha- and beta1-subunits. *Circ Res* 83: 141–146
- Anderson ME. 2004. Calmodulin kinase and L-type calcium channels: a recipe for arrhythmias? *Trends Cardiovasc Med*. 14(4):152-61. Review.
- Anderson ME, Braun AP, Schulman H, Premack BA. 1994. Multifunctional Ca²⁺/calmodulin-dependent protein kinase mediates Ca²⁺-induced enhancement of the L-type Ca²⁺ current in rabbit ventricular myocytes. *Circ Res*. 75(5):854-61.
- Antzelevitch C, Brugada P *et al*. Brugada Syndrome:1992-2002. 2003. A Historical Perspective. *J Am Coll Cardiol*. 41:1665-1671.
- Antzelevitch C, and Fish J. 2001 Electrical heterogeneity within the ventricular wall. *Basic Res Cardiol*. 96: 517-527.
- Antzelevitch C, Yan G, Shimuzu W, and Burashnikov A. Electrical heterogeneity, the ECG, and cardiac arrhythmias. 2000. In: *Cardiac Electrophysiology: From Cell to Bedside*, edited by Zipes DP and Jalife J. Philadelphia, PA: Saunders, p. 222–238.
- Armstrong CM, and Bezanilla F. 1977. Inactivation of the sodium channel. II. Gating current experiments. *J Gen Physiol* 70, 567-90.
- Banyasz T, Fulop L, Magyar J, Szentandrassy N, Varro A, and Nanasi PP. 2003. Endocardial versus epicardial differences in L-type calcium current in canine ventricular myocytes studied by action potential voltage clamp. *Cardiovasc Res*. 58: 66-75.
- Bassani JWM, Bassani RA, and Bers DM, 1994. Relaxation in rabbit and rat cardiac cells: Species-dependent differences in cellular mechanisms. *J. Physiol*. 476:279–293.
- Bassani RA, Altamirano J, Pugliesi JL, and Bers DM. 2004. Action potential duration determines sarcoplasmic reticulum Ca²⁺ reloading in mammalian ventricular myocytes. *J. Physiol*. 559(Pt 2):593-609.

REFERENCES

- Beeler GW, Reuter H. 1977. Reconstruction of the action potential of ventricular myocardial fibers. *J. Physiol.* 268, 177–210.
- Benhorin J, Taub R, Goldmit M, Kerem B, Kass RS, Windman I, and Medina A. 2000. Effects of flecainide in patients with new *SCN5A* mutation: mutation-specific therapy for long-QT syndrome? *Circulation.* 101: 1698-1706.
- Benndorf K, and Nilius B. 1987. Inactivation of sodium channels in isolated myocardial mouse cells. *Eur Biophys J.* 15: 117-127.
- Bernus O, Wilders R, Zemlin CW, Verscelde H, Panfilov AV. 2002 A computationally efficient electrophysiological model of human ventricular cells. *Am J Physiol Heart Circ Physiol.* 282(6):H2296-308.
- Bers DM. 2001. Excitation-Contraction Coupling and Cardiac Contractile Force. Kluwer Academic, Dordrecht, Netherlands.
- Bers DM, Allen LAH, and Kim YJ. 1986. Calcium binding to cardiac sarcolemmal vesicles: Potential role as a modifier of contraction. *Am. J. Physiol.* 251:C861–C871.
- Bers DM, Peskoff A. 1991. Diffusion around a cardiac calcium channel and the role of surface bound calcium. *Biophys. J.* 59, 703–721.
- Beuckelmann DJ, Erdmann E, 1992. Ca^{2+} currents and intracellular $[Ca^{2+}]_i$ transients in single ventricular myocytes isolated from terminally failing human myocardium. *Basic Res. Cardiol.* 87, I235–I243.
- Beuckelmann DJ, Nabauer M, Erdmann E, 1993. Alterations of K^+ currents in isolated human ventricular myocytes from patients with terminal heart failure. *Circ. Res.* 73, 379–385.
- Bezanilla F, and Armstrong CM. (1977). Inactivation of the sodium channel. I. Sodium current experiments. *J Gen Physiol* 70, 549-66.
- Bloise R, Napolitano C *et al.* 2002. Romano-Ward and other congenital long QT syndromes. *Cardiovasc Drugs Ther.* 16:19-23.
- Bondarenko VE, Sziget GP, Bett GCL, Kim SJ, and Rasmusson RL. 2004. Computer model of action potential of mouse ventricular myocytes. *Am J Physiol Heart Circ Physiol.* 287: H1378-H1403
- Braun Ap, Schulman H. 1995. The multifunctional calcium/calmodulin-dependent protein kinase: from form to function. *Annu Rev Physiol* 57: 417-445
- Brugada P, and Brugada J. 1992. Right bundle branch block, persistent ST segment elevation and sudden cardiac death: a distinct clinical and electrocardiographic syndrome. A multicenter report. *J Am Coll Cardiol.* 15: 1391-1396.
- Brugada R, Brugada J, Antzelevitch C, Kirsch GE, Potenza D, Towbin JA, and Brugada P. 2000. Sodium channel blockers identify risk for sudden death in patients with ST-segment elevation and right bundle branch block but structurally normal hearts. *Circulation* 101: 510–515

REFERENCES

- Brugada J, Brugada R, and Brugada P. 1998. Right bundle-branch block and ST-segment elevation in leads V1 through V3: a marker for sudden death in patients without demonstrable structural heart disease. *Circulation* 97, 457-60.
- Cabo C., Boyden PA. 2003. Electrical remodeling of the epicardial border zone in the canine infarcted heart: a computational analysis. *Am. J. Physiol.* 284, H372–H384.
- Cheng HM, Cannell B, and Lederer WJ. 1995. Models of Ca²⁺ release channel adaptation. *Science* 267:2009–2010.
- Chanda B, Asamoah OK & Bezanilla F. 2004. Coupling interactions between voltage sensors of the sodium channel as revealed by site-specific measurements. *J Gen Physiol* 123, 217-30.
- Chandra R, Starmer CF, and Grant AO. 1998. Multiple effects of the KPQ deletion on gating of human cardiac Na⁺ channels expressed in mammalian cells. *Am J Physiol Heart Circ Physiol* 274: H1643–H1654
- Chen Q, Kirsch GE, Zhang D, *et al.* 1998 Genetic basis and molecular mechanism for idiopathic ventricular fibrillation. *Nature.* 19;392(6673):293-6.
- Ching CK, Tan Ec. 2006 Congenital long QT syndromes: clinical features, molecular genetics and genetic testing. *Expert Review of Molecular Diagnostics.* 6(3):365-74.
- Clancy CE and Rudy Y. 1999. Linking a genetic defect to its cellular phenotype in a cardiac arrhythmia. *Nature* 400: 566–569.
- Clancy CE and Rudy Y. 2001. Cellular consequences of HERG mutations in the long QT syndrome: precursors to sudden cardiac death. *Cardiovasc Res* 50: 301–313.
- Clancy CE and Rudy Y. 2002. Na⁺ Channel Mutation That Causes Both Brugada and Long-QT Syndrome Phenotypes. *Circulation* 105:1208-1213.
- Clancy CE, Tateyama M, and Kass RS. 2002. Insights into the molecular mechanisms of bradycardia-triggered arrhythmias in long QT-3 syndrome *J Clin Invest.* 110, pp. 1251-1262
- Clancy CE, Tateyama M, Liu H, Wehrens XHT, and Kass RS. 2003. Non-equilibrium gating in cardiac Na⁺ channels: an original mechanism of arrhythmia. *Circulation* 107: 2233–2237
- Collier M, Levesque P, Kenyon J and Hume J. 1996. Unitary Cl⁻ channels activated by cytoplasmic Ca²⁺ in canine ventricular myocytes. *Circ Res.* 78:936-944.
- Cormier JW, Rivolta I and Tateyama M *et al.* 2002. Secondary structure of the human cardiac Na⁺ channel C terminus: Evidence for a role of helical structures in modulation of channel inactivation, *J Biol Chem* 277: 9233–9241.
- Correa AM, Latorre R, Bezanilla F. 1991. Ion permeation in normal and batrachotoxin-modified Na⁺ channels in the squid giant axon. *J Gen Physiol.* 97:605–625.
- Courtemanche M, Ramirez, RJ, Nattel, S. 1998. Ionic mechanisms underlying human atrial action potential properties: insights from a mathematical model. *Am. J. Physiol.* 44, H301–H321.
- Davis Ba, Schwartz A, Samaha Fj, Kranias Eg. 1983. Regulation of cardiac sarcoplasmic reticulum calcium transport by calcium-calmodulin-dependent phosphorylation. *J Biol Chem* 258: 13 587-13 591.

REFERENCES

- Demir SS, Clark JW, Murphey CR, Giles WR. 1994. A mathematical model of a rabbit sinoatrial node cell. *Am. J. Physiol.* 266, C832–C852.
- Demir SS. 2004. Computational modeling of cardiac ventricular action potentials in rat and mouse: review. *Jpn J Physiol.* 54(6):523-30. Review.
- Despa S, Islam MA, Weber CR, Pogwizd SM, Bers DM. 2002. Intracellular Na⁺ Concentration Is Elevated in Heart Failure But Na/K Pump Function Is Unchanged. *Circulation* 105:2543-2548.
- DiFrancesco D, and Noble D. 1985. A model of cardiac electrical activity incorporating ionic pumps and concentration changes. *Phil Trans Roy Soc B.* 307:353-398.
- Drouin E, Charpentier F, Gauthier C, Laurent K, and Le M. 1995. Electrophysiologic characteristics of cells spanning the left ventricular wall of human heart: evidence for presence of M cells. *J Am Coll Cardiol.* 26: 185-192.
- Dumaine R, Wang Q, Keating MT, Hartmann HA, Schwartz, PJ, Brown AM, and Kirsch GE. 1996. Multiple Mechanisms of Na⁺ Channel-Linked Long-QT Syndrome. *Circ Res.* 78: 916-924
- Dumaine R, Towbin JA, Brugada P, Vatta M, Nesterenko DV, Nesterenko VV, Brugada J, Brugada R, and Antzelevitch C. 1999. Ionic mechanisms responsible for the electrocardiographic phenotype of the Brugada syndrome are temperature dependent. *Circ Res* 85: 803–809.
- Edman Cf, Schulman H. 1994. Identification and characterization of δ_B -CaM kinase and δ_C -CaM kinase from rat heart, two new multifunctional Ca²⁺/calmodulin-dependent protein kinase isoforms. *Biochim Biophys Acta* 1221:89-101.
- Etheridge SP, Compton SJ *et al.* 2003. A new oral therapy for long QT syndrome: long-term oral potassium improves repolarization in patients with HERG mutations. *J Am Coll Cardiol.* 42:1777-1782.
- Faber GM, Rudy Y. 2000. Action potential and contractility changes in [Na⁺]_i overloaded cardiac myocytes: a simulation study. *Biophys J* 78:2392-2404.
- Fabiato A. 1985. Time and calcium dependence of activation and inactivation of calcium-induced release of calcium from the sarcoplasmic reticulum of a skinned canine cardiac purkinje cell. *J. Gen. Physiol.* 85:247–289.
- Fish JM and Antzelevitch C. 2004. Role of sodium and calcium channel block in unmasking the Brugada syndrome. *Heart Rhythm.* 1: 210-2171.
- Fitzhugh R. 1960. Thresholds and plateaus in the Hodgkin-Huxley nerve equation. *J Gen Physiol.* 43:867-896.
- Follmer CH, Cullinan CA, and Colatsky TJ. 1992. Differential block of cardiac delayed rectifier current by class Ic antiarrhythmic drugs: evidence for open channel block and unblock. *Cardiovasc Res.* 26: 1121-1130.
- George AL Jr. 2005. Inherited disorders of voltage-gated sodium channels. *J Clin Invest.* 115(8): 1990–1999. Review.

REFERENCES

- Gima K, and Rudy Y. 2002. Ionic current basis of electrocardiographic waveforms: a model study. *Circ Res.* 90: 889-896.
- Goldin AL. 2001. Resurgence of sodium channel research. *Annu Rev Physiol* 63: 871–894.
- Grant AO, Carboni MP, Neplioueva V, Starmer CF, Memmi M, Napolitano C, and Priori S. 2002. Long QT syndrome, Brugada syndrome, and conduction system disease are linked to a single sodium channel mutation. *J Clin Invest* 110: 1201–1209.
- Groenewegen WA, Bezzina CR, van Tintelen JP, Hoorntje TM, Mannens MMAM, Wilde AAM, Jongsma HJ, and Rook MB. 2003. A novel LQT3 mutation implicates the human cardiac sodium channel domain IVS6 in inactivation kinetics. *Cardiovasc Res* 57: 1072–1078.
- Greenstein JL, Wu R, Po S, Tomaselli GT, Winslow RL. 2000. Role of the calcium-independent outward current Ito1 in shaping action potential morphology and duration. *Circ. Res.* 87, 1026–1033.
- Greenstein JL, and Winslow RL. 2002. An Integrative Model of the Cardiac Ventricular Myocyte Incorporating Local Control of Ca²⁺ Release. *Biophysical J* 83: 2918–2945
- Hain J, Onoue H, Mayrleitner M, Fleischer S, Schindler H. 1995. Phosphorylation modulates the function of the calcium release channel of sarcoplasmic reticulum from cardiac muscle. *J Biol Chem* 270: 2074-2081.
- Hancox JC, and Convery M. 1997. Inhibition of L-type calcium current by flecainide in isolated single rabbit atrioventricular nodal myocytes. *Experimental and Clinical Cardiology.* 2: 163-170.
- Hatem S, Le G, Le, H, Couetil JP, and Deroubaix E. 1992. Differential effects of quinidine and flecainide on plateau duration of human atrial action potential. *Basic Res Cardiol.* 87: 600-609.
- Herbert E, Trusz G *et al.* 2002. KCNQ1 gene mutations and the respective genotype-phenotype correlations in the long QT syndrome. *Med Sci Monit.* 8:RA240-RA248.
- Hering S, Bodewei R, and Wollenberger A. 1983. Sodium current in freshly isolated and in cultured single rat myocardial cells: frequency and voltage-dependent block by mexiletine. *J Mol Cell Cardiol.* 15: 431-444.
- Hilgemann, D. W., A. Collins, and S. Matsuoka, 1992. Steady-state and dynamic properties of cardiac sodium-calcium exchange. Secondary modulation by cytoplasmic calcium and ATP. *J. Gen. Physiol.* 100:933–961.
- Hille B. 1992. *Ionic Channels of Excitable Membranes.* Sinauer Associates Inc., Sunderland.
- Hoch B, Meyer R, Hetzer R, Krause EG, Karczewski P. 1999. Identification and expression of d-isoforms of the multifunctional Ca²⁺/calmodulin-dependent protein kinase in failing and nonfailing human myocardium. *Circ Res* 84:713-721.
- Hodgkin AL, Huxley AF, and Katz B. 1949. Ionic currents underlying activity in the giant axon of the squid. *Arch Sci Physiol.* 3:129-150.
- Hodgkin AL., and Huxley AF. 1952a. The components of membrane conductance in the giant axon of *Loligo*. *J Physiol.* 116:473-496.

REFERENCES

- Hodgkin AL., and Huxley AF. 1952b. Currents carried by sodium and potassium ions through the membrane of the giant axon of *Loligo*. *J Physiol*. 116:449-472.
- Hodgkin AL., and Huxley AF. 1952c. The dual effect of membrane potential on sodium conductance in the giant axon of *Loligo*. *J Physiol*. 116:497-506.
- Hodgkin AL., and Huxley AF. 1952d. A quantitative description of membrane current and its application to conduction and excitation in nerve. *J Physiol*. 117:500-544.
- Hund TJ, and Rudy J. 2004 Rate dependence and regulation of action potential and calcium transient in a canine cardiac ventricular cell model. *Circulation*. 110(20):3168-74.
- Hvalby Q, Hemmings Jr Hc, Paulsen O, Czernik Aj, Nairn Ac, Godfraind J-M, Jensen V, Raastad M, Storm Jf, Andersen P, Greengard P. 1994. Specificity of protein kinase inhibitor peptides and induction of long-term potentiation. *Proc Natl Acad Sci USA* 91: 4761-4765
- Irvine La, Jafri Ms, And Winslow RL. 1999. Cardiac sodium channel Markov model with temperature dependence and recovery from inactivation. *Biophys J*. 76: 1868-1885
- Iyer V, Mazhari R, and Winslow RL. 2004. A Computational Model of the Human Left-Ventricular Epicardial Myocyte. *Biophys J*. 87: 1507-1525.
- Jafri S, Rice JJ, and Winslow RL. 1998. Cardiac Ca^{2+} dynamics: The roles of ryanodine receptor adaptation and sarcoplasmic reticulum load. *Biophys J*. 74:1149-1168.
- Jett Mf, Schworer Cm, Bass M, Soderling Tr. 1987. Identification of membrane-bound calcium, calmodulin-dependent protein kinase II in canine heart. *Arch Biochem Biophys* 255: 354-360.
- Katz A. 1992. Physiology of the Heart. Raven Press, New York.
- Keating MT, and Sanguinetti MC. 1996. Molecular genetic insights into cardiovascular disease. *Science* 272, 681-5.
- Keating M, Atkinson D, Dunn C, Timothy K, Vincent GM, Leppert M. 1991. Linkage of a cardiac arrhythmia, the long QT syndrome, and the Harvey ras-1 gene. *Science*. 252:704-706.
- Kirchhefer U, Schmitz W, Scholz H, Neumann J. 1999. Activity of cAMP-dependent protein kinase and Ca^{2+} /calmodulin-dependent protein kinase in failing and nonfailing human hearts. *Cardiovasc Res* 42:254-261.
- Kneller J, Ramirez RJ, Chartier D, Courtemanche M, Nattel S. 2002. Time-dependent transients in an ionically based mathematical model of the canine atrial action potential. *Am. J. Physiol*. 282, H1437–H1451.
- Kohlhaas M, Zhang T, Seidler T, Zibrova D, Dybkova N, Steen A, Wagner S, Chen L, Brown JH, Bers DM, Maier LS. 2006. Increased sarcoplasmic reticulum calcium leak but unaltered contractility by acute CaMKII overexpression in isolated rabbit cardiac myocytes. *Circ Res*. 98(2):235-44.
- Kontis KJ and Goldin AL. 1997. Sodium channel inactivation is altered by substitution of voltage sensor positive charges. *J Gen Physiol* 110: 403–413.

REFERENCES

- Krishnan SC, and Antzelevitch C. 1991. Sodium channel block produces opposite electrophysiological effects in canine ventricular epicardium and endocardium. *Circ Res.* 69: 277-291.
- Kyndt F, Probst V, Potet F, Demolombe S, Chevallier JC, Baro I, Moisan JP, Boisseau P, Schott JJ, Escande D, and Le Marec H. 2001. Novel *SCN5A* mutation leading either to isolated cardiac conduction defect or Brugada syndrome in a large French family. *Circulation* 104: 3081–3086.
- Langer GA, and Peskoff A. 1996. Calcium concentration and movement in the dyadic cleft space of the cardiac ventricular cell. *Biophys J.* 70:1169-1182.
- Leblanc N, Hume JR. 1990. Sodium current-induced release of calcium from cardiac sarcoplasmic reticulum. *Science* 248, 372–376.
- Li GR, Feng J, Yue L, Carrier M, Nattel S. 1996. Evidence for two components of delayed rectifier K^+ current in human ventricular myocytes. *Circ. Res.* 78, 689–696.
- Li J, Marionneau C, Zhang R, Shah V, Hell JW, Nerbonne JM, Anderson ME. 2006. Calmodulin kinase II inhibition shortens action potential duration by upregulation of K^+ currents. *Circ Res.* 99(10):1092-9.
- Li L, Chu G, Kranias EG, Bers DM. 1998. Cardiac myocyte Ca transport in phospholamban knockout mouse: relaxation and endogenous CaMKII effects. *Am J Physiol* 274:H1335-1347.
- Liu DW, Gintant GA, and Antzelevitch C. 1993. Ionic bases for electrophysiological distinctions among epicardial, midmyocardial, and endocardial myocytes from the free wall of the canine left ventricle. *Circ Res* 72: 671–687.
- Liu DW and Antzelevitch C. 1995. Characteristics of the delayed rectifier current (IKr and IKs) in canine ventricular epicardial, midmyocardial, and endocardial myocytes. A weaker IKs contributes to the longer action potential of the M cell. *Circ Res.* 76: 351-365.
- Liu H, Tateyama M, Clancy CE, Abriel H, and Kass RS. 2002. Channel openings are necessary but not sufficient for use-dependent block of cardiac Na(+) channels by flecainide: evidence from the analysis of disease-linked mutations. *J Gen Physiol.* 120: 39-51.
- London B, Sanyal S, Michalec M, Pfahnl AF, Shang LL, Kerchner L, Lagana S, Aleong RG, Mehdi H, Gutmann R, Weiss R, and Dudley SC. 2006. *Heart Rhythm* 3(5) Suppl 1 Page S32
- Lossin C, Wang DW, Rhodes TH, Vanoye CG, and George AL. 2002. Molecular basis of an inherited epilepsy. *Neuron* 34: 877–884.
- Luo CH, Rudy Y. 1991 A model of the ventricular cardiac action potential. Depolarization, repolarization, and their interaction. *Circ Res.* 68(6):1501-26.
- Luo CH, and Rudy Y. 1994a. A dynamic model of the cardiac ventricular action potential. I. Simulations of ionic currents and concentration changes. *Circ Res.* 74: 1071-1096.
- Luo CH, and Rudy Y. 1994b. A dynamic model of the cardiac ventricular action potential. II. Afterdepolarizations, triggered activity, and potentiation. *Circ Res.* 74: 1097-1113.

REFERENCES

- Maier LS, Bers DM. 2002. Calcium, calmodulin, and calcium-calmodulin kinase II: heartbeat to heartbeat and beyond. *J Mol Cell Cardiol* 34:919-939.
- Maier LS, Zhang T, Chen L, DeSantiago J, Brown JH, Bers DM. 2003. Transgenic CaMKII δ_C overexpression uniquely alters cardiac myocyte Ca^{2+} handling: reduced SR Ca^{2+} -load and activated SR Ca^{2+} -release. *Circ Res* 92:904-911.
- Maltsev VA, and Undrovinas AI. 2006. A Multi-Modal Composition of the Late Na^+ Current in Human Ventricular. Cardiomyocytes. *Cardiovasc Res.* 69(1): 116–127.
- Mantegazza M, Yu FH, Catterall WA, and Scheuer T. 2001. Role of the C-terminal domain in inactivation of brain and cardiac sodium channels. *Proc Natl Acad Sci USA* 98: 15348–15353.
- Marban E. 2002. Cardiac channelopathies. *Nature.* 415:213-218.
- Marban E, Yamagishi T, and Tomaselli GF. 1998. Structure and function of voltagegated sodium channels. *J Physiol (Lond).* 508:647-57.
- Milburn T, Saint DA, Chung SH. 1995. The temperature dependence of conductance of the sodium channel: implications for mechanisms of ion permeation. *Receptors Channels* 3:201–211.
- Mitcheson JS, and Hancox JC. 1997. Modulation by mexiletine of action potentials, L-type Ca current and delayed rectifier K current recorded from isolated rabbit atrioventricular nodal myocytes. *Pflugers Arch.* 434: 855-858.
- Morita H, Nagase S, Kusano K, and Ohe T. 2002. Spontaneous T wave alternans and premature ventricular contractions during febrile illness in a patient with Brugada syndrome. *J Cardiovasc Electrophysiol.* 13: 816-818.
- Morita H, Zipes DP, Lopshire J, Morita ST, and Wu J. 2006. T wave alternans in an in vitro canine tissue model of Brugada syndrome. *Am J Physiol Heart Circ Physiol.* 291: H421-H428.
- Motoike HK, Liu H and Glaaser IW *et al.* 2004. The Na^+ channel inactivation gate is a molecular complex: a novel role of the COOH-terminal domain, *J Gen Physiol* 123: 155–165.
- Näbauer M, Beuckelmann DJ, and Erdmann E. 1993. Characteristics of transient outward current in human ventricular myocytes from patients with terminal heart failure. *Circ Res.* 73:386-394.
- Nagatomo T, January CT, and Makielski JC. 2000. Preferential block of late sodium current in the LQT3 DeltaKPQ mutant by the class I(C) antiarrhythmic flecainide. *Mol Pharmacol* 57: 101–107.
- Negretti N, O’Neil SC, and Eisner DA. 1993. The effects of inhibitors of sarcoplasmic reticulum function on the systolic Ca^{2+} transient in rat ventricular myocytes. *J. Physiol.* 468:35–52.
- Noble D. 1962. A modification of the Hodgkin-Huxley equations applicable to Purkinje fibre action and pacemaker potentials. *J Physiol.* 160:317-352.
- Noble D, and Rudy Y. 2001. Models of cardiac ventricular action potentials: iterative interaction between experiment and simulation. *Phil Trans R Soc Lond A.* 359:1127-1142.

REFERENCES

- Noble D, Varghese, Kohl P, and Noble P. 1998. Improved Guinea-pig ventricular cell model incorporating a diadic space, I_{Kr} and I_{Ks} , and length- and tension-dependent processes. *Can J Cardiol.* 14:123-134.
- Nordin C. 1993. Computer model of membrane current and intracellular Ca flux in the isolated guinea pig ventricular myocyte. *Am. J. Physiol.* 34, H2117–H2136.
- Nordin C, Ming Z. 1995. Computer model of current-induced early afterdepolarizations in guinea pig ventricular myocytes. *Am. J. Physiol.* 37, H2440–H2459.
- Nygren A, Fiset C, Firek L, Clark JW, Lindblad DS, Clark RB, Giles WR. 1998. Mathematical model of an adult human atrial cell: the role of K^+ currents in repolarization. *Circ. Res.* 82, 63–81.
- Oehmen CS, Giles WR, Demir SS. 2002. Mathematical model of the rapidly activating delayed rectifier potassium current I_{Kr} in rabbit sinoatrial node. *J. Cardiovas. Electrophysiol.* 13, 1131–1140.
- Ohkubo KIMI, Watanabe ICHI, Okumura YASU, Yamada TAKE, Masaki RIKO, Kofune TATS, Oshikawa NAOH, Kasamaki YUJI, Saito SATO, Ozawa YUKI, and Kanmatsuse KATS. 2003. Intravenous Administration of Class I Antiarrhythmic Drug Induced T Wave Alternans in an Asymptomatic Brugada Syndrome Patient. *Pacing and Clinical Electrophysiology.* 26: 1900-1903.
- Ono K, Kiyosue T, and Arita M. 1986. Comparison of the inhibitory effects of mexiletine and lidocaine on the calcium current of single ventricular cells. *Life Sci.* 39: 1465-1470.
- Ou Y, Stregé P and Miller SM *et al.* 2003. Syntrophin gamma 2 regulates *SCN5A* gating by a PDZ domain-mediated interaction, *J Biol Chem* 278: 1915–1923.
- Page E, McCallister LP, and Power B. 1971. Stereological measurements of cardiac ultrastructures implicated in excitation-contraction coupling. *Proc. Natl. Acad. Sci.* 68:1465–1466.
- Page, E. and M. Surdyk-Droske, 1979. Distribution, surface density and membrane area of diadic junctional contacts between plasma membrane and terminal cisterns in mammalian ventricle. *Circ. Res.* 45:260–267.
- Pandit SV, Clark RB, Giles WR, and Demir SS. 2001. A Mathematical Model of Action Potential Heterogeneity in Adult Rat Left Ventricular Myocytes. *Biophys J.* 81:3029-3051.
- Pandit SV Giles WR, and Demir SS. 2003. A mathematical model of the electrophysiological alterations in rat ventricular myocytes in type-I diabetes. *Biophys. J.* 84, 832–841.
- Paul AA, Witchel HJ, and Hancox JC. 2002. Inhibition of the current of heterologously expressed HERG potassium channels by flecainide and comparison with quinidine, propafenone and lignocaine. *Br J Pharmacol.* 136: 717-729.
- Peterson BZ, DeMaria CD, Adelman JP, and Yue DT. 1999. Calmodulin is the Ca^{2+} sensor for Ca^{2+} -dependent inactivation of L-type calcium channels. *Neuron.* 22:549–558.

REFERENCES

- Piacentino III V, Weber CR, Chen X, Weisser-Thomas J, Margulies KB, Bers DM, Houser SR. 2003. *Circ.Res.* 92, 651–658.
- Pogwizd SM, Schlotthauer K, Li L, Yuan W, Bers DM. 2001. Arrhythmogenesis and contractile dysfunction in heart failure: Roles of sodium-calcium exchange, inward rectifier potassium current, and residual beta-adrenergic responsiveness. *Circ Res.* 88(11):1159-67.
- Priebe L, Beuckelmann DJ. 1998. Simulation study of cellular electric properties in heart failure. *Circ. Res.* 82, 1206–1223.
- Priori SG, Napolitano C, Cantu F, Brown AM, and Schwartz PJ. 1996. Differential response to Na⁺ channel blockade, beta-adrenergic stimulation, and rapid pacing in a cellular model mimicking the *SCN5A* and *HERG* defects present in the long-QT syndrome. *Circ Res.* 78: 1009-1015.
- Priori SG., Barhanin J, Hauer RN, Haverkamp W, Jongsma, HJ, Kleber AG, McKenna WJ, Roden DM, Rudy Y, Schwartz K, Schwartz PJ, Towbin JA and Wilde AM. (1999a). Genetic and molecular basis of cardiac arrhythmias: impact on clinical management part III. *Circulation* 99, 674-81.
- Priori SG, Barhanin J, Hauer RN., Haverkamp W, Jongsma HJ., Kleber AG, McKenna WJ, Roden DM, Rudy Y, Schwartz K, Schwartz PJ, Towbin JA and Wilde AM. (1999b). Genetic and molecular basis of cardiac arrhythmias: impact on clinical management parts I and II. *Circulation* 99, 518-28.
- Liu CJ, Dib-Hajj SD and Renganathan M *et al.* 2003. Modulation of the cardiac sodium channel Nav1.5 by fibroblast growth factor homologous factor 1B, *J Biol Chem* 278: 1029–1036.
- Priori SG, Napolitano C, Schwartz PJ, Bloise R, Crotti L, and Ronchetti E. 2000. The thin border between long QT and Brugada syndromes: the role of flecainide challenge. *Circulation* 102: 676.
- Priori SG, Napolitano C, Schwartz PJ, Bloise R, Crotti L, and Ronchetti E. 2000. The elusive link between LQT3 and Brugada syndrome: the role of flecainide challenge. *Circulation.* 102: 945-947.
- Priori SG, Rivolta I, and Napolitano C. 2003. Genetics of long QT, Brugada and other Channelopathies. In: *Cardiac Electrophysiology, Fourth Edition*, pp. 462-470. Eds D. P. Zipes, J. Jalife. Elsevier: Philadelphia.
- Puglisi JL, Bassani RA, Bassani JWM, Amin JN, and Bers DM. 1996. Temperature and relative contributions of Ca transport systems in cardiac myocyte relaxation. *Am. J. Physiol.* 270:H1772–H1778.
- Puglisi JL, Yuan W, Bassani JWM, and Bers DM. 1999. Ca influx through Ca channels in rabbit ventricular myocytes during action potential clamp: Influence of temperature. *Circ. Res.* 85:e7–e16.
- Puglisi JL, and Bers DM. 2001. LabHEART: an interactive computer model of rabbit ventricular myocyte ion channels and Ca transport. *Am J Physiol Cell Physiol.* 281(6):C2049-C2060.
- Qin N, Olcese R, Branby M, Lin T, and Birnbaumer L. 1999. Ca²⁺-induced inhibition of the cardiac Ca²⁺ channel depends on calmodulin. *Proc. Natl. Acad. Sci.* 96:2435–2438.

REFERENCES

- Ramirez RJ, Nattel S, Courtemanche M. 2000. Mathematical analysis of canine atrial action potential. *Am. J. Physiol.* 279, H1767–H1767.
- Rice JJ, Jafri MS, and Winslow RL. 1999. Modeling gain and gradedness of Ca^{2+} release in the functional unit of the cardiac diadic space. *Biophys J.* 77:1871-84.
- Rivolta I, Abriel H, Tateyama M, Liu H, Memmi M, Vardas P, Napolitano C, Priori SG, and Kass RS. 2001. Inherited Brugada and long QT-3 syndrome mutations of a single residue of the cardiac sodium channel confer distinct channel and clinical phenotypes. *J Biol Chem.* 276: 30623-30630.
- Rivolta I, Clancy CE, Tateyama M, Liu H, Priori SG. and Kass RS. 2002. A novel *SCN5A* mutation associated with long QT-3: altered inactivation kinetics and channel dysfunction. *Physiol.Genomics*, 10: 191-197
- Rudy Y, Silva JR.2006. Computational biology in the study of cardiac ion channels and cell electrophysiology. *Q Rev Biophys.* 39(1):57-116. Review.
- Schwartz PJ, Priori SG, Locati EH, Napolitano C, Cantu F, Towbin JA, Keating MT, Hammoude H, Brown AM., and Chen LS. 1995. Long QT syndrome patients with mutations of the *SCN5A* and *HERG* genes have differential responses to Na^+ channel blockade and to increases in heart rate. Implications for gene-specific therapy. *Circulation.* 92: 3381-3386.
- Schwartz PJ, Priori SG, and Napolitano C. 2000a. The long QT syndrome. In: *Cardiac Electrophysiology: From Cell to Bedside*, pp. 597-615.
- Schwartz PJ, Priori SG, Dumaine R, Napolitano C, Antzelevitch C, Stramba-Badiale M, Richard TA, Berti MR, and Bloise R. 2000b. A Molecular Link between the Sudden Infant Death Syndrome and the Long-QT Syndrome. *N Engl J Med.* 343: 262-267.
- Schwartz PJ, Priori SG, Spazzolini C, Moss AJ, Vincent GM, Napolitano C, Denjoy I, Guicheney P, Breithardt G, Keating MT, Towbin JA, Beggs AH, Brink P, Wilde AA, Toivonen L, Zareba W, Robinson JL, Timothy KW, Corfield V, Wattanasirichaigoon D, Corbett C, Haverkamp W, Schulze B, Lehmann MH, Schwartz K, Coumel P, and Bloise R. 2001. Genotype-phenotype correlation in the long-QT syndrome: gene-specific triggers for life-threatening arrhythmias. *Circulation.* 103: 89-95.
- Schwartz PJ, Priori SG, Napolitano C. 2003. How Really Rare Are Rare Diseases?: The Intriguing Case of Independent Compound Mutations in the Long QT Syndrome. *Journal of Cardiovascular Electrophysiology.* 14(10):1120-1.
- Schwarz JR. 1986. The effect of temperature on Na currents in rat myelinated nerve fibres. *Pflugers Arch.* 406: 397-404.
- Scriven DR, Dan P, and Moore ED. 2000. Distribution of proteins implicated in excitationcontract coupling in rat ventricular myocytes. *Biophys. J.* 79:2682–2691.
- Scriven DRL, Klimek A, Lee KL, and Moore EDW. 2002. The molecular architecture of calcium microdomains in rat cardiomyocytes. *N. Y. Acad. Sci.* 976:488–499.
- Shampine LF, M. Reichelt MW, and Kierzenka JA. 1999. Solving Index-1 DAEs in MATLAB and Simulink. *SIAM Review*, 41: 538-552.

REFERENCES

- Shampine LF, and Reichelt MW. 1997. The MATLAB ODE Suite. *SIAM Journal on Scientific Computing*. 18: 1-22.
- Shannon T, Chu G, Kranias E, and Bers D. 2001. Phospholamban decreases the energetic efficiency of the sarcoplasmic reticulum Ca pump. *J Biol Chem* 276:7195–201.
- Shannon TR, and Bers DM. 1997. Assessment of intra-SR free [Ca] and buffering in rat heart. *Biophys. J.* 73:1524–1531.
- Shannon TR, Ginsburg KS, and Bers DM. 2000a. Potentiation of fractional SR Ca release by total and free intra-SR Ca concentration. *Biophys. J.* 78:334–343.
- Shannon TR, Ginsburg KS, and Bers DM. 2000b. Reverse mode of the SR Ca pump and load-dependent cytosolic Ca decline in voltage clamped cardiac ventricular myocytes. *Biophys. J.* 78:322–333.
- Shannon TR, Wang F, Puglisi J, Weber C, Bers DM. 2004. A mathematical treatment of integrated Ca dynamics within the ventricular myocyte. *Biophys J.* 87(5):3351-71.
- Shimizu W. 2005. The Brugada Syndrome –An Update- *Internal Medicine* 44(12): 1224-31
- Shimizu W, Aiba T, Kamakura S. 2005. Mechanisms of disease: current understanding and future challenges in Brugada syndrome. *Nat Clin Pract Cardiovasc Med.* 2(8):408-14. Review.
- Shimizu W, Antzelevitch C, Suyama K, Kurita T, Taguchi A, Aihara N, Takaki H, Sunagawa K, and Kamakura S. 2000. Effect of sodium channel blockers on ST segment, QRS duration, and corrected QT interval in patients with Brugada syndrome. *J Cardiovasc Electrophysiol.* 11: 1320-1329.
- Sicouri S, Quist M, and Antzelevitch C. 1996. Evidence for the presence of M cells in the guinea pig ventricle. *J Cardiovasc Electrophysiol.* 7: 503-511.
- Simmerman Hkb, Collins Jh, Theibert JI, Wegener Ad, Jones Lr. 1986. Sequence analysis of PLB: Identification of phosphorylation sites and two major structural domains. *J Biol Chem* 261: 13 333-13 341.
- Slawsky MT, and Castle NA. 1994. K⁺ channel blocking actions of flecainide compared with those of propafenone and quinidine in adult rat ventricular myocytes. *J Pharmacol Exp Ther.* 269: 66-74.
- Soeller C, and Cannell MB. 1997. Numerical simulation of local calcium movements during L-type calcium channel gating in the cardiac diad. *Biophys J.* 73:97-111.
- Stern MD, and Lakatta EG. 1992. Excitation–contraction coupling in the heart: the state of the question. *FASEB J.* 6, 3092–3100.
- Stern MD, Song LS, Cheng H, Sham JS, Yang HT, Boheler KR, and Rios E. 1999. Local control models of cardiac excitation-contraction coupling. A possible role for allosteric interactions between ryanodine receptors. *J Gen Physiol.* 113:469-89.

REFERENCES

- Stuhmer W, Conti F, Suzuki H, Wang XD, Noda M, Yahagi N, Kubo H, and Numa S. 1989. Structural parts involved in activation and inactivation of the sodium channel. *Nature* 339: 597–603.
- Sun YM, Favre I, Schild L, and Moczydlowski E. 1997. On the structural basis for size-selective permeation of organic cations through the voltage-gated sodium channel: effect of alanine mutations at the DEKA locus on selectivity, inhibition by Ca^{2+} and H^+ , and molecular sieving. *J Gen Physiol* 110: 693–715.
- Tan HL, Bezzina CR and Smits JP *et al.* 2003. Genetic control of sodium channel function, *Cardiovasc Res* 57: 961–973.
- Tan H, Kupershmidt S, Zhang R, Stepanovic S, Roden D, Wilde A, Anderson M., Balser J. 2002. A calcium sensor in the sodium channel modulates cardiac excitability. *Nature* 415:442-447.
- Tan HL, Bink-Boelkens MTE, Bezzina CR, Viswanathan PC, Beaufort-Krol GCM, van Tintelen PJ, van den Berg MP, Wilde AAM, and Balser JR. 2001. A sodium-channel mutation causes isolated cardiac conduction disease. *Nature* 409: 1043–1047.
- Tateyama M, Kurokawa J, Terrenoire C, Rivolta I, and Kass RS. 2003. Stimulation of Protein Kinase C Inhibits Bursting in Disease- Linked Mutant Human Cardiac Sodium Channels. *Circulation*, 107: 3216-3222
- ten Tusscher KH, Noble D, Noble PJ, Panfilov AV. 2004. A model for human ventricular tissue. *Am J Physiol Heart Circ Physiol*. 286(4):H1573-89
- ten Tusscher KH, and Panfilov AV. 2006. Alternans and spiral breakup in a human ventricular tissue model. *Am J Physiol Heart Circ Physiol*. 291(3):H1088-100.
- Tian XL, Yong SL, Wan X, Wu L, Chung MK, Tchou PJ, Rosenbaum DS, Van Wagoner DR, Kirsch GE, and Wang Q. 2004. Mechanisms by which *SCN5A* mutation N1325S causes cardiac arrhythmias and sudden death in vivo. *Cardiovasc Res*. 61: 256-267.
- Tobimatsu T, Fujisawa H. 1989. Tissue-specific expression of four types of rat calmodulin-dependent protein kinase II mRNAs. *J Biol Chem* 264: 17 907-17 912
- Tohse N. 1990. Calcium-sensitive delayed rectifier potassium currents in guinea pig ventricular cells. *Am. J. Physiol*. 258:H1200–1207.
- Uemura A, Okazaki K, Takesue H, Matsubara T, Hidaka H. 1995. A novel Ca/calmodulin-dependent protein kinase lacking autophosphorylation activity in the rabbit heart. *Biochem Biophys Res Commun* 211: 562-569.
- Vecchietti S, Rivolta I, Severi S, Napolitano C, Priori S, and Cavalcanti S. 2006. Computer simulation of wild-type and mutant human cardiac Na^+ current. *Med Biol Eng Comput*. 44(1-2):35-44.
- Vecchietti S, Grandi E, Severi S, Rivolta I, Napolitano C, Priori SG, Cavalcanti, S. 2007. In silico assessment of Y1795C and Y1795H *SCN5A* mutations. Implication for inherited arrhythmogenic syndromes. *Am J Physiol Heart Circ Physiol* 292: H56–H65.

REFERENCES

- Veldkamp MW, Viswanathan PC, Bezzina C, Baartscheer A, Wilde AAM, and Balseer JR. 2000. Two distinct congenital arrhythmias evoked by a multidysfunctional Na⁺ channel. *Circ Res* 86: E91–E97.
- Viswanathan PC, and Rudy Y. 1999. Pause induced early afterdepolarizations in the long QT syndrome: a simulation study. *Cardiovasc Res*. 42: 530-542.
- Viswanathan PC, Shaw RM *et al.* 1999. Effects of I_{Kr} and I_{Ks} heterogeneity on action potential duration and its rate dependence: a simulation study. *Circulation*. 99:2466-2474.
- Wagner S, Seidler T, Picht E, Maier LS, Kazanski V, Teucher N, Schillinger W, Pieske B, Isenberg G, Hasenfuss G, *et al.* 2003. Na⁺-Ca²⁺ exchanger overexpression predisposes to reactive oxygen species-induced injury. *Cardiovasc Res* 60:404-412.
- Wagner S, Dybkova N, Rasenack EC, Jacobshagen C, Fabritz L, Kirchhof P, Maier SK, Zhang T, Hasenfuss G, Brown JH, Bers DM, Maier LS. 2006a. Ca/calmodulin-dependent protein kinase II regulates cardiac Na channels. *J Clin Invest*. 116(12):3127-3138.
- Wagner S, Hacker E, Dybkova N, Fabritz L, Kirchhof P, Bers DM *et al.* 2006b. Ca/calmodulin kinase II differentially modulates transient outward potassium current in heart failure. *Circulation* 114(Suppl II):60.
- Wang DW, Kiyosue T, Sato T, and Arita M. 1996. Comparison of the effects of class I anti-arrhythmic drugs, cibenzoline, mexiletine and flecainide, on the delayed rectifier K⁺ current of guinea-pig ventricular myocytes. *J Mol Cell Cardiol*. 28: 893-903.
- Wang DW, Yazawa K, Makita N, George AL Jr, and Bennett PB. 1997. Pharmacological targeting of long QT mutant sodium channels. *J Clin Invest* 99: 1714–1720.
- Wang DW, Makita N, Kitabatake A, Balseer JR, and George AL. 2000. Enhanced Na⁺ channel intermediate inactivation in Brugada syndrome. *Circ Res* 87: E37–E43.
- Weber C, Ginsburg K, Philipson K, Shannon T, and Bers D. 2001. Allosteric regulation of Na/Ca exchange current by cytosolic Ca in intact cardiac myocytes. *J. Gen. Physiol*. 117:119–31.
- Weber CR., Piacentino V, Ginsburg KS, Houser SR, and Bers DM. 2002. Na⁺-Ca²⁺ exchange current and submembrane [Ca²⁺] during the cardiac action potential. *Circ. Res*. 90:182–189.
- Wehrens XH, Vos MA *et al.* Novel insights in the congenital long QT syndrome. 2002. *Ann Intern Med*. 137:981-992.
- Westenskow P, Splawski I, Timothy KW, Keating MT, Sanguinetti MC. 2004. Compound Mutations: A Common Cause of Severe Long-QT Syndrome. *Circulation*.109(15):1834-41.
- Winslow RL, Rice JJ, Jafri MS, Marban E, and O'Rourke B. 1999. Mechanisms of Altered Excitation-Contraction Coupling in Canine Tachycardia-Induced Heart Failure. II. Model Studies. *Circ Res*. 84:571-586.
- Witcher Dr, Kovacs Rj, Schulman H, Cefali Dc, Jones Lr. 1991. Unique phosphorylation site on the cardiac ryanodine receptor regulates calcium channel activity. *J Biol Chem* 266: 11 144-11 152.

REFERENCES

- Wu Y, Temple J, Zhang R, Dzhura I, Zhang W, Trimble R, Roden DM, Passier R, Olson, EN, Colbran RJ, *et al.* 2002. Calmodulin kinase II and arrhythmias in a mouse model of cardiac hypertrophy. *Circulation* 106:1288-1293.
- Yan GX and Antzelevitch C. 1999. Cellular basis for the Brugada syndrome and other mechanisms of arrhythmogenesis associated with ST-segment elevation. *Circulation* 100: 1660–1666.
- Yan GX and Antzelevitch C. 1998. Cellular basis for the normal T wave and the electrocardiographic manifestations of the long-QT syndrome. *Circulation* 98: 1928–1936.
- Yuan W and Bers DM. 1994. Ca-dependent facilitation of cardiac Ca current is due to Ca-calmodulin-dependent protein kinase. *Am J Physiol.* 267(3 Pt 2):H982-93.
- Yue DT, and Marban E. 1988. A novel cardiac potassium channel that is active and conductive at depolarized potentials. *Pflugers Arch.* 413:127-33.
- Zang H, Holden AV, Kodama I, Honjo H, Lei M, Varghese T, Boyett MR. 2000. Mathematical models of action potentials in the periphery and center of the rabbit sinoatrial node. *Am. J. Physiol.* 279, H397–H421.
- Zeng J, and Rudy Y. 1995. Early afterdepolarizations in cardiac myocytes: mechanism and rate dependence. *Biophys J.* 68:949-64.
- Zeng J, Laurita KR, Rosenbaum DS, and Rudy Y. 1995. Two components of the delayed rectifier K⁺ current in ventricular myocytes of the guinea pig type. Theoretical formulation and their role in repolarization. *Circ Res.* 77: 140-152.
- Zhang T, Maier LS, Dalton ND, Miyamoto S, Ross J, Bers DM, Brown JH. 2003. The δ_C isoform of CaMKII is activated in cardiac hypertrophy and induces dilated cardiomyopathy and heart failure. *Circ Res* 92:912-919.
- Zhang R, Khoo MS, Wu Y, Yang Y, Grueter CE, Ni G, Price EE, Thiel W, Guatimosim, S, Song LS, *et al.* 2005. Calmodulin kinase II inhibition protects against structural heart disease. *Nat Med* 11:409-417.
- Zygmunt AC, and Gibbons WR. 1991. Calcium-activated chloride current in rabbit ventricular myocytes. *Circ. Res.* 68:424–437.

Publications

Peer-reviewed Journal Publications

S. Severi, S. Cavalcanti, A. Ciandrini, **E. Grandi**, Stefano Bini, F. Badiali, A. Gattiani, L. Cagnoli. 'Cardiac response to hemodialysis with different cardiovascular tolerance: heart rate variability and QT interval analysis', Hemodial Int. 2006 Jul;10(3):287-93.

S. Vecchiotti, **E. Grandi**, S. Severi, I. Rivolta, C. Napoletano, S. G. Priori, S. Cavalcanti. 'In silico assessment of Y1795C and Y1795H *SCN5A* mutations. Implication for inherited arrhythmogenic syndromes', Am J Physiol Heart Circ Physiol 2007 292:H56-H65

Book Chapters

E. Grandi, S. Vecchiotti, S. Severi, E. Giordano & S. Cavalcanti "Effects of β -adrenergic stimulation on the ventricular action potential: a simulation study", In Modelling in Medicine and Biology VI , edited by M. Ursino, C.A. Brebbia, G. Pontrelli, and E. Magosso: 87-94, WIT press, Southampton, 2005 (ISBN: 1-84564-024-1)

International Conference Proceedings

E. Grandi, S. Vecchiotti, S. Severi, S.G. Priori, S. Cavalcanti. 'Effects of Nitric Oxide on the QT Interval during Hemodialysis Sessions: a Simulation Study', X Mediterranean Conference on Medical and Biological Engineering and Computing 2004, Ischia, 31 luglio-5 agosto, 2004

S. Vecchiotti, **E. Grandi**, S. Severi and S. Cavalcanti. 'Effects of Potassium and Calcium Changes on Ventricular Action Potential: a Simulation Study' X Mediterranean Conference on Medical and Biological Engineering and Computing 2004, Ischia, 31 luglio-5 agosto, 2004

E. Grandi, S. Vecchiotti, S. Severi, E. Giordano, S. Cavalcanti 'Simulated effects of sympathetic stimulation on the action potential of ventricular cardiomyocytes', EMBEC 2005 3rd European Medical and Biological Engineering Conference, Praga, 20-25 Novembre 2005

E. Grandi, J.L. Puglisi, D.M. Bers, S. Severi 'Compound Mutations in Long QT Syndrome Assessed by a Computer Model' 33rd Computers in Cardiology, Valencia, Spain, 17-20 settembre 2006

S. Severi, **E. Grandi**, G. Alessandrini, A. Santoro, S. Cavalcanti 'Principal Component Analysis of the T Wave: 24 Hour Monitoring of Repolarization Complexity in Dialysis Patients' 33rd Computers in Cardiology, Valencia, Spain, 17-20 settembre 2006

National Conference Abstracts

E. Grandi, S. Vecchiotti, S. Severi, E. Giordano, S. Cavalcanti. *'Simulazione Numerica degli Effetti dell'Ossido di Azoto sul Potenziale d'Azione dei Cardiomiociti'* XI Congresso Nazionale della Società Italiana di Ricerche Cardiovascolari, Latina, 23-25 settembre 2004, p.107

S. Vecchiotti, S. Severi, **E. Grandi**, S. Cavalcanti, I. Rivolta, C. Napoletano, S.G. Priori. *'Applicazione di un Simulatore di Cellula Cardiaca a Studi di Proteomica Funzionale'* XI Congresso Nazionale della Società Italiana di Ricerche Cardiovascolari, Latina, 23-25 settembre 2004, p.62

M. Govoni, **E. Grandi**, S. Furini, S. Severi, V. Mazzone, M. Carboni, A. Santoro, S. Cavalcanti, E. Giordano *'Bicarbonato-dialisi verso biofiltrazione in assenza di acetato nell' induzione della sintasi dell'ossido nitrico in cardiomiociti di ratto'* XIII Congresso Nazionale della Società Italiana di Ricerche Cardiovascolari, Imola, 21-23 settembre 2006

S. Furini, M. Govoni, **E. Grandi**, S. Severi, F. Lodesani, M. Bennati, I. Olla, M. Tartagni, P. Iorio, A. Miano, C.M. Caldarera; S. Cavalcanti, E. Giordano *'Macrolides antibiotics and ion transport across plasma membrane'* XIII Congresso Nazionale della Società Italiana di Ricerche Cardiovascolari, Imola, 21-23 settembre 2006

S. Furini, M. Govoni, **E. Grandi**, S. Severi, G. Alessandrini, P. Iorio, A. Miano, V. Mazzone, C.M. Caldarera; S. Cavalcanti, E. Giordano. *'Effetto degli antibiotici macrolidi sul trasporto ionico attraverso la proteina-canale CFTR'* IV Convention d'autunno dei ricercatori italiani per la Fibrosi Cistica, Verona, 17 – 18 Novembre 2006